DEFINING THE EXTRACELLULAR MATRIX COMPOSITION OF THE ACUTE MYELOID LEUKEMIA CELL NICHE: TOWARDS DEVELOPMENT OF A FUNCTIONAL 3D DRUG SCREENING SYSTEM

VLADISLAVA SADETCKAIA

A THESIS SUBMITTED TO THE FACULTY OF GRADUATE STUDIES

IN PARTIAL FULFILMENT OF THE REQUIREMENTS FOR

THE DEGREE OF MASTER OF SCIENCE

GRADUATE PROGRAM IN BIOLOGY

YORK UNIVERSITY

TORONTO, ONTARIO

APRIL 2022

©Vladislava Sadetckaia, 2022

Abstract

Acute Myeloid Leukemia is a heterogeneous hematopoietic malignancy, which has been shown to modify the bone marrow microenvironment towards cooperating with the cancer cell to promote their proliferation. In this research I optimized a procedure for growing AML cells in a novel culture system in vitro in order to provide the cells with a microenvironment more closely resembling the native cell niche. Next, an analysis of various ECM components was undertaken to assess whether their presence may affect AML cell survival. In a proof-of-concept study, I employed the novel culture system to analyze the effect of 160 chemical agents on cell survival and compared the traditional polystyrene cultures with the novel 2D and 3D collagen culture systems. By recapitulating the tumor microenvironment with three-dimensional collagen scaffolds, I was able to demonstrate a microenvironment-dependent variation in drug response and identify novel targets that may not have been detected with a traditional screening assay.

Acknowledgements

First and foremost, I would like to thank Dr. Eleftherios Sachlos for taking me on and allowing me the opportunity to explore the field of biomedical engineering. I would like to express my sincere appreciation for his continued support, ongoing encouragement and patience. I have learned so much during this short time and am thankful to have had him as a mentor.

To my supervisory committee Dr. Samuel Benchimol, thank you for your guidance, for the thoughtful and interesting discussions and for your encouragement.

I would like to thank all the members of the Stem Cell Engineering lab group for their encouragement and support. Each person in the lab has helped me throughout these years, they have created a friendly and encouraging research environment and supported each other even when we were forced to stay apart. I would especially like to thank Milad Falahat Chian for spending so much time teaching me methods and techniques essential for my degree and always being there to bounce ideas off. And a special thank you to Sara Hajari, for continuing on with this project.

Lastly, I would like to thank my parents for giving me the freedom to pursue my passions and encouraging me to always explore. I am thankful to my sister for always being there for me and reminding me of my worth. And to all my friends for supporting me throughout this entire degree, thank you for your everlasting love, patience, and encouragement. I would not be where I am today without your support.

Table of Contents

List of Abbreviations

AML	Acute Myeloid Leukemia
Ara-C	Cytarabine arabinoside
C	Collagen
CDC42	Cell division control protein 42
CD44	Cluster of Differentiation 44
CSC	Cancer Stem Cell
CXCR4	Chemokine Receptor 4
DMSO	Dimethyl Sulfoxide
DNA	Deoxyribonucleic Acid
FBS	Fetal Bovine Serum
E	Elastin
EDC	1-ethyl-3-(3-dimethylaminopropyl) carbodiimide hydrochloride
EDTA	Ethylenediaminetetraacetic Acid
ECM	Extracellular Matrix
GAG	Glycosaminoglycan
HA0.1	Hydroxyapatite nano powder, <200 nm particle size (BET)
HA10	Hydroxyapatite powder, 10 μm, ≥100 m2/g
HSC	Hematopoietic Stem Cell
LSC	Leukemia Stem Cell
NHS	N-hydro-xysuccinimide
NR	Nuclear Receptor
OCI	Ontario Cancel Institute
PBS	Phosphate Buffered Saline
PCR	Polymerase Chain Reaction
PEF	PBS, EDTA, FBS
PS	Polystyrene
ROS	Reactive Oxygen Species
SNS	Sympathetic Nervous System
RHAMM	Receptor for Hyaluronan Mediated Motility
TDZ	Thioridazine
VEGF	Vascular Endothelial Growth Factor
VLA-4	Very Late Antigen – 4

αMEM	alpha Minimum Essential Medium
2D	Two-dimensional
3D	Three-dimensional
7-TM	7 Transmembrane

List of Figures

Chapter 1. Introduction

1.1 The Bone Marrow Niche Components and Inhabitants

1.1.1 The Hematopoietic System

The hematopoietic system is the collection of organs and tissues in the body involved in the production and maintenance of cellular blood components. Blood cells in turn are responsible for constant maintenance of the organism tissues, as well as oxygen delivery and immune protection of the body. A single cell type is responsible for the production of all blood cells in the body – the hematopoietic stem cell (HSC), capable of giving rise to platelets, white and red blood cells and responsible for the constant renewal of blood in the body. First evidence of a blood forming progenitor cells came in 1945 when studies emerged on people who were exposed to high levels of radiation. After studying radiation exposure in mice, it was found that these animals could be rescued with a bone marrow transplant[1]. Subsequently in the 1960s, two Canadian scientists Till and McCulloch analyzed the bone marrow and identified the hematopoietic stem cell – responsible for regenerating blood [2]. They defined the two unique hallmarks of the hematopoietic stem cell: self renewal and multipotency by differentiation[2]. Self-renewal refers to the capacity of these cells to sustain their population number while still producing billions of blood cells each day. Multipotency refers to the cell's ability to give rise to multipotent progenitors which are capable of differentiating into specialized progenitors, such as blood cells in the case of HSC, which, have a restricted lineage differentiation and self-renewal capacity[3,4].

To maintain homeostasis, the stem cell pool is sustained at a relatively constant number – the amount of cells lost to differentiation is balanced with proliferation of the stem cells[5]. During stress, however, such as injury the HSCs are capable of extensive in vivo self-renewal. Studies showed that a single purified HSC is capable of reconstituting long-term hematopoiesis[6]. This robust self-replicating capacity warrants a high degree of regulation in order to support the needs of the organism, through expansion and differentiation. Excessive differentiation or insufficient self-renewal can deplete the HSC pool, whereas insufficient differentiation or unrestrained self-renewal can lead to myeloproliferative diseases or leukaemia[7].

Although HSCs constitute the most important blood component, they are a rare population of cells, representing less than 0.01% of all cells in the bone marrow[5]. Another vital occupant of the bone marrow is the Mesenchymal stromal cells (MSCs) – an adherent cell capable of self-renewal and clonal expansion with the capacity to differentiate into multilineage precursors of bone, fat, and cartilage[8]. These serve a multitude of functions, from musculoskeletal tissue formation to hematopoietic support and immune system regulation[9]. MSCs progenitor descendants also play an important role in niche formation as they assemble

into a sustainable framework, occupied by cells, where external signals can be spatially regulated. The cells derived from MSCs express molecules that aid in HSC maintenance and proliferation regulation and studies have shown that their depletion results in a decline of the HSC pool[10]. MSCs modulate hematopoiesis through regulation of balance between self-renewal and differentiation and achieve this through direct cell-cell interactions as well as secretion of cytokines and extracellular matrix (ECM) molecules[11].

The diversity of the bone marrow cells ranges from mesenchymal stromal cells to mature hematopoietic cells. Some examples of candidate niche cells include endothelial cells of the sinusoids and arterioles[12], perivascular cell[12,13], osteo-lineage cells[14], adipocytes[15], neuronal cells[16] and a large variety of the HSC progenitor cells[17]. Paradoxically almost all cellular components found within the bone marrow microenvironment may play an important function for the control of HSCs[7].

Blood stem cells in culture behave like ordinary white blood cells making them difficult to identify and isolate and when they are isolated the yield is very low, with proportions being as low as 1 in 100,000 blood cells. Currently in clinical studies there are three sources of hematopoietic stem cells. The first most traditional source is the bone marrow tissue, transplants of bone marrow have been performed for over 40 years. Typically, the donor's bone is punctured, and the bone marrow is drawn out with a syringe. Not only is this procedure extremely painful for the donors, it also has a low yield of stem cells with only 1 in 100,000 cells having the blood-forming potential[18]. Although the hematopoietic stem cells proliferate and differentiate in the marrow, it has been known that occasionally these cells can travel outside the marrow and circulate through the bloodstream. Scientists have found that by using certain cytokines they can coax the cells into travelling into the peripheral blood stream more rapidly, using this approach a second method for HSC harvesting was derived. The donor is administered the treatment a few days prior to the transplant to allow the cells to move, then during the harvesting the blood is filtered removing all the blood forming cells and filtering the red blood cells back to the donor. This procedure not only has a higher yield of cells with about 5-20% of the cells collected identified as HSCs, but it also shows a lower risk to the transplant recipient with faster engraftment time. The last source of these cells is the umbilical cord, it has low yield of stem cells, which are not enough for adult transplant, but are often enough for a child[18]. Cord blood is also the primary source of hematopoietic stem cells for studies as it is able to be stored in a much more efficient manner.

Although the hematopoietic stem cells are among the longest studied and utilized somatic stem cells, they cannot yet be maintained and expanded in vitro. This is primarily due to an extremely complex and dynamic environment that these cells reside in in vivo – the bone marrow niche. The cells form a network of crosstalk

between the endogenous cellular and molecular components of the bone marrow, which in turn dictate HSCs fate[19].

1.1.2 The Bone Marrow Niche

Hematopoietic stem cell proliferation and differentiation occurs mostly within the bone marrow, where these cells reside in specific areas known as the "stem cell niche". The niches represent a complex intricate interplay of cell- extrinsic factors encompassing not only signals from other cells, such as MSCs, immune cells, bone lining (osteoblasts and osteoclasts) cells, sinusoidal endothelium and perivascular stromal cells, but also various extracellular matrix components[10,12–14,20]. The bone marrow contains two defined distinct niches, each housing a different type of HSC[21]. The first is often referred to as the vascular niche, HSCs located in the perivascular spaces are considered to be highly active cells and exhibit rapid self-renewal and differentiation[7]. These cells, however, are unable to sustain themselves long term, and studies show that when used for transplant these cells are not able to re-establish normal hematopoiesis on their own as their populations die off quickly. These type of cells are referred to as short-term progenitor cells. The second niche is termed the endosteal niche and is defined as a relatively oxygen poor environment compared to the vascular niche. Endosteum is the lining of the inner surface of the bone marrow cavity, lining both cortical and trabecular bone types[10]. The endosteum is occupied by bone cells such as osteoblasts and osteoclasts – progenitor bone-forming and resorbing cells that work in tandem to maintain osteogenesis[22]. The HSCs residing adjacent to the endosteum are quiescent in nature and are considered long-term repopulating hematopoietic stem cells[21].

Although the genetic information that establishes cell behaviour is regulated by intrinsic cues, such as transcriptional regulators, the triggers for activating certain pathways are provided by the cell's environment[23]. The HSCs residing in their specific niches perceive a large variety of signals from their surroundings. These range from cell-cell interactions, signaling molecules, nutrition availability, as well as physical and mechanical cues such as tensile strain, hydrostatic pressure, surface stiffness and elasticity etc[24–29]. Evidently the two niches described above demonstrate the varying constituents contributing to HSC fate. Due to this evident dependency on their microenvironment, HSCs cannot be sustainably expanded in vitro, and they quickly differentiate in culture. Genetic mouse models demonstrated that deletion of even one factor from the niche can result in hematopoietic collapse[30]. This has greatly impeded the efforts to study these cells and effectively transplant HSCs in clinical contexts[18].

Several cell types have been examined for their roles in the bone marrow niches. The osteo-lineage cells have not only been implicated in aiding the quiescent HSCs[14,31], but also play a role in guiding B and T

lymphopoiesis, as regulators of the adaptive immune system[32]. Endothelial cells have been shown to regulate the homeostasis of the HSCs through secretion of specific paracrine growth factors, cytokines and adhesion molecules[33]. Another resident of the bone marrow – adipocytes, have been implicated as negative regulators of hematopoiesis, with studies demonstrating that an adipocyte-rich BM has reduced numbers of HSCs and an impaired cycling capacity[15]. Finally, bone marrow macrophages are indispensable cellular participants required for mobilization and retention of HSCs in the niche. Additionally, they play an indirect role in hematopoiesis by signalling other stromal cells[34].

Regulation of HSC trafficking as well as acute stress response is regulated by the sensory and autonomic innervation of the bone marrow. Signals emanating from the sympathetic nervous system (SNS) suppress osteoblast function and regulate stem cell trafficking[35]. These regulatory pathways are currently being investigated as potential therapeutic modalities to overcome poor HSC mobilization in clinical settings.

The spatial organization of the bone marrow also leads to factors such as nutrition and oxygen availability to function as stem cell mediators in the niche. The bone marrow is a physiologically hypoxic organ and hypoxia has been established as a key mediator of stem cell biology, acting through hypoxia-induced factors (HIF) – a cellular oxygen sensor. In particular cell signaling induced by HIFs maintains HSC quiescence, survival, and metabolic phenotype. The metabolic dormancy resulting from the anaerobic glycolytic energetic metabolism also leads to a low production of endogenous reactive oxygen species (ROS). Low ROS levels are crucial for maintaining genetic stability and self-renewal. As more metabolically active cells the HSC progenitors have higher ROS levels and an increase in ROS levels can induce differentiation and maturation of HSC cells[36].

It is evident that a variety of niche factors contribute to the appropriate stem cell behaviour, however, the proteins of the extracellular matrix provide the structural organization of the anatomically and functionally distinct nodes of the niche[23]. The relationship between the extracellular matrix and the hematopoietic stem cells is crucial for cell survival, adhesion, mobilization, proliferation, lineage specification, differentiation as well as cell death[37]. The extracellular matrix consists of a complex organisation of insoluble proteins that define the structural and mechanical environment within tissues, some of these include fibronectin, collagen, elastin, laminin, hydroxyapatite etc. These proteins create specialized compartments within the bone marrow with localized chemokines and cytokines, resulting in a variety of microenvironments for the cells to grow[21].

1.1.3 The Extracellular Matrix of the Bone Marrow

The ECM is a multifunctional network of molecules which comprises the interstitial elements within tissues and organs for all metazoan organisms[38]. It facilitates architectural support, anchorage for cell adhesion, a reservoir for water, and various growth factors, as well as inductions for intracellular signaling pathways – establishing itself as vital in most biological processes[38]. Studying the cellular response to these various stimuli will aid in understanding the underlying cell mechanisms necessary for normal hematopoiesis as well as aid in establishing appropriate conditions for the cells to survive in vitro.

Both the physical and biochemical characteristics of the ECM modulate cell function, the former being involved in modulation of cell cycle, adhesion, proliferation and migration and the latter function through interaction with cell-surface receptors in a cascade that controls cell fate. The two properties, however, are not independent and function in tandem in order to provide bi-directional communication of the cells with their environment[39].

In mammalian organisms ECM is composed of around 1000 proteins, most of which can be classified into two categories: glycosaminoglycans (GAGs) and fibrous proteins. The former are polysaccharide compounds, which are further classified based on their core disaccharide unit: hyaluronic acid and chondroitin, keratan and heparan sulfates[40]. They function not only as structural scaffolding, but sustain cell hydration and participate in cell signaling, modulating a vast amount of biochemical processes[41]. Fibrous proteins contain polypeptide chains organized in parallel along a single axis, which produce long fibers sheets. They mainly function in structural support, and include proteins like collagens, fibronectin, elastin and laminin, keratin[38]. The proteins of the ECM interact with cells directly through binding a range of cell receptors, such as integrins, syndecans, lectins, discoidin domain receptors[39]. However, they can also influence the cells indirectly this is achieved through sequestering of growth factors and morphogens, creating reservoirs that can be released in response to cellular demands. Additionally, it has been demonstrated that the cells are able to sense and respond to the mechanical properties of the matrix, such as tissue elasticity and stiffness. Discussed below are several members of the extracellular matrix that may play a role in hematopoiesis.

1.1.3.1 Collagen

Collagen (C) is the most abundant protein found in mammalian tissues, and in the bone it comprises approximately 89% of the organic matrix. The protein consists of polymers bound together to form a triple helix of elongated fibers. There are at least 28 different types of collagens in human tissues, which contribute to structural stability of various tissues of an organism, which can be categorized based on

polymeric structures they form: fibrils, beaded filaments, anchoring fibrils, and networks[42]. Type I collagen is the major structural protein in the extracellular compartment of the bone, it's synthesized by osteoblasts and directionally aligned when secreted into the matrix, creating dense lamellar structures[43]. In addition to maintaining tissue architecture, collagen also functions in cell signaling, accomplished by binding of the repetitive amino acid sequences present on the fibers by cell receptors. These signaling events are able to dictate differential cell signaling mechanisms, spanning from cell survival and differentiation to cell adhesion and paracrine signals induction[39].

In BM, collagen type I is mainly expressed by osteoblasts, but also by bone marrow stromal cells, like MSCs[44]. HSCs isolated from cord blood have been shown to express the integrin receptor, CD44, specific for type I collagen and this expression increases during in vitro cultures. Culturing of these stem cells on surfaces coated with type I collagen results in diminished proliferation and altered differentiation, leading researchers to believe that it plays a role in maintaining cell quiescence in the endosteal niche[45]. Additionally, the protein has been described as an adhesive ligand for myeloid and erythroid progenitor cells, suggesting a function in mediating adhesion and localization of the committed progenitor cells within the BM[46].

1.1.3.2 Fibronectin

Fibronectin is another representative of fibrillar proteins, although in the body it exists in two forms, as a soluble molecule in the blood plasma and in an insoluble form deposited in the ECM. The latter is secreted by cells in a soluble form and further modified and assembled into an insoluble matrix in a cell-mediated process. It's composed of a protein dimer, consisting of two monomers linked via a disulfide bridge. Several fibronectin isoforms have been identified; however, all arise as a product of alternative splicing of a single gene[47].

Due to a vital role of fibronectin in the body where knockout of fibronectin is lethal during embryonal development, studies evaluating its specific role in the hematopoietic system are difficult[48]. In vitro studies were able to demonstrate that in hematopoiesis fibronectin plays a major role in stem cell trafficking and homing of both normal and malignant cells by acting on various receptors. Additionally, the protein provides adhesion and enhances proliferation of some primitive hematopoietic progenitor cells[49]. It has been demonstrated that myeloid progenitors neither adhere nor respond to fibronectin molecules, in contrast to erythroid progenitors, differentiation of which is highly dependent on presence of fibronectin. This suggests a loss of sensitivity, which may be part of the myeloid progenitor developments[50].

1.1.3.3 Laminin

Another integral component of the structural scaffolding of ECM are laminins, a large glycoprotein, secreted and incorporated into cell-associated matrices. Laminins are composed of as α-β-γ heterotrimers, with genetic variants of five α chains, three β and three γ chains that have been characterized thus far for a total of 15 combinations. The α chains of the laminin molecule have been implicated in binding of cellular surface receptors and thus characterized as responsible for the biological function of laminins[51].

Laminins are considered a major component of basement membranes, where they bind several other proteins to create a cross-linked network, in the bone marrow laminin is associated with the perivascular niches where it is present in the basement membrane of sinusoids and larger blood vessels. Studies conducted in vitro have shown that laminin α4 and α5 favor HSCs adhesion in the BM. Knockout of α4 laminin in mice results in impairment of HSC circulation and promotion of cell quiescence. Additionally, although cycling of progenitor cells is reduced, differentiation of HSCs does not appear to be impacted by absence of laminin[52]. Therefore, in hematopoiesis laminin functions in supporting the active HSCs residing in the endosteal niche as well as stem cell and progenitor circulation and homing.

1.1.3.4 Elastin

The final constituent of the fibrous protein group discussed here is elastin (E). It is a primary component of elastic fibers and mainly found in ligaments and vascular walls to accommodate tissue elasticity. Elastin is secreted from cells in a soluble monomeric form – tropo-elastin, and upon entering the extracellular space it is cross-linked into insoluble fibers, which are highly resilient and resistant to deformation[53].

Data on the role of elastin in hematopoiesis is scarce as it is not considered to be a major constituent of the bone marrow. Although elastin fibers are found in bone, their location is limited to the outer fibrous layer of the periosteum, not the inner cellular layer. Activated lymphocytes express the elastin receptors with varied frequency, indicating a role of the protein in immunopathological processes[54]. Additionally, a study conducted by Helbig et al demonstrated an association between elastin metabolism and prognosis of hematopoietic recovery after bone marrow transplantation, highlighting a potential role of the protein in hematopoiesis[55].

1.1.3.5 Hyaluronic Acid

Hyaluronic acid has the simplest structure of all GAGs, consisting of sequentially bound glucuronic acid and *N*-acetylglucosamine residues. The highly polar structure of the polysaccharide allows it to attract water molecules and facilitates its function in tissue regeneration, however it has also been implicated in

angiogenesis control[56]. Hyaluronic acid also provides compression strength to the ECM and in different tissues has been implicated in biological functions such as cell adhesion and aiding in control of cell proliferation and differentiation[57–59]. Additionally, it's been found that the biological function of hyaluronic acid is strongly related to its molecular weight (MW): low MW polysaccharide (>700 kDa) induces angiogenesis, while high MW fragments inhibit it[60,61].

In the bone marrow hyaluronic acid functions in HSC motility, it can bind to several receptors as well as growth factors of the niche. Human and murine HSCs not only express cell surface receptors for hyaluronic acid but have been shown to secrete the compound as well, although progenitor cells do not maintain this expression[62]. Overall, hyaluronic acid binding by HSCs is linked to the proliferative state of the cell and differentiation to progenitors, depletion of polysaccharides in the niche leads to reduced support of hematopoiesis by the matrix[62,63]. In hematopoietic progenitors, hyaluronic acid binding appears to be induced during cell cycle, providing a direct signal of proliferation to the cells and in vitro studies have shown that exogenous HA directly promoted the proliferation of HSC progenitor cells[64,65]. Additionally, the two major receptors for hyaluronic acid found on progenitor cells: CD44 and receptor for hyaluronan mediated motility (RHAMM), have been described as an anchoring molecule and motility mediator respectively. The two receptors function in tandem to facilitate mobilization of HSC progenitor cells into the circulation[64–66]. Overall, the amount of hyaluronic acid in the bone marrow niche is tightly regulated as lack or excess of the polysaccharide can lead to adverse effects and hematological malignancies[67].

1.1.3.6 Mineral ECM Component

Hydroxyapatite (HA) is the main inorganic constituent of hard tissues, such as bone and dentine and is comprised primarily of calcium and phosphate. In bone it accounts for almost 70% of the bone mass and forms a crystal lattice providing structural support. Formation of the mineral network is controlled by osteo-lineage cells and other ECM components, where collagen serves as a template for deposition of mineral, followed by maturation of crystal to form stable bone mineral[68,69]. Although it has not been demonstrated whether the mineral component of the bone directly interacts with HSC cells, it is modulated in response to cellular demands. Additionally, it provides the physical cues, such as tissue stiffness and topography which HSC cells are capable of sensing[29,70–72]. It has been demonstrated that hydroxyapatite can alter gene expression profiles of MSCs and influence osteoblast lineage commitment, however the mechanisms underlying this behavior remain to be elucidated[73–75].

1.1.3.7 Physical Cues of the ECM

The mechanical environment of the cell has only recently been recognized as a key driver of cellular growth, development and in some cases, disease progression. However, manipulating the local microenvironment of cells in vivo is challenging, thus the majority of studies on cell response to biophysical cues largely depends on successful cultivation of three dimensional (3D) in vitro cultures. Further complicating these investigations is the heterogeneity of bone, throughout the bone marrow the physical properties of the ECM are not homogenous and differ between different regions, additionally it is possible that ageing might also lead to alterations of these mechanical properties of the niche.

Thus far evidence has been accumulated that HSCs are able to respond to a variety of biophysical cues. First the presentation of ligand patterns, with parameters such as the lateral distance between ECM protein surface ligands influences HSC and progenitor cell adhesion and subsequent cell signaling[76]. Additionally, under unfavorable conditions, when ligands required for HSC adhesion are absent or spread out too far from each other, the cells are able to modify their environment and actively participate in the formation and regulation of the niche[77]. The topography of the matrix surface is another parameter that is sensed by the cells. In a study conducted on electrospun nanofibers, HSCs responded differently to a different topographical feature, with synergistic influence on cell adhesion, proliferation and phenotype maintenance[71]. The 3D architecture of the matrix has also been shown to affect cell behaviour, achieved in part due to effects of local accumulation and depletion of diffusible components of the niche[78]. Biomechanical forces such as shear stress and hydrostatic pressure have also been identified as regulators of cell behaviour, where increase in shear stress has been shown to increase hematopoietic colony-forming potential[79,80]. Finally, it has been demonstrated that HSCs react to substrate stiffness, by increasing cell adhesion and migration, facilitating the egress of HSCs from their niche[72,81,82]. The spreading of HSC progenitor cells, characterized by increase in cell size and decrease in circularity, increased with substrate stiffness[72]. Additionally, it was demonstrated that when plated on soft substrate bone-marrow derived MSCs become quiescent and are reactivated when introduced to stiffer substrate, which may elicit an indirect effect of HSC fate[83]. Stiffness of bone ECM generally increases with increasing collagen type I concentration, whereas increased concentrations of collagen type III in collagen type I structures leads to increased matrix elasticity[84,85].

The mechanisms that facilitate mechano-transduction in HSCs are still largely unexplored. The environmental cues are translated into biological responses via cellular receptors, such as integrins, which not only connect the cells to the ECM, but often connect internally to the elements of the cytoskeleton and

may also elicit intracellular signaling. This results in generation of internal forces inside the cell that counteract the extrinsic forces, facilitating a direct mechanical crosstalk of the cell with its environment[86,87].

1.1.3.8 ECM Cell Receptors

The ECM is a dynamic environment, which is constantly remodelled through deposition, modification, and degradation of its components in response to tissue demands[38]. These effects are mediated by a large diversity of cell receptors, known as cell adhesion molecules, which function in facilitating both cell-matrix and cell-cell interactions and allow the cells to respond to environmental cues intrinsically.

The primary cell receptors mediating signal transduction from ECM are the transmembrane integrin receptors, a non-covalently linked heterodimer composed of an α- and a β-subunit. They generally possess a single transmembrane domain and a short cytoplasmic chain and bind ECM components such as fibronectin, collagen, and laminin. For example, the α4β1 and α5β1 integrins are both involved in fibronectin adhesion and have been shown to play a role in HSC survival and self-renewal[88,89]. Numerous studies have demonstrated the importance of integrins in hematopoiesis and HSCs express a variety of integrins on their surface, with some integrins being recognised as markers of cell fate[90,91]. For example, the β3 subunit has been correlated with quiescent HSC properties[92]. There is also a variety of other cell adhesion molecules that facilitate cell-ECM interactions. Transmembrane discoidin domain receptors are tyrosine kinase proteins, which are capable of binding several types of collagens[93]. Dystroglycan is a laminin receptor highly expressed on human CD34 HSCs, however the knowledge of the effect of this interaction on hematopoiesis is still rudimentary[94]. Syndecans are a family of transmembrane proteoglycans, which have demonstrated affinity for fibronectin, collagen and several growth factors, this allows for colocalization of ECM molecules and growth factors on the cell surface deifying a unique characteristic of the receptor. Finally, glycoprotein I (CD44) – a major hyaluronic acid receptor, which also has a propensity for fibronectins, laminin and collagen type I and IV[95]. This receptor is involved in several cellular processes and in HSCs it can directly contribute to cell homing, quiescence and cell survival through inhibition of apoptosis. Additionally, CD44 can also trigger hyaluronan metabolism within the cells demonstrating direct involvement in matrix remodelling[65,96].

1.2 Hematopoietic Malignancies

1.2.1 Acute Myeloid Leukemia

Malignancies of the immune system are termed hematopoietic cancers or leukemias and are considered "liquid tumors"[97]. They affect the blood, bone marrow, lymph and lymphatic system, and the immune

system since these tissues are intimately connected through the circulatory system[98]. The cancer is derived from either a hematopoietic precursor in the bone marrow or one of the matured hematopoietic cells in the circulation. Leukemias are generally classified into subtypes, defined by the lineage of the cell – lymphoid or myeloid, and by onset – acute or chronic[97]. Lymphoid lineage is responsible for producing B, T, NK and plasma cells and the myeloid lineage generates erythrocytes, thrombocytes, mast cells and cells of the myeloblast lineage: granulocytes macrophages[99]. Lymphomas, lymphocytic cancers, and myelomas (cancer of plasma cells) are all derived from cells of the lymphoid lineage and acute and chronic myelogenous leukemias and myeloproliferative diseases are myeloid in origin[97,98,100].

Acute Myeloid Leukemia (AML) is a heterogeneous hematopoietic malignancy characterized by an irregular expansion of undifferentiated myeloid blasts. It is considered to be the most common acute leukemia in adults and incidence rate increases with age[101]. Although advances in the treatment of AML have led to improved outcomes for younger patients, the prognosis remains poor in the elderly, with approximately 70% mortality in patients over 65 years[101]. Clinical manifestations of this disease reflect alterations to the cells of the hematopoietic myeloid lineage, such as erythrocytes, platelets, myeloblasts, and granulocytes, resulting in poorly differentiated myeloid cells[102]. High levels of self-renewal and stalled differentiation causes expulsion of the normal hematopoietic system and loss of function[103]. Patients generally present with signs of bone marrow failure, such as anemia, thrombocytopenia, and leukocytosis. In majority of cases AML presents as a de novo malignancy in previously healthy individuals, however it can arise in patients with underlying hematological disorders or as a consequence of other therapy[97,104]. Current treatment involved induction chemotherapy of eligible patients, after which minimal residual disease often persists and must be followed by consolidation therapy in order to minimize chances of relapse. However, these treatment options lead to treatment-related toxicities and favorable response in elderly patients is poor[101]. Therefore, development of new treatments would result in incremental gains in long-term survival and remission.

1.1.1 Leukemia Stem Cell

Recent studies suggest that AML is a hierarchical disease based on a small subset of leukemia initiating cells, this would imply the existence of a stem-like leukemia cells that possess long-term repopulating potential. AML is characterized by the accumulation of vast numbers of abnormal cells that fail to differentiate into functional granulocytes or monocytes[105]. AML leukemia stem cells (LSCs) are homologous to normal HSCs in many ways, including a $CD34^{+}CD38^{-}$ phenotype, however, they demonstrate enhanced self-renewal and divergent expression of cell surface markers[106]. The leukemic blasts have limited proliferative capacity, suggesting that a small subpopulation of leukemic stem cells that

possess extensive proliferative capacity and the potential for self-renewal must maintain the leukemia[105]. AML was the first malignancy where a population of distinct cancer stem cells (CSCs) was identified and has since been adopted as a model study of CSCs[107]. Clonal expansion is considered the first step in leukemogenesis, which occurs through acquisition of founder mutations leading to a formation of a preleukemic stem cells[108]. Subsequent acquisition of progressor mutations generates AML stem cells capable of self-renewal and thereby disease development[109,110]. Normal HSCs exhibit self-renewal properties, that disappear as the cells commit to myeloid development, giving rise to committed progenitor cells that no longer possess long-term self-renewing properties, but maintain multipotency[99]. One theory has proposed the presence of long-term and short-term LSCs, similarly to normal hematopoietic stem cells[107]. In some cases leukemia stem cells have been shown to possess an immunophenotype more consistent with committed myeloid cells, where a mature cell exhibits an ectopic re-activation of genes associated with self-renewal[111]. However, it is unknown whether these cells are capable of recapitulating leukemia populations long-term[105]. In other cases, however, a multipotent stem cell seemed to be involved and the heterogeneity was found to have resulted from the variable ability of the primitive leukemic stem cells to differentiate or to acquire lineage markers[105,112].

Eradication of the leukemia stem cells is a critical part of any successful anti-cancer therapy. Similarly to the endosteal niche-residing HSCs, some LSCs remain quiescent, which offers an insight into why conventional therapies, targeting DNA replication, may be effective at reducing tumor burden through destruction of AML blasts, but are not curative, as they are unable to target the quiescent cells, leading to high degree of relapse in AML patients[113]. Current therapies do not offer a targeted treatment approach, given the similarity between the healthy HSCs and LSCs and lack of studies on the variation of the two cells, leads to destruction of the healthy hematopoietic system during treatment[10,97,104]. Similarly to the hematopoietic stem cells, the leukemia stem cells are difficult to investigate in vitro and assessment of phenotypic differences between the two cells is challenging[108,110]. Samples obtained from patients investigated in vitro differentiate rapidly, causing the cells to lose their self-renewing potential and alter the phenotype of interest[105]. Just as in the case of healthy HSCs this rapid differentiation is attributed to the lack of environmental cues the cells rely on for maintenance[7,10]. LSCs transplanted into mice have demonstrated an ability to home to the epiphyseal osteoblastic surface of the endosteum prior to their dispersion to the perivascular niches[114]. The LSCs tend to occupy the same spaces in the endosteal and sinusoidal niches of the HSCs in the bone marrow, however they are able to outcompete the healthy cells and hijack the bone marrow microenvironment in order to promote tumor growth[10,17].

1.1.2 Cancer-Driven Alterations of The Bone Marrow Niche

Current findings report that the myeloid malignancies modify the HSC niche into a leukemia niche, where the altered components cooperate with the leukemia cell to promote its proliferation and are detrimental to normal HSC function[115,116]. Several niche parameters demonstrate significant changes associated with the disease and have been closely correlated with an LSC niche, where the microenvironment is able to accelerate development and provide chemoresistance to AML cells[117,118].

1.1.2.1 Cell Components

Mesenchymal stem cells of the bone marrow have been shown to exhibit alterations in the expression of cell adhesion molecules and cytokines in a malignant cell niche[119]. These alterations turn the BM environment hostile toward healthy HSCs and supportive of leukemic cells, contributing to therapy resistance and disease evolution[119]. Previous studies have demonstrated how presence of mesenchymal stem cells in a co-culture with LSCs can increase long-term proliferation of primary AML cells in a largely quiescent state[120]. This enhancement is achieved through cytokine-mediated crosstalk as well as direct cell-cell contact[110]. AML-derived bone marrow MSCs are considered functionally distinct from healthy HSC-derived MSCs and provide the cells protection against chemotherapy[121].

1.1.2.2 Angiogenesis

Over the course of AML, an overall increase in the bone marrow vasculature can be observed, as the malignancy drives vascular remodelling[7,122]. The changes occur as a result of accumulation of local pro-inflammatory and anti-angiogenic cytokines produced by the endosteal AML cells[7]. Vascular endothelial growth factor (VEGF) and angiopoietin are considered the most influential angiogenic cytokines that are secreted by several types of leukemic as well as stromal cells. AML-secreted VEGF activates the appropriate receptors expressed on endothelial cells as well as AML cells[123]. Binding to endothelial cells stimulates growth factors which promote angiogenesis[123,124], while in AML cells VEGF participates in a cascade that protects the cells from apoptosis[125]. Some studies also indicated that the malignancy alters not only the vascular density, but also enhances vascular permeability[126]. Alterations in angiopoietin expressions result in vessel destabilization and facilitate vascular leakiness[127]. These alterations to the vasculature of the niche can function as prognostic markers, as VEGF up-regulation in AML blasts has been closely associated with increased failure of complete remission and low overall survival[128].

1.1.2.3 Soluble Mediators

A wide range of soluble mediators released by both the primary AML cells and the non-leukemic stromal cells can promote leukemogenesis[110]. Expression of CXCR4 is universal across both HSCs and LSC cells of AML, however internal expression of the molecule is upregulated in AML even in cells that do not express surface CXCR4[129]. Pathways regulated by this molecule play a crucial role in survivability and proliferation of leukemia stem cells and inhibition has demonstrated significant impairment of AML proliferation in vitro[130,131]. It has also been demonstrated that CXCR4 plays a role in migration and homing of the cancer stem cells and its activation is more closely associated with the leukemia stem cells rather than other mature AML cells. Hence targeting this pathway, in the form of CXCR4 inhibition, may overcome the observed resistance to chemotherapy by AML[132]. Another molecule that has been implicated in drug-resistance of AML is very late antigen 4 (VLA-4) – an integrin dimer, which functions in cell adhesion with primary ligands including fibronectin and VCAM-1[133]. In normal HSCs VLA-4 plays a critical role in localization and circulation of progenitor cells[134]. VLA-4 mediates anti-apoptotic signals through binding with stromal cells, providing a microenvironment-mediated chemotherapy resistance[134]. Gaining insight into how these normal adhesion molecules interplay with the malignant niche to affect leukemogenesis will aid researchers in developing innovative therapeutic interventions.

1.1.2.4 Adipogenesis

Another mechanism observed in AML remodelling of the bone marrow is suppression of adipogenesis in favor of AM-supportive osteo-lineage differentiation of MSCs[135]. Adipocytes located in spaces of haematopoietically active myeloid lineage cells provide important support to regenerating blood populations[136]. Early on in the development of AML the disease causes an interruption of adipogenesis leading to compromised myelo-erythroid maturation[137]. Hence, targeting the bone marrow adipose tissue could be utilized as a potential strategy to arrest leukemia progression[118]. The uncontrolled expansion of AML cells in the limited bone marrow cavity causes shrinkage of the available adipocyte living space, inducing a series of adipocyte remodeling events like morphological and metabolic changes[136]. The bone marrow microenvironment in induced into a lipolytic state under the impact of AML, enabling transfer of fatty acids from adipocytes to the leukemic blasts, maintaining cancer nutrient supply[118,136].

1.1.2.5 Sympathetic nervous system

Sympathetic neuropathy accelerated the progression of AML by reducing the density of the sympathetic nervous system bone marrow nerve network leading to depletion of niche cells that maintain healthy HSCs and expand leukemia-supportive mesenchymal progenitors[122].

1.1.2.6 Hypoxia and ROS

Although no detectable difference of hypoxic levels has been reported between healthy and leukemic bone marrow, the leukemic cells are capable of enhanced adaptation to hypoxic conditions[118]. Although the oxidation state of the two cell types is consistent, the metabolic strategies differ[36]. LSCs demonstrate a greater dependency on oxidative respiration and are more sensitive to oxidative stress than normal HSCs which can effectively achieve normal homeostasis with glycolysis[36,118]. This leads to increased expression of reactive oxygen species (ROS) and superoxide production[138]. This increase is attributable to constitutive activation of nicotinamide adenine dinucleotide phosphate oxidases (NOX)[138]. ROS may function in leukemogenesis in several ways. First, they promote oxidative DNA damage and the resulting mutagenesis aids in disease progression[139]. Additionally, it plays a role in suppressing antileukemic immune responses, protecting the blast from the body's defense system[140]. Finally, it has also been demonstrated that ROS overproduction in AML can act to promote proliferation of leukemic blasts conferring a competitive advantage over healthy HSCs[138].

1.1.2.7 Extracellular Matrix

The extracellular matrix, comprising of the interstitial elements, providing structural support to the niche, has not been extensively investigated as a contributor to AML development. However, studies have shown that a large number of ECM genes in AML cells as well as in the AML-supporting MSCs, were differentially expressed[141]. Recently researchers were able to identify a common mechanism of ECM gene regulation in AML and define a prognostic value based on ECM protein composition in patients[141,142]. However, the direct impact of matrix composition on cancer initiation, progression and treatment resistance has not been previously investigated.

The ability of LSCs and AML cells to interact with the ECM is a detrimental feature, which has been shown to not only facilitate disease development, but also foster resistance to therapy and survival of minimal clones, causing a large relapse rate[142]. Normal signal transduction of the bone marrow is disrupted and favors LSCs quiescence, autophagy or decreased apoptosis, thereby impairing drug sensitivity [143–146]. Due to these complex interactions of the cancer cells with its environment, research is now shifting towards understanding the underlying mechanisms of the niche, which will not only allow for the development of more effective culture systems in order to study these cells, but also provide new targets for drug therapies[147,148].

1.1.2.7.1 Collagen

As the major component of the ECM, collagens undergo tremendous modifications during cancer development, resulting in a fundamental influence on the fate of cancer cells as well as neighbouring cells[38]. Studies have reported that several collagen types are overexpressed by cancer cells. Presence of collagen type I promotes expression of stem-like phenotype in colorectal cancers[149] and maintains and propagates glioblastoma cells in adherent cultures[150]. Collagen type III is highly expressed in ovarian cancers and may provide a potential mechanism of drug resistance[151]. Head and neck cancer cells grown in cultures coated with collagen type IV demonstrate an increased growth rate and maintain stem-like traits[152]. Expression of collagen type XI promotes chemoresistance in ovarian cancer and is associated with poor clinical outcomes[153,154]. Collagen type XVII expression in lung cancers is required for cell metastasis capacity and has been an indicator of poor prognosis, especially when laminin 322 overexpression was also reported. Blockage of collagen XVII pathway reduced metastasis potential in vitro, thereby highlighting this pathway as a novel therapeutic target for lung cancer treatment[155].

In leukemia association of collagen type I with its integrin receptor α2β1 has demonstrated a significant effect on drug resistance, where doxorubicin induced DNA damage was minimized in acute T-cell lymphoblastic and myeloid leukemic cells[156,157]. This was achieved through a combination of efflux of the chemotherapeutic enhanced by the α2β1 integrin as well as collagen induced inhibition of cell death induction[156]. High levels of α2β1 expression on AML cells were related to worse overall patient survival and targeting this pathway alongside doxorubicin treatment may improve relapse rate by preventing emergence of drug-resistant leukemia cells[156]. Collagen type IV has also exhibited remodelling in the BM niche throughout AML development, as demonstrated from analysis of bone marrow samples from patients[158]. Its associated receptor - Discoidin Domain Receptor Tyrosine Kinase 1 is implicated in modulation of cell motility. In vitro experiments demonstrated that exposure of AML cells to collagen IV significantly increased cell migration and adhesion.

1.1.2.7.2 Fibronectin

The role of fibronectin in cancer is controversial. On one hand it has played a tumor-suppressive role to halt early cancer progression, but on the other hand fibronectin is associated with provoking tumor metastasis in late stages of cancer and is associated with poor prognosis[159]. Fibronectin appears capable of directly stimulating cell proliferation, demonstrated in vitro supplementation of cell lines with fibronectin doubles cell proliferation rate[160]. Additional roles of fibronectin in tumor angiogenesis have also been

characterized, where fibronectin is implicated in forming tumor vessels, providing the framework for vessel maturation[161,162].

Specifically in AML, fibronectin has been shown to increase cancer stem cell self-renewal and drug resistance[163,164]. Adhesion to fibronectin increased the proliferation rate of AML cells with accelerated S-phase entry, however in normal CD34 cells proliferation was decreased as a result of fibronectin adhesion, suggesting that adhesion-mediated signaling of fibronectin is altered during leukemogenesis[163].

An elevated expression of an integrin associated with fibronectin binding (α4β1 or VLA-4) has been associated with reduced chemosensitivity of cells facilitated by the interaction with fibronectin. And has been reported as a prognosis marker in poor induction of remission[133]. An in vitro study in a 3D culture model coated with fibronectin displayed elevated adhesion of AML cell phenotype as well as high adhesion-mediated resistance to chemotherapeutic drugs[165].

1.1.2.7.3 Laminin

This class of adhesive glycoproteins, constitute a major structural part of basement membranes, and various forms of laminin have been implicated in supporting cancer stem cell self-renewal. In breast cancer laminin 511 through its interaction with α6β1 can induce expression of several stemness transcription factors, demonstrating a role in supporting breast cancer stemness[166]. Laminin 332 has been shown to maintain cancer stem cells characteristics in several epithelial cancer types. In normal tissues this form of laminin promotes epithelial cell polarity, but during cancer the protein favors migration and tumorigenesis[167]. In lung cancer over-expression of laminin 332 along with collagen XVII is associated with poor prognosis[155]. Although laminin 332 is not detected in normal liver, an integrin receptor associated with the protein demonstrated increased expression in hepatocellular carcinomas and in vitro cultures supplemented with laminin 332 induce an enhanced resistance to chemotherapy[168,169].

In AML laminin binding receptors have been implicated in cancer prognosis. Laminin α4 – a receptor binding several laminin types is altered in the bone marrow niche presenting with AML. Mice deficient in the protein expression exhibited drastic alteration of the niche, including upregulation of inflammatory cytokines that favor AML growth. As a result of laminin α4 deficiency AML progression and relapse were accelerated[170]. Another laminin adhesion molecule integrin α7 demonstrates increased expression in AML, its binding to laminin 211 stimulates the ERK signaling cascade signalling implicating this ECM association with formation of extramedullary disease[171]. Finally, a nonintegrin laminin receptor 67LR has been associated specifically with AML cancers and its expression was not present in normal HSCs,

lymphocytic leukemias or chronic myeloid leukemia. Increased expression of 67LR in AML patients has been associated with poor prognosis[172].

1.1.2.7.4 Elastin

Soluble elastin and elastin degradation products have been shown to induce motility signals in cancel cells. Expression of two major elastin binding proteins by a tumor is associated with an invasive potential in several types of cancer[173–175]. Certain cancers, such as breast and gastric, exhibit an elastic tumor phenotype, which has been attributed to an induced elastin synthesis by the tumor cells[173]. Additionally, elastin has been shown to exhibit chemotactic properties for tumor cells, signifying its role in cancer metastasis[176,177].

Data on the role of elastin in hematopoietic malignancies, and specifically AML, is sparse. However, the protein has been implicated in immunological processes occurring after HSC transplantation as part of treatment of hematopoietic malignancies[178]. Elastase, an elastin degradation enzyme, activity varies with leukemia subtype, where chronic myeloid leukemia patients exhibited the highest elastase activity, followed by AML and lymphocytic leukemias[178]. As a consequence of elastase activity endothelial cell inflammation can sometimes be observed, which causes an inflammatory response by the immune cells, potentially leading to inflammation, which can often protect cancers from drug therapy.

1.1.2.7.5 Hyaluronic Acid

Hyaluronic acid associated receptor proteins have been implicated in cancer progression and treatment resistance for quite some time. Hyaluronic acid in tumors is produced by both the tumor cells and associated stroma cells. Binding of the polysaccharide to its associated CD44 receptor activates various pathways inside the cells that promote cancer cell survival, stemness and induce motility and invasion through remodelling of cytoskeletal constituents inside the cell[66,179]. Overexpression of CD44 is widely reported in many types of cancers[38] and the interaction of CD44 with hyaluronic acid has been shown to promote chemoresistance in breast, ovarian and head and neck cancers[179–182]. Efforts are already underway to utilize the hyaluronic acid – CD44 signaling pathway as a target in cancer therapy[183].

Expression of CD44 in AML cells is associated with an aggressive cancer phenotype and resistance to chemotherapy[96]. In parallel to CD44 upregulation AML cells also upregulate genes directly[184] and indirectly[95] associated with CD44 signaling, driving matrix modifications to establish an ECM-CD44 network[141]. It has been demonstrated that CD44 is required for maintenance of AML LSCs, as the cells were effectively eradicated in vivo by manipulation of CD44 specific antibody which blocked homing of

leukemia cells to the bone marrow, however this effect did not extend to normal HSCs, demonstrating a therapeutic targeting potential of this adhesion molecule in AML[106].

1.1.2.7.6 Hydroxyapatite

The mineral component of bone has not been extensively investigated for contribution to cancer progression. One study indicated a potential of hydroxyapatite to selectively target cancer cells, where HA has a much greater inhibitory effect on cancer cell proliferation and extended longevity of animals with tumors. This was achieved through direct blocking of protein synthesis and cell cycle arrest[185]. In breast cancer presence of hydroxyapatite exhibited direct influence on gene expression patterns of cancer cells, promoting tumor adhesion and growth and promoting a migratory axis of signaling[186]. Increased production of bone degradation molecules was also notes as a response to HA interaction, demonstrating a propensity to metastasize into bone. This effect was also observed to be dependent on the physical properties of hydroxyapatite with larger crystalline particles enhanced bone degradation protein production, whereas a smaller less crystalline form of mineral induced cell adhesion and growth[186]. Cytotoxic effect of hydroxyapatite was also investigated in hepatocytes, where hydroxyapatite nanoparticles induced decreased cell viability and even cytotoxicity at higher concentrations[187].

Although studies of hydroxyapatite effect on AML development have not been conducted, close association of AML with the mineral component of the bone marrow niche as well as increasing utilization of HA in fabrication of scaffolds for investigation of hematopoiesis, warrants in depth investigations of HA-AML interaction.

1.1.2.7.7 Biophysical Cues

Cancer cells are thought to actively participate in ECM remodelling, compared to their non-malignant counterparts achieved through upregulated expression of matrix metalloproteases. This reorganization can induce formation of reservoirs for factors facilitating sustained malignant transformations, while limiting availability of these molecules for normal cell development. For example, in myeloma patients acute bone lesions as a result of extreme matrix remodelling by the cancer cells is reported [188].

Mechanical properties such as ECM rigidity, topography and porosity have all been implicated as contributors to tumor development. In solid tumors, stiffening of the ECM is related to poor clinical outcomes due to its association with increased tumor growth and metastatic rate[189]. The stiffening effect is facilitated by accumulation of collagen and fibronectin in tumor periphery and hyaluronic acid in central parts counteracts the compressive stress exerted by the peripheral layer[190,191]. ECM stiffening is a key

biological process for cancer development as it can induce uncontrolled proliferation, increased motility, metastasis formation, angiogenesis, and even drug resistance. Leukemias do not exhibit formation of solid tumors and only form temporary connection with ECM in specific niches of the bone marrow and lymphoid organs, with the exception of LSCs, which are believed to permanently reside in the BM niche. These cells do exhibit a distinct niche compared to healthy HSCs and certain bone marrow ECM signatures have been associated with AML outcomes[142].

The ECM also provides a physiologic resistance of cancer cells to treatment[192]. Matrix stiffness is obstructive for effective drug reuptake and collagen has been shown to bind certain chemotherapeutics preventing their diffusion into the target cells. In vitro mechanistic study of variation in matrix stiffness revealed that cells exhibited distinct growth patterns and drug sensitivity in response to the physical cues from their environment[192]. This underscores the importance of further understanding the interaction of cancer with its environment and addresses a potential new avenue of addressing drug resistance in cancers through modulation of ECM.

1.2 Niche mimicry approaches

The study of hematopoietic stem cells has so far been limited to in vivo studies or simplistic 2D cultures which fail to mimic the complex environment provided by the extracellular matrix and essential for stem cell survival. Studies are beginning to explore three-dimensional biomaterial platforms that would be able to not only provide the structural support for these cells, but also the extrinsic cues from the environment as well as the cell-cell interactions which are present in vivo, therefore capturing the physiological conditions of the native niches[193]

In traditional cultures HSCs and primary AML cells rapidly differentiate (hours to days) and undergo apoptosis, which researchers have hypothesized occurs due to the lack of the extrinsic cues involved in cell fate that is provided by the various components of the bone marrow niche[34,192,194]. Studies showed that varying level of topography, elasticity and lateral spacing causes different responses from the hematopoietic stem cells, for example it has been demonstrated that changes in the stiffness of the extracellular matrix causes cells to commit to certain lineages when differentiating[190]. These physiological conditions need to be considered when developing a three-dimensional culture system. Another important factor is the cell-cell interactions, the stem cells need to be co-seeded with those cells occurring in their natural niche. Once a scaffold is built where the biophysical cues are controlled and the cell-cell interactions are present the stromal cells will begin to produce the biochemical cues and signals for cell survival, creating a fully functional in vitro study mechanism. This system could then be used not only to expand the cell populations

in order to grow and study these cells, but researchers would also be able to investigate the niche mechanisms that are in play as well as develop disease models and drug screening platforms.

Tissue-engineering strategies developing scaffolds must take into consideration several basic elements: biocompatibility, biodegradability, biomechanical properties, scaffold architecture and manufacturing technology[193]. Biocompatibility ensures that the components chosen for the scaffold are not cytotoxic. Additionally, in scaffolds which are transplanted into living tissues consideration must be taken in regard to the immune response elicited by the construct, as a severe inflammatory response to the components of the scaffold may cause rejection and further tissue damage[195]. Scaffolds must demonstrate biodegradability in order to allow infiltrating cells to produce their own ECM, replacing the scaffold tissues. The by-products of this degradation must also not exhibit any cytotoxic effects in the tissue and have the capability to safely exit the tissue[194]. Mechanical properties of the engineered scaffolds must be consistent with the anatomical site they are capturing, this includes not only the material strength, but stiffness, elasticity and permeability[190–192]. The architecture of the scaffold itself is of critical importance as it should represent an interconnected pore structure and high porosity to model the natural tissue and facilitate cell infiltration and adequate nutrient diffusion within the constructs[196–198]. Finally, in order for these models to be clinically an commercially applicable they must be reproducible, cost-efficient and allow for scaled manufacturing.

Currently a few different platforms are being explored for establishing in vitro cultures of HSCs, some of which are summarized below. However, a consensus on an optimal scaffold material or manufacturing technique has yet to be established. An optimized *in vitro* culture system of the bone marrow niche will permit researchers to study the mechanisms of hematopoiesis in a relevant environment. Understanding the pathways leading to cell proliferation, differentiation, apoptosis, and matrix remodelling will lead to extensive clinical applications in health and disease. This will establish a platform for drug screening for new therapeutic discoveries in treatment of hematological malignancies. Moreover, it will provide a foundation for the development of screening platforms aimed at personalized therapy.

1.2.1 Animal Models

Murine models are considered best-characterized animal models of the BM niche and remain as standard for hematopoietic studies. Although these models have advanced our understanding of the hematopoietic system and AML, they demonstrate limited predictivity in the human hematopoietic system due to species-related differences[199]. Additionally, they demand extensive animal facilities and expertise for use and are often considered unsuitable for drug discovery studies as they provide limited mechanistic insight, exhibit inconsistency in disease onset, low penetrance and overall poor response to therapy. Regarding

investigations of drug treatments for hematopoietic malignancies, murine models are generally less sensitive to many cytotoxic compounds. Co-existence on non-malignant mouse cells with the leukemic cells invoke complex tumor-host interactions which can have an adverse effect on drug resistance, self-tolerance, angiogenesis, tumor growth, and response to therapy[199]. Finally animal models are unsuitable for high-throughput drug screening applications.

1.2.2 Suspension Culture

The easiest models employ ECM molecules as a coating for surfaces or a supplementary solute[17]. The harvested cells are placed into medium, that is supplemented with a cocktail of growth factors, cytokines and ECM components, and cultured[134]. Although these are able to enhance stem cell cultures in comparison to traditional suspension cultures, they fail to consider the spatial presentation of the molecules, which leads to inefficient cell stimulation and lack of translational value[17]. Additionally, these cultures are often unable to sustain stem cell cultures long-term and alter symmetrical self-renewal divisions[135].

1.2.3 Cell Co-Culture

Increasing the culture complexity, the next model introduces addition of other cell types for co-cultures[200]. These include the employ of supporting stromal or endothelial cells, with HSCs and LSCs often cultured on top of the adherent cells either directly or separated by a trans-well system. Studies demonstrate that in vitro co-cultures of blood forming stem cells with mesenchymal cells exhibit long term survival and maintenance of HSCs as well as cell expansions[119,200,201]. These models however fail to capture the influence of the spatial component on cell behaviour and would be better suited to employ in combination with three-dimensional approaches.

1.2.4 Electrospun nanofibers

One system that has been used in engineering of bone tissue is the use of electrospun nanofibers. These manufactured scaffolds provide excellent interconnectivity and control of porosity can be achieved through adjustment of fiber sizes[202,203]. Several types of polymers have been used, ranging from synthetic materials to organic and inorganic components of the bone matrix. The natural ECM components demonstrate a more effective stimulation of HSC cell growth, likely due to existence of cell binding moieties associated with natural bone component[202,204]. The electrospun nanofiber meshes, however, do not possess mechanical properties similar to that of osseous tissue and limit the interactions the cells with their environment[71].

1.2.5 Synthetic Scaffolds

Synthetic scaffolds offer another study model of the BM niche environment. They are capable of embodying the physical and mechanical intricacies of the niche and are able to establish several cellular mechanisms, such as mechanosensitivity and controlled release of biomolecules. The hydrogels are typically cross-linked 3D polymeric networks with high water retention capacity, made with synthetic polymers such as poly (ethylene glycol) (PEG)[205], (PU)[206] and poly (l-lactic acid) (PLLA)[207]. The polymers are covalently crosslinked permitting the fabrication of well-defined network structures with tailorable properties. Cultures of HSCs on these polymer scaffolds demonstrate an increased efficiency in long-term cell maintenance with the cell differentiation period delayed compared to standard cultures[102,206].

Although synthetic materials offer exceptional mechanical properties, where architecture can be carefully tailored[207], they present several drawbacks in terms of biodegradability. Although the synthetic polymers have been shown to not elicit an immune response when transplanted, they degrade via hydrolysis, producing carbon dioxide which can lead to pH changes resulting in cell and tissue necrosis[208]. Additionally, these scaffolds lack the ligands for binding of integrins which prevents the native cell-matrix interactions, although coating of these polymers with native components can overcome these limitations, monocausality of results cannot be clearly established[21].

1.2.6 Decellularized Bone Marrow

Another approach currently being explored is de-cellularized bovine bone marrow repopulated by human stromal and blood progenitor cells, which shows promising results[209]. Bovine bone marrow tissue is processed and decellularized through physical, enzymatic, or chemical processes[39]. Scaffolds obtained from decellularized tissues are able to maintain the tridimensional structure of the native tissue and are composed of natural extracellular matrix proteins. They are therefore highly biocompatible and present low cytotoxicity and immunogenic response[209]. Studies have demonstrated that this employ of bone as a scaffold is capable of not only maintaining, but expanding HSCs in long term culture, especially effective when co-seeded with MSCs [209,210].

Although they are capable of expanding stem cells, the composition of these matrices cannot be fully defined, hampering the interpretation of results when determining specific pathways linked to ECM components[17]. Additionally, the processing of the matrix prior to cell seeding must achieve an optimal balance between cellular removal and structural tissue maintenance as the procedures can be quite destructive to the native proteins of the bone, which may alter subsequent cellular response[210]. Finally, scaling of the model to improve translation and provide-high throughput techniques is difficult.

1.2.7 ECM Extract

One of the most used "biological" ECM systems is Matrigel, extracted from Engelbreth-Holm-Swarm mouse sarcoma cells and commercially available. This tumor derived matrix has the characteristics of a basement membrane and is composed of mainly type IV collagen, laminins (mainly LM-111), perlecan, nidogen and trophic factors[17]. Although Matrigel has proven useful in cultures of endothelial cells as well as breast-, colon-, prostate-, and lung-derived tumor cells, it has limited physiological relevance to HSCs or leukemia cells as it does not accurately recapitulate the microenvironment of the bone marrow niche[211,212]. Other limitations of this model system also include high batch-to-batch variability and inability to accurately demonstrate native mechanical properties of the basement membrane[211]. Additionally, it has limited application in clinical application due to its source of a murine tumor model.

1.2.8 Scaffolds constructed with native ECM materials

The final ECM-mimicking model involves an artificial scaffold fabricated with native components of the BM niche microenvironment. Imitating the natural bone, these composites contain the signaling motifs, which are able to modulate cell fate by facilitating the native ligands of cell receptors[39].

Collagen is an attractive target for biomedical applications as it is the main component of natural ECM and the most abundant protein in mammalian tissues[213]. Collagen is composed of three polypeptide chains that self-aggregate to wrap around each other and form a rope structure which is held together by covalent and hydrogen bonds. Collagen type I has been employed in construction of collagen scaffolds for studies of hematopoiesis as it is the most abundant component of the BM niche. This model system presents great biodegradability as collagen is naturally degraded by metalloproteases, specifically collagenase, and serine proteases, released by local cellular components[213]. Additionally, due to the preserved nature of the collagen molecule the immunogenic response across species is minimized. Another advantage of this scaffold is that collagen is readily available, abundant in nature and has demonstrated ease of manipulation into different forms[195].

The fabrication of collagen scaffolds involved an initial step of rehydration of the collagen fibrils in acetic acid, resulting in a collagen slurry. The interstitial fluid of the suspension is then frozen to create ice crystals within the material, and thin films of collagen nucleate and grow on the edges of the ice, eventually forming the pore walls[214]. Acetic acid facilitates formation of dendritic arrangements, leading to formation of inter-connected pore networks within the scaffold. Additionally manipulating acetic acid concentration can adjust the size of the ice crystals, therefore regulating pore size and scaffold interconnectivity[215]. By reducing the

environmental pressure imposed on the scaffold the material initiates sublimation, yielding a highly porous structure[214].

Due to the thin pore walls collagen scaffolds have been characterized as having poor mechanical properties compared to their synthetic counterparts, especially when mimicking bone. However, employing physical (i.e. UV irradiation, freeze-drying, heating)[216,217] and chemical (i.e. glutaraldehyde, formaldehyde, carbodiimide)[217–219] cross-linking agents can improve structure stability by enhancing the compressive and tensile strength of the scaffolds[208]. Latest studies with collagen scaffolds have also demonstrated that specific microstructure, porosity, pore size and pore morphology can be achieved through manipulation of preparation protocol, such as adjustments of concentration, freezing rate and temperature[220–224]. Another strategy to enhance the mechanical strength of collagen scaffolds is incorporation of mineral components as biomaterials. Hydroxyapatite has been investigated as bone replacement strategy for some time and scaffolds reinforced with HA have demonstrated improved mechanical property and good biocompatibility, without affecting the histocompatibility of the scaffolds[225,226].

These collagen scaffolds enable co-cultures with other cell types, such as MSCs, which allows for a greater encapsulation of the niche components contributing to cell fate. Studies demonstrated that HSC co-cultures with BM-derived MSCs in type I collagen scaffolds enable expansion, with cells retaining their proliferative potential and self-renewal. The model significantly enhanced the stem cells phenotype even 14 days after expansion compared to conventional cultivation and co-culturing techniques that do not incorporate the synthesized collagen matrix[201].

1.3 Aim of Thesis and Research Design

Acute myeloid leukaemia (AML) is a cancer of hematopoietic cells that develops in 3D bone marrow niches in vivo. Mounting evidence demonstrates the focal role of the cell microenvironment in governing decisions of cell fate. However, a predictive in vitro model for study of hematopoietic cells and associated malignancies has yet to be developed and the study of AML has been hampered by lack of appropriate culture systems that mimic this microenvironment. AML cells possess unique requirements for interaction with their environment and targeting these associations may provide a novel therapeutic approach to control their proliferation, induce differentiation, or stimulate apoptosis. However, the employment of 3D culturing methods is technically challenging and labor intensive with complicated cell seeding and retrieval procedures. I hypothesize that the establishment of a collagen-based culture system would permit the study of physiological as well as pathophysiological mechanisms of the cells and their interactions with the microenvironment and allow us to develop a more physiologically accurate high-throughput drug screening system.

The first objective is aimed at establishing and optimizing a collagen-based environment for AML cells as an analog to human 3D bone marrow niche environment native to the cells. Due to the multitude of advantages of the collagen scaffold system previously listed, it was elected as a model of choice for the present study and optimization of the system was undertaken in order to tailor the system for application for a high-throughput drug screening of AML. The established protocols for manufacture of collagen films and scaffolds were amended to incorporate other extracellular matrix components as well as optimize these systems for cell culture. Next, the processes by which the cells are introduced, harvested and analyzed were honed to deliver the most accurate results. Finally, the various extracellular matrix components are systematically screened to reveal the optimal conditions for cell survival and growth.

The second objective is aimed at utilizing the optimized culture system to conduct a proof-of-concept high-throughput drug screening assay. Seeking further evidence in support of the notion that interaction of AML cells with their niche can increase survival rates during drug treatment through cell adhesion mediated drug resistance, ultimately influencing treatment outcomes. The model culture system developed here has the potential to mimic the disease microenvironment and therefore partially recapitulate at least some attributes of leukemia in patients, allowing for selection of “microenvironment-stable” drugs with potential for translation into clinical applications.

Chapter 2. Materials and Methods

2.1 Collagen Scaffold Preparation

Type I collagen flakes (insoluble Type I collagen from bovine Achilles tendon, Cat.# C9879, Sigma-Aldrich Co. Ltd., UK) were mixed with 0.05M Acetic Acid Solution (prepared from diluted Glacial acetic acid purchased as Acetic Acid, ACS reagent, ≥99.7%, Cat.# 695092, Sigma-Aldrich Co. Ltd., UK and MilliQ water) in order to produce the desired concentration of collagen mixture. The collagen solution was rehydrated overnight and then homogenised in order to generate a uniform suspension. To prepare 3D collagen scaffolds the collagen was dispensed onto each well of a flat-bottom 96-well plate (VWR, US). The plate was then frozen overnight at -20°C causing suspension of ice crystals within the scaffold. This was followed by a freeze-dry cycle (Harvest Right) to remove the ice crystals resulting in a porous scaffold which can be infiltrated by the cells. To produce 2D film, the collagen was dispensed onto a flat-bottom 96-well plate (VWR, US) and the water was allowed to evaporate in a fume hood for a minimum of 24 hours (Figure 1).

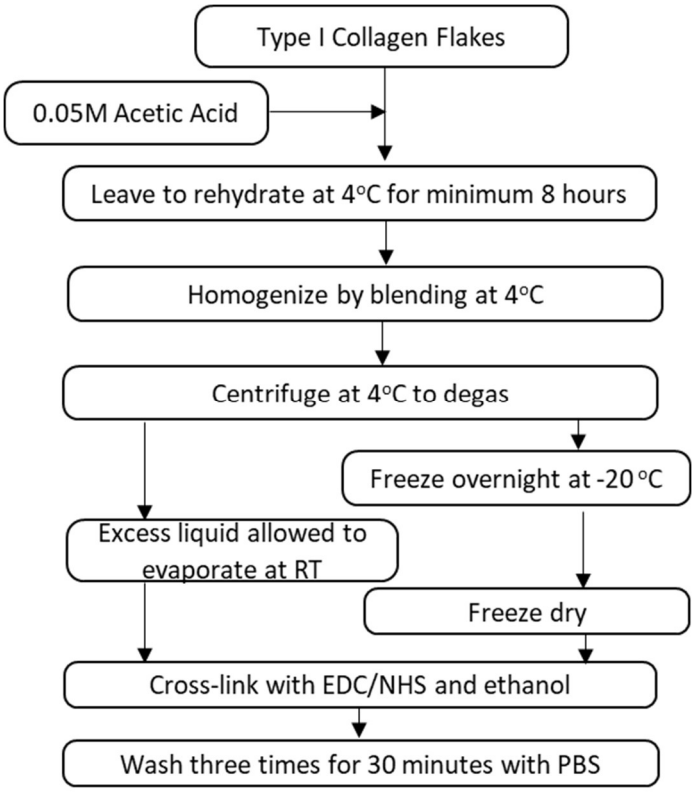

Figure 1: **Collagen Films and Scaffolds fabrication process.** Collagen flakes are suspended in acetic acid and allowed to rehydrate overnight. The mixture is then homogenized using a conventional blender and air bubbles are removed. The collagen suspension is then cast into appropriate wells and allowed to evaporate to produce 2D collagen films or freeze-dried in order to generate a porous 3D network. The structures are then cross-linked and washed.

2.2 Collagen Slurry Degasification

Air bubbles were removed from the blended collagen slurry by two different methods. Vacuum degasification was performed by placing the solution beaker into a vacuum chamber and pressure reduction was applied. In the second method the slurries were centrifuged (Heraeus, Megafuge 40R) at 200g at 4°C. The collagen suspensions did not precipitate during the centrifugal degassing.

2.3 Degasification Evaluation

To evaluate the number of air bubbles present in 2mL of each sample was spread over a 3 cm area with the layer thickness of 2mm and an image was captured (Olympus SZ61, AxioCam ERc5s). The images were analyzed by using ImageJ software[227]. The amount and size of bubbles present per 3 cm area were analyzed with GraphPad to exclude outliers and plotted.

2.4 Slurry pH Measurements

The pH of each collagen slurry prepared with various components was evaluated by measuring 5 mL of each slurry with pH Meter (sympHony SB70P, VWR, US).

2.5 Rheological Measurements

Viscosity for each component slurry was analyzed with the Discovery HR30 (TA Instruments) rheometer, using the 40mm parallel Peltier steel plate. Results were plotted using GraphPad.

2.6 Cross-Linking of Collagen 2D Films and 3D Scaffolds

EDC-NHS crosslinking solution of 1-ethyl-3-(3-dimethylaminopropyl) carbodiimide hydrochloride (EDC, Cat.# 161462, Sigma-Aldrich Co. Ltd., UK) and N-hydro-xysuccinimide (NHS, Cat.# 6066-82-6, Sigma-Aldrich Co. Ltd., UK) was prepared using a 5:2:1 M ratio for EDC: NHS: Collagen, hereafter referred to as the '100% concentration'. For every 1 mg of collagen, the 100% concentration standard of crosslinking solution consisted of 1.15 mg EDC and 0.276 mg NHS dissolved in 80% ethanol. Films and scaffolds were submerged in crosslinking solution and allowed to react for 3 hours at room temperature on the microplate shaker (FisherBrand, US) at 200 rpm. After reaction the scaffolds were washed thoroughly in Phosphate Buffer Solution (Dulbecco's phosphate buffered saline (PBS) powder (Cat. # D5652, Sigma-Aldrich Co. Ltd., UK) diluted in MilliQ water and sterilized) three times for 30 minutes. Scaffolds were then stored in PBS solution until ready to use.

To obtain scaffolds with different cross-linked states the EDC:NHS concentration was serially diluted to produce 10%, 50% and 100% solutions. Following the crosslinking procedure described above, the

scaffolds were imaged (Olympus SZ61, AxioCam ERc5s) and the images were analyzed by using ImageJ software. The degree of scaffold shrinking was measured and compared to the control sample treated with ethanol as the cross-linking agent. Data was analyzed with GraphPad.

2.7 Scanning Electron Microscopy

The microstructure of the scaffolds was examined using scanning electron microscopy (SEM) (Quanta 3D, Thermofisher, US). Prior to observation, samples were placed on stand and secured with double-sided adhesive carbon tape and imaged under low vacuum. The resulting images were analyzed with ImageJ[227] software to determine the number of pores observed within a section and to calculate the pore area. Pore size is reported as the calculated pore area in μm^2, all pores reported under 10 μm^2 were excluded from calculations. The reported values were then analyzed with Prism® 5.03 (GraphPad Software Inc., La Jolla, CA, USA) to exclude outliers.

2.8 pH Measurement of Collagen 2D Films and 3D Scaffolds

After films and scaffolds were prepared in duplicate plates, half were washed by submerging the films and scaffolds in 200 µL of Phosphate Buffer Solution (Dulbecco's phosphate buffered saline (PBS) powder (Cat. # D5652, Sigma-Aldrich Co. Ltd., UK) diluted in MilliQ water and sterilized) and washed for 30 minutes at room temperature on the microplate shaker (FisherBrand, US) at 200 rpm. The wash solution was then completely removed and these along with the unwashed scaffolds were analyzed by adding 200 µL solution of 0.05% Phenol Red Indicator (0.5% Phenol Red Solution (Cat. # P0290, Sigma-Aldrich Co. Ltd., UK) diluted in in PBS) to each well and allowed to equilibrate for 10 minutes at room temperature on the microplate shaker (FisherBrand, US) at 200 rpm. Thereafter, 100 µL from each well was transferred to a fresh 96-well plate (VWR, US) and the absorbance of each solution was measured using the Plate Reader (Synergy H4 Hybrid) at 560 nm with the parameters Read Speed: Normal, Delay: 100 msec, Measurements/Data Point: 8. Absorbance at 560 nm was normalized with 750nm with GraphPad and converted to pH values by using a calibration curve of solutions with known pH, as measured by the pH Meter (sympHony SB70P, VWR, US).

2.9 Cell Culture

Acute Myeloid Leukemia OCI-2 and OCI-3 cell lines were obtained from Dr Mark Minden's lab. The cells were expanded and cultured in media with αMEM (Cat.# 12-169F, Lonza, BioWhittaker, Switzerland) with 10% Fetal Bovine Serum (Cat.# 12483-020, Thermo-Fisher Scientific, US) and 1% Penicillin-Streptomycin (Cat.# 10378-016, Thermo-Fisher Scientific, US) and 1% L-Glutamine (Cat.# 25030164, Thermo-Fisher Scientific, US).

K-562-GFP cell line was obtained from ATCC (CCL-243-GFP). The cells were expanded and cultured in media prepared by mixing IMDM Modified (Cat.# SH30228.01, HyClone, US) with 10% Fetal Bovine Serum (Cat.# 12483-020, Thermo-Fisher Scientific, US) and 0.5 µg/mL Puromycin (Cat.# A1113803, Gibco, US).

2.10 Scaffold Seeding

Following expansion, the AML OCI-2 cells were harvested for cell seeding experiments. Three seeding methods (static surface seeding, cell seeding using a centrifuge and cell seeding with an orbital shaker) were evaluated for seeding efficiency on 2D films and 3D collagen scaffolds. A cell density of $5x10^4$ cells/scaffold (of film) was used across all conditions. 100 µL of complete AML OCI media was dispensed onto the structures, followed by 100 µL of concentrated cell suspension evenly added on top of the films/scaffold. For static seeding the films/scaffolds were then allowed to incubate. For seeding by centrifugation, the plates were centrifuged (5804 Eppendorf, Germany) at 1500 rpm for 10 seconds and allowed to incubate. For last seeding method the plates were placed on an orbital shaker inside the incubator at 200 rpm. Incubation lasted 72 hours at 37.0^0C, 5% CO_2 saturation (Thermo-Scientific, Forma, Steri-Cycle) (Figure 2).

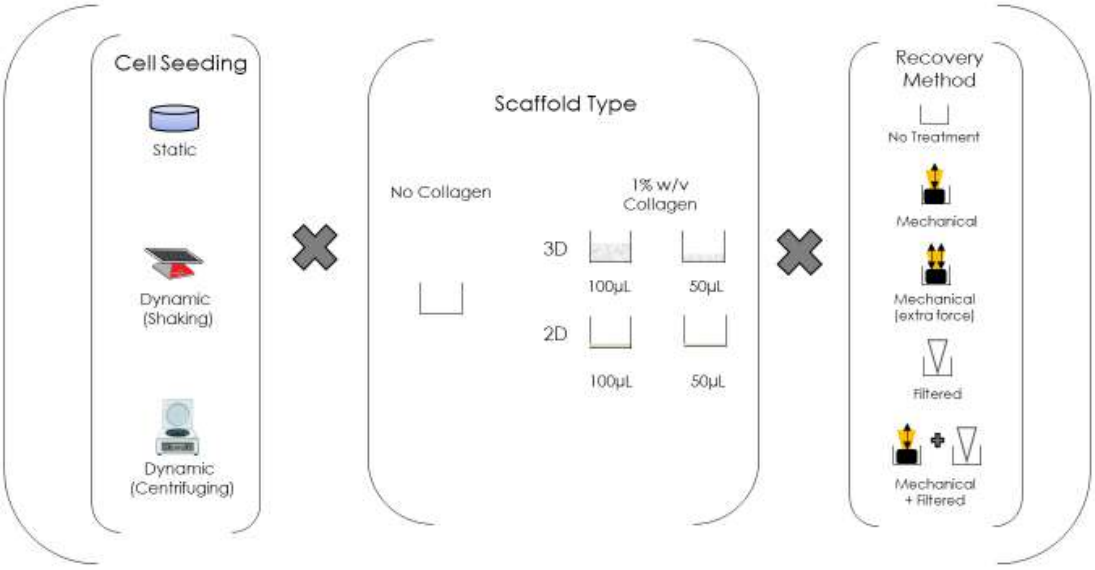

Figure 2. Cell Seeding and Recovery Experiment Layout. Evaluated a total of three seeding conditions – static seeding, orbital shaker and centrifugation, five ECM conditions: polystyrene control, 2D films and 3D scaffolds of two sizes each, and four recovery methods: no treatment, mechanical, mechanical extra force, filtered and a combination of mechanical and filtered are evaluated.

2.11 Cell Recovery from Seeded 2D Films and 3D Scaffolds

To harvest the cells from films and scaffolds five recovery methods were evaluated. Direct recovery entailed pipetting the cells from the scaffold without any additional treatment. Mechanical recovery includes dissociation of cells from the scaffold by using of a small plunger to depress the scaffold for a total of six repetitions (Figure 3A). A third recovery method involved similar dissociation technique but doubled in number of repetitions. Fourth recovery method included a scaffold filter, made from 0.8 mL PCR Tubes (NEST) which depresses the scaffold during the pipetting process (Figure 3B). Last recovery method combined the second and fourth methods: the cells were first agitated by plunger depression and then the scaffold was depressed with a PCR tube filter (Figure 2). Cell suspension from the scaffolds was added to a new 96-well round bottom plate (Thermo Scientific, US) all films and scaffold were washed with 100 µL of PBS after cell recovery and the rinse was also added into the appropriate wells. The plates were centrifuged at 1500 rpm for 5 minutes. Supernatant was removed and cells were resuspended in 100 µL of PEF solution (diluted and sterilized Dulbecco's phosphate buffered saline (PBS) powder (Cat. # D5652, Sigma-Aldrich Co. Ltd., UK) in MilliQ water, 0.1 M of UltraPure 0.5M EDTA, pH 8.0 (Cat.# 15575-020, Invitrogen, US) and 10% Fetal Bovine Serum (Cat.# 12483-020, Thermo-Fisher Scientific, US) and transferred onto a new 96-well flat bottom plate (Figure 4).

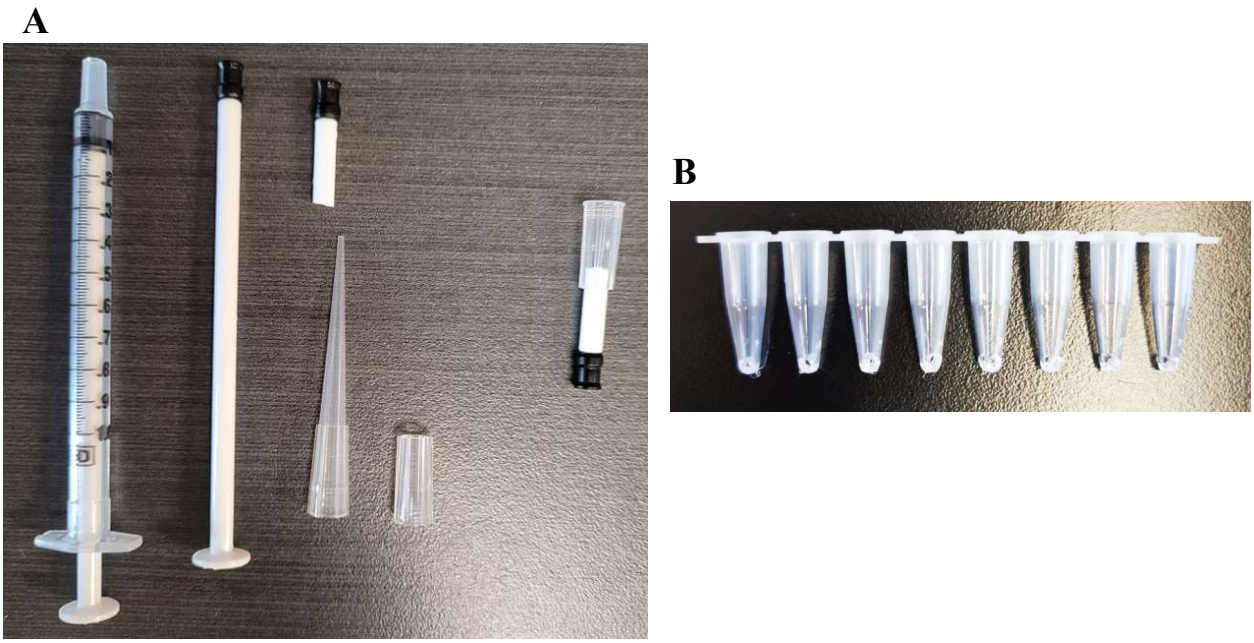

Figure 3. Preparation of Plungers for Mechanical Agitation of Cells and Filters for Cell Recovery. (**A**). The syringe head is removed from a 1 mL syringe (Becton Dickinson, US) and cut down to a 2-3 cm length. The syringe tip is then inserted into a cut centrifuge tip to create a small plunger equivalent which can be attached onto a pipette for easier handling. (**B**). An 8-strip PCR tube is modified to contain holes on either side of its tip. The strip is then inserted into 96-well plates for cell suspension recovery.

2.12 Cell Staining and Evaluation

To observe the effects of 2D films and 3D scaffolds on cell viability, the cells were stained with Alamar Blue (Cat.# DAL1100, Invitrogen, US) and Hoechst 33342 (Cat.#H3570, Invitrogen, US) at 1:1000 and incubated for 1 hour following scaffold recovery protected from light at 37.0^{0}C, 5% CO_2 saturation (Thermo-Scientific, Forma, Steri-Cycle). A calibration curve for the cells was prepared for each plate with appropriate cell concentrations for the range of cell numbers being evaluated. Alamar Blue assay was also performed on the scaffolds to evaluate the number of cells left-over after recovery (Figure 4). The plates were then analyzed using the Microplate Reader (Synergy H4, BioTek) at 361:497 and 560:590 Emission: Excitation wavelengths. Parameters Read Speed: Normal, Delay: 100 msec, Measurements/Data Point: 10. The values were processed using GraphPad.

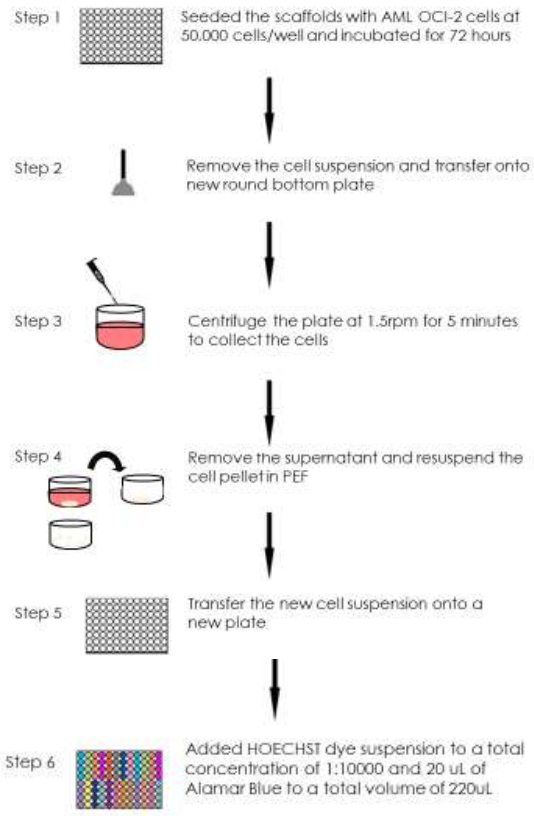

Figure 4. Procedure for Cell Evaluation with Fluorescent Assay. Cells are seeded onto the scaffolds and allowed to incubate. The solutions are carefully removed from the structures and placed into a new round-bottom plate, the collagen structures are washed wish PBS and the wash solution is added to the round-bottom plate. Upon plate centrifugation the supernatant is removed, and the pellets are resuspended in PEF solution. The resulting cell suspension is then transferred onto a new flat-bottom 96-well plate and the dye solution is added. The cells are then incubated with the dye and fluorescence is evaluated with a plate reader.

2.13 Evaluation of alteration in cell growth in response to ECM Component Variation

Three cell lines were evaluated separately, each was seeded onto the scaffolds at the concentration of 50,000 cells/well by centrifugation (5804 Eppendorf, Germany) at 1500rpm for 10 seconds. The analysis of drug response variation involved an additional step of adding one of three chemical agents (DMSO, TDZ or Ara-C) to the assay at the time of seeding for a final drug concentration of 10 μM. The plates were then incubated for 72 hours at 37.0^{0}C, 5% CO_2 saturation (Thermo-Scientific, Forma, Steri-Cycle). Cell recovery from the plates was carried out using the combination of mechanical agitation and filtering as well as a rinse step. The scaffolds and the 96-well round bottom plates were stained with Alamar Blue in PEF solution. The recovered cells were stained with Alamar Blue (Cat.# DAL1100, Invitrogen) and all plates were incubated for 1 hour protected from light at 37.0^{0}C, 5% CO_2 saturation (Thermo-Scientific, Forma, Steri-Cycle). The plates were then analyzed using the Microplate Reader (Synergy H4, BioTek) at 361:497 and 560:590 Emission: Excitation wavelengths. Parameters Read Speed: Normal, Delay: 100 msec, Measurements/Data Point: 10. The resulting data was processed using GraphPad.

2.14 High -Throughput Drug Screening

Collagen scaffolds and films were manufactured, irradiated, and cross-linked using the methodology established over the course of this manuscript and the OCI AML-2 cell line was employed in the evaluation. The cells were seeded onto the films, scaffolds and polystyrene plates at a concentration of 50,000 cells/well by centrifugation (5804 Eppendorf, Germany) at 1500rpm for 10 seconds. TOCRIS Mini 2.0 Drug Library (Cat. #7151, Tocris Bioscience, UK), containing 1,120 biologically active compounds was used to conduct the screening assay, 157 compounds were randomly selected from the library for the screen as well as three additional compounds: DMSO control, thioridazine and cytarabine (Ara-C), for a total of 160 screened chemical agents. After cell seeding each compound was added to the media to a final concentration of 10 μM, each compound was scanned in triplicate within each of the three conditions: PS, 2D collagen films and 3D collagen scaffolds. After incubation for 72 hours at 37.0^{0}C, 5% CO_2 saturation (Thermo-Scientific, Forma, Steri-Cycle) the samples were stained with Alamar Blue (Cat.# DAL1100, Invitrogen) and incubated for 1 hour protected from light at 37.0^{0}C, 5% CO_2 saturation (Thermo-Scientific, Forma, Steri-Cycle). A calibration curve was developed for each plate type and analyzed alongside the samples on the Microplate Reader (Synergy H4, BioTek) at 361:497 and 560:590 Emission: Excitation wavelengths. Parameters Read Speed: Normal, Delay: 100 msec, Measurements/Data Point: 10. The resulting data was normalized to the relative control treated with DMSO and plotted using GraphPad.

2.15 Statistical Analysis

Data were analyzed using Prism® 5.03 (GraphPad Software Inc., La Jolla, CA, USA) and reported as the mean ± standard deviation (SD). Welch Anova multiple comparison tests were used to determine statistical significance (sample size specified for all experiments). For the drug screening assay multiple two-tailed t-tests were conducted to establish significance. P-values considered statistically significant are indicated with asterisks: less than 0.05*, less than 0.01**, less than 0.001*** or less than 0.0001****.

Chapter 3. Results

3.1 Optimization of Collagen Suspension Preparation

Preparation of collagen suspension for casting was performed as previously described[220,228]. However, several adjustments had to be considered in order to optimize the procedure for the desired purposes.

3.1.1 Degassing of Collagen Suspension

The homogenized collagen suspension was refined to remove trapped air bubbles from solution. Two methods were evaluated for their efficacy: pressure reduction by vacuum application and centrifugation. Although both methods were successful in significantly reducing both the number and the size of bubbles present within a sample (Figure 5A and 5B), the centrifugation method was more efficient at reducing the amount of trapped air bubbles - t-test ** p value <0.01 between vacuum method and all the centrifugation trials. Centrifugation time of 4 minutes was chosen as optimal for future formulations of collagen suspension.

3.1.2 Incorporation of Components into Collagen Suspension

Addition of extracellular matrix components into the collagen suspension leads to disruption of equilibrium and additional optimization measures are required in order to maintain it. Three extracellular matrix components, aside from type I collagen were tested (Figure 5C): Elastin from bovine neck ligament (Cat.# E1625, Sigma-Aldrich Co. Ltd., UK), and hydroxyapatite of two different particle sizes Hydroxyapatite nanopowder, <200 nm particle size (BET) (Cat.# 677418, Sigma-Aldrich Co. Ltd., UK) and Hydroxyapatite powder, 10 µm, ≥100 m2/g (Cat.# 900203, Sigma-Aldrich Co. Ltd., UK). For both Micro ~10 µm and Nano <200nm Hydroxyapatite powders, a significant increase in apparent pH can be observed at both temperatures, hence the procedure for preparation of scaffolds with these components requires modification. The solution is buffered with concentrated acetic acid ≥99.7% (Sigma-Aldrich Co. Ltd., UK) to prevent the sudden pH increase caused by the addition of basic hydroxyapatite powders. Different amounts of acetic acid were assessed in order to determine the optimal concentration at which the precipitation of collagen would be minimized. Supplementation with 2% of concentrated acetic acid does not cause sufficient buffering of the solution as the pH remains significantly higher than that of the control 1% Collagen Suspension (*p<0.05 and **p<0.01). Addition of 4% of concentrated acetic acid restores the system to it's original pH for both sizes of hydroxyapatite used (Micro ~10 µm and Nano <200nm) across both temperatures assessed (5ºC and 25ºC). Addition of elastin does not appear to cause any statistically significant pH changes in the collagen suspension; therefore, no additional modifications are required for collagen formulations with this component.

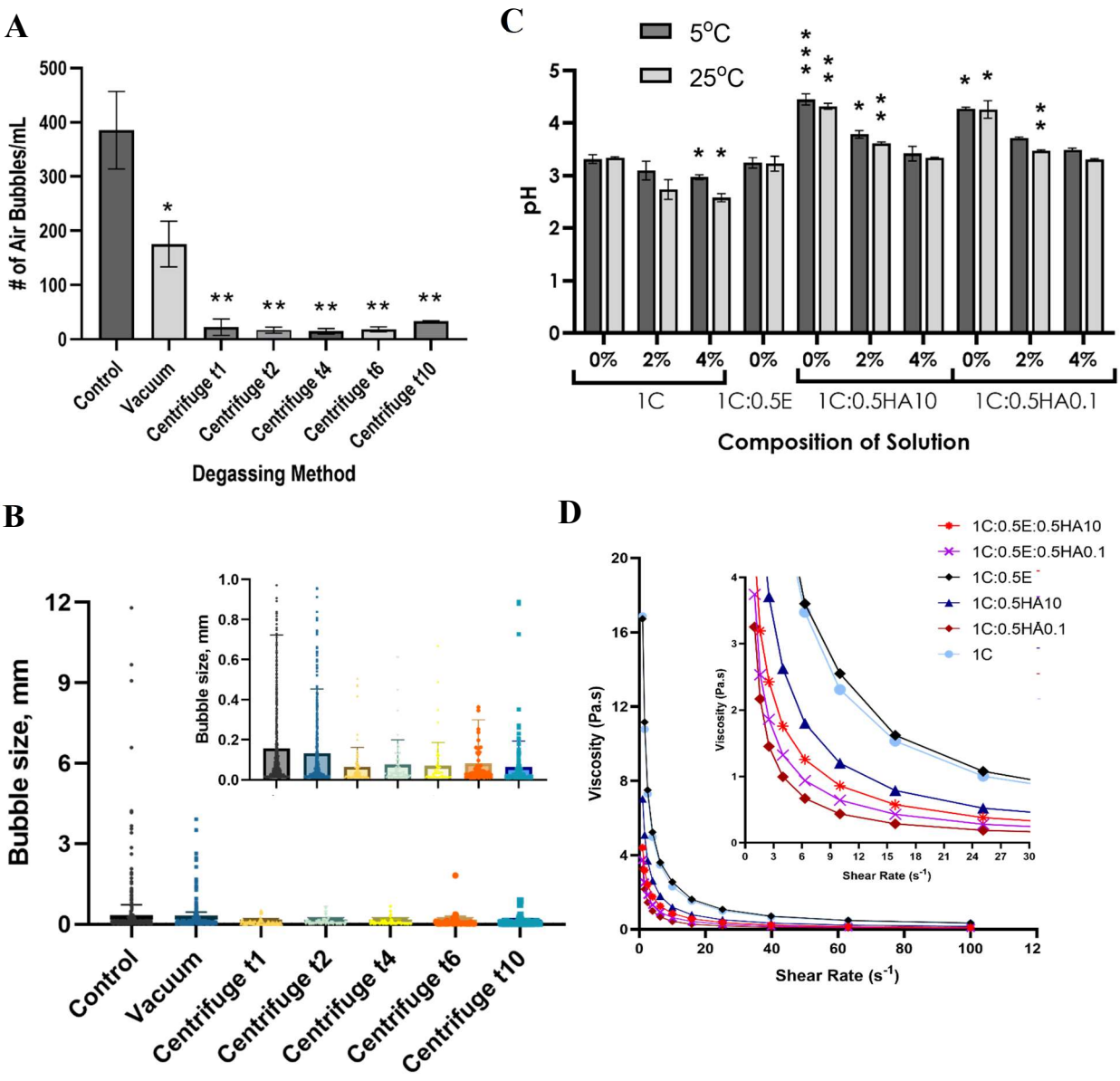

Figure 5. Optimization of collagen suspension and preparation for dispensing (**A**). Variation in amount of bubbles present per 1 mL of collagen suspension after degasification (Data reported as Mean±SD, *n*=4) (**B**). Reported size of bubbles present in 1 mL of collagen suspension after degasification treatment, reported average and size distribution, smaller scale is provided to highlight the averages (Data reported as Mean±SD, *n*=4) (**C**). pH Measurements of Collagen Suspension assembled with various combinations of components and concentrations of acetic acid (C-collagen, E- Elastin, HA10 – Micro Hydroxyapatite <200nm, HA0.1 – Nano Hydroxyapatite ~10 µm), performed at temperatures of 5°C and 25 °C (Data reported as Mean±SD, *n*=3, multiple comparison t-tests compared to control - 0% acetic acid 1% Collagen solution). (**D**) Rheological Measurements of collagen suspension prepared with combinations of components, smaller scale is highlighted to demonstrate the slight variation present at low shear rate, measurements performed at 5°C. (Welch Anova multiple comparison test (*) $p < 0.05$, (**) $p < 0.01$, (***) $p < 0.001$).

Collagen suspension solution is a viscous fluid and when tested with a rheometer exhibits shear thinning behaviour, where viscosity decreases with an increase in shear rate (Figure 5D). Addition of other ECM components does not alter this overall behavior where the viscosity decreased, in the same range of rates, with rising frequency. Some decrease in viscosity is observed, however, with addition of hydroxyapatite powders to the collagen suspension. Elastin does not alter the reported viscosity values.

3.2 Optimization of Collagen Scaffold for Cell Culture

Collagen sponges and films produced from the processing of the collagen suspension (Figure 1) offer a remarkable system for assessing cell behavior as they provide a suitable environment for cell adhesion and proliferation. Porous structure of the 3D scaffolds, the adhesion properties for cell attachment as well as biocompatibility are essential to ensuring proper cell growth in these model systems[217].

3.2.1 Cross-Linking of Collagen Films and Scaffolds

In order to enhance the mechanical strength of the cast 2D films and 3D scaffolds and improve enzymatic stability a cross-linking reagent is employed (Figure 6A). The combination of 1-ethyl-3-(3-dimethylaminopropyl) carbodiimide (EDC) and N-hydroxysuccinimide (*NHS*) was used as the cross-linker for the films and scaffolds as it has been extensively characterized in the past [89,146,217,220,229–232]. Scaffolds that do not undergo cross-linking are prone to significant shrinkage and collapse, seemingly unable to provide sufficient tensile strength to support the cell media. The scaffolds that have undergone the cross-linking procedure demonstrate a significant increase in resistance to shrinkage (Figure 6B). The 100% as well as the 50% cross-linking solutions demonstrates the most drastic change in reduction of scaffold shrinkage, approximately 10% area reduction as compared to 25% for our control treated with ethanol as the cross-linking agent (***$p<0.001$), the 10% cross-linker sample, however, fails to provide any statistically significant increase in the scaffold resistance to shrinkage. In our experiments going forward the 100% concentration of cross-linking solution will be employed as it demonstrates the highest degree of scaffold resistance to shrinkage (Figure 6B).

3.2.2 Scaffold Porosity

Three-dimensional scaffold structures were analyzed by imaging the top surface of each scaffold type. Five different scaffold types manufactured with various combinations of ECM components were screened and the images obtained revealed that all samples exhibit a sponge-like porous appearance (Figure 6C). The scaffolds still sustained a favorable interconnected porous structure when ECM components were added, indicating that these components do not change the porous properties of the collagen scaffold, additionally all scaffolds show heterogeneous pore size distribution. However, incorporation of components other than

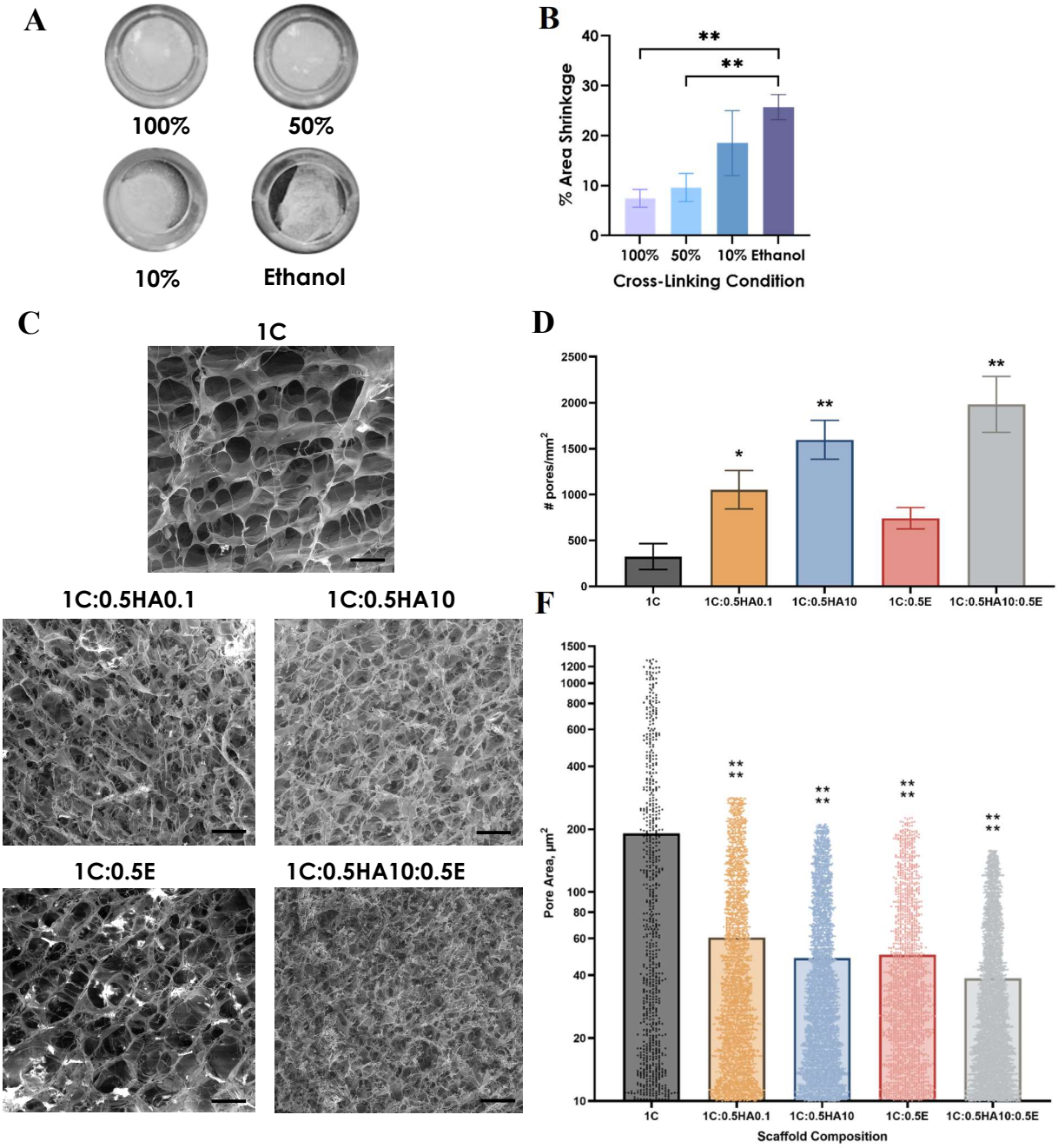

Figure 6. Characterization of 3D collagen scaffolds (A). Representative images of 3D scaffolds cross-linked with various concentration of EDC-NHS. (**B**). Estimation of size reduction of 3D scaffolds after treatment with various concentrations of EDC-NHS cross-linking solution, images obtained with Olympus SZ61 (AxioCam ERc5s), processed with ImageJ[227] and analyzed with GraphPad (*n*=4). (**C**). Comparison of pore structures in representative SEM images of collagen scaffolds composed with various combinations of extracellular components, Scale bars: 100 µm (C-collagen, E – elastin, HA10 – Micro Hydroxyapatite <200nm, HA0.1 – Nano Hydroxyapatite ~10 µm). (**D**). Reported number of pores in the various scaffold composition samples calculated with ImageJ[227] software (n=3) (**F**). The reported and average areas of the pores found in scaffolds composed with various ECM components, area is shows on a log10 scale. (All data reported as Mean±SD, Welch Anova multiple comparison, (*) $p < 0.05$, (**) $p < 0.01$, (***) $p < 0.001$, (****) $p < 0.0001$).

collagen increases the number of pores present per area and causes a decrease in the average size of the pores observed. This is most evident with the hydroxyapatite in both the nano (~10 μm) and micro (<200nm) forms with the micro hydroxyapatite demonstrating a statistically significant increase in the number of pores observed (Figure 6D), here addition of Micro Hydroxyapatite <200nm powder alone caused an almost 5-fold increase in the number of pores reported (**$p<0.01$) and with three components, in the presence of elastin, an even greater increase is observed (***$p<0.001$). The increase in the number of pores correlates with the decreased pore size in the scaffolds constructed with additional components (Figure 6F). Scaffolds composed with collagen alone demonstrate an average pore size of 190.8±280.5 μm2, however the average pore size for composite scaffolds were 60.7±62.3 μm2 (1% collagen 0.5% nano hydroxyapatite ~10 μm), 48.3±45.5 μm2 (1% collagen 0.5% micro hydroxyapatite <200nm), 50.2±46.8 μm2 (1% collagen 0.5% elastin) and the three component scaffolds exhibited the lowest average pore size 38.68±33.4 μm2 (1% collagen 0.5% micro hydroxyapatite <200nm and 0.5% elastin). Additionally, all components were imaged in the absence of collagen matrix (Appendix 1).

3.2.3 2D Film and 3D Scaffold pH

The production of the collagen suspension material occurs at an acidic pH, and although the evaporation of acid in 2D films and lyophilization of 3D scaffolds should remove any residual acidity, investigation was undertaken into whether increased concentrated acid content, required to produce component scaffolds, would cause significant decreases in pH of resulting structures. The 2D films demonstrate an overall lower apparent pH than their 3D scaffold counterparts across both scaffold sizes tested (Figure 7A). A clear correlation between increasing percentage of concentrated acetic acid added into the collagen suspension and decreased pH of the 2D films produced was observed, where films manufactured with the addition of acetic acid are significantly different from the control 1% collagen formulation films. This linear correlation is not present for the 3D scaffolds, however, high percentage of added acetic acid does cause an apparent decrease to pH, especially for the larger scaffold size. The introduction of a wash step allows for sufficient buffering of the system to adjust the pH to the physiological range for the collagen suspension prepared without addition of concentrated acetic acid, however, is not sufficient when higher acid content is present. It is also evident that a larger structure size has a greater impact on the resulting system pH, this correlation required further investigation. From Figures 7B and it can be ascertained that larger structure size is inversely proportional to the resulting pH measurements, as a linear decrease is detected. Additionally, scaffolds of 100 μL and larger are not restored to the physiological pH range following a single 30-minute wash with PBS. However, a wash does significantly increase the pH (****$p<0.0001$) of the structures across all sizes of both films and scaffolds when compared with the untreated samples. Following these findings, it was evaluated whether an increase in the time of the wash step would improve the restoration

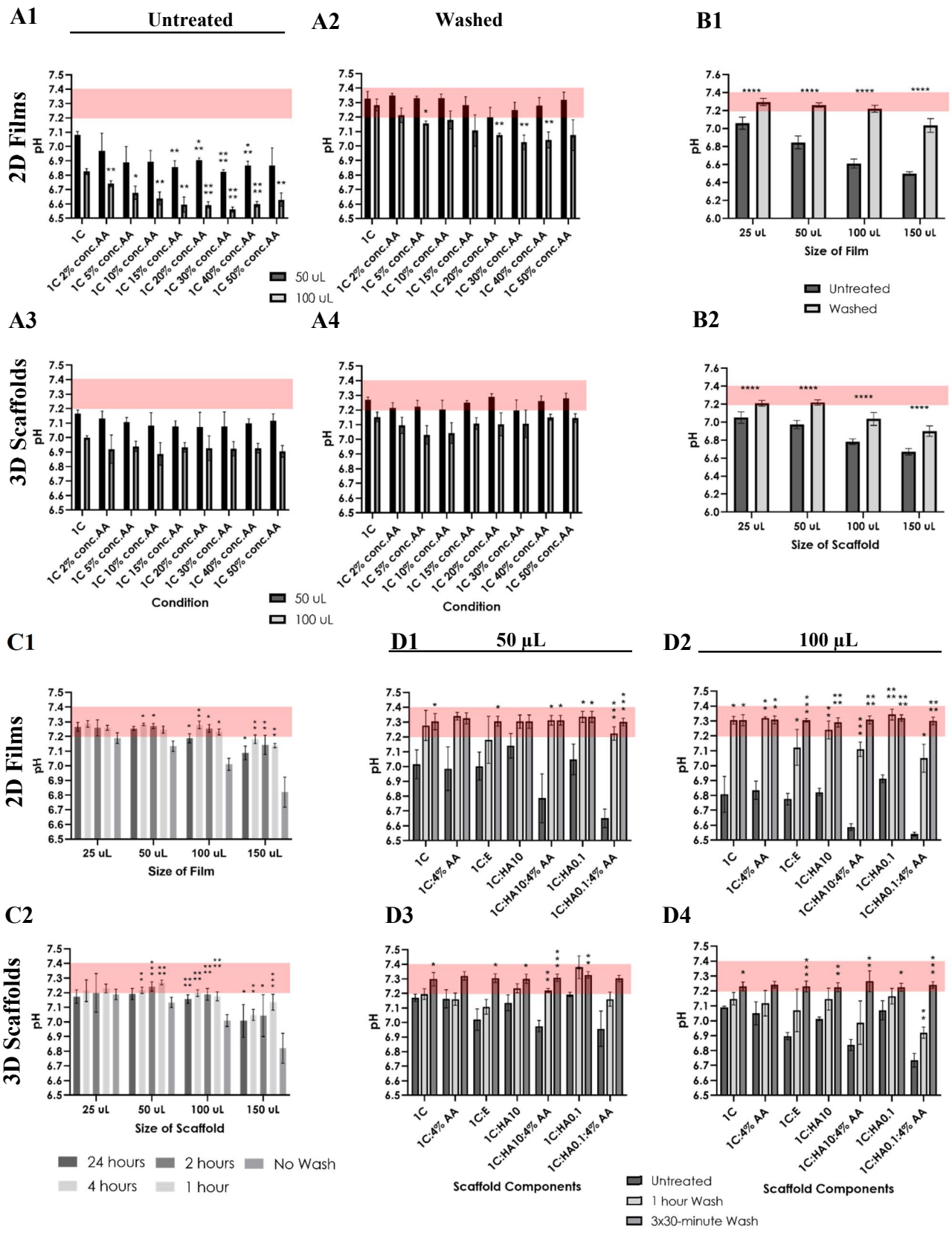

Figure 7: Legend on next page

of pH of these structures to the physiological range. In Figures 7C the pH of untreated films and scaffolds of various sizes were compared with those washed for either 1, 2, 4 or 24 hours. For the largest structures evaluated (150 µL) the increased wash time was still unsuccessful in raising the pH to our desired range, and a 24-hour wash demonstrated the smallest pH increase as compared to the untreated control for both 2D films and 3D scaffolds (*$p<0.01$). Across all conditions, the longer wash step does not result in a larger pH increase, with the 24-hour wash seemingly causing the smallest pH increase across all formulation sizes. For films and scaffolds made from 50 µL and 100 µL the shorter washes do significantly alter the final pH of the system.

Finally, investigation was conducted into how addition of other components, and the accompanying changes in the formulation protocol, would alter the pH of the resulting structures (Figures 7D). Samples prepared with elastin or hydroxyapatite powders do not appear to have a significantly different pH from the 1% collagen formulation across the untreated sample, however samples prepared with the protocol alteration, namely the addition of 4% concentrated acetic acid, demonstrate an apparent pH decrease as compared to the 1% Collagen formulation in the untreated samples for both 2D films and 3D scaffolds. This pH reduction appears so significant that a single wash with PBS is inadequate in restoring the pH to the physiological range for the 100 µL structures. However, a different treatment composed of three washes each consisting of 30 minutes appears to be sufficient and the pH for all structures falls into the 7.2-7.4 pH range. Therefore, the three 30-minute washes were chosen as standard treatment for all scaffolds prior to cell seeding.

3.3 Seeding and Recovery of Cells from Collagen Films and Scaffolds

To provide the most efficient seeding technique for our manufactured collagen structures a comparison between static and dynamic seeding methods was carried out. Data was obtained through a variety of

---

Figure 7. Evaluation of culture system pH for 2D films and 3D scaffolds. pH of structures was measured by using the phenol indicator and analyzing absorbance at 560nm and converted to pH values with a standard calibration curve**.** (**A**). pH Measurements of 2D Films (**A1 and A2**) and 3D scaffolds (**A3 and A4**) across two different sizes either untreated or washed with PBS for a range of structures prepared from collagen formulations with various amount of concentrated acetic acid (*n*=4, One-way Anova multiple comparison t-test). (**B**). Effect of dispensed collagen suspension volume on final 2D film and 3D scaffold pH untreated and washed (*n*=20, One-way Anova multiple comparison t-test between untreated and washed) (**C**). Correlation of pH value with the structure volume observed across four different wash times (*n*=8, One-way Anova multiple comparison t-test to untreated controls). (**D**). Representation of component 2D films (**D1-D2**) and 3D scaffolds (**D3-D4**) pH measurements for two size variations demonstrated for three components (C-collagen, E – elastin, HA10 – Micro Hydroxyapatite <200nm, HA0.1 – Nano Hydroxyapatite ~10 µm) prepared with and without the addition of concentrated acetic acid as previously described. The untreated samples were compared to a single 1-hour wash and three 30-minute washes. *(n*=4, One-way Anova multiple comparison t-test to untreated controls). (All data reported as Mean±SD, (*) $p < 0.05$, (**) $p < 0.01$, (***) $p < 0.001$, (****) $p < 0.0001$).

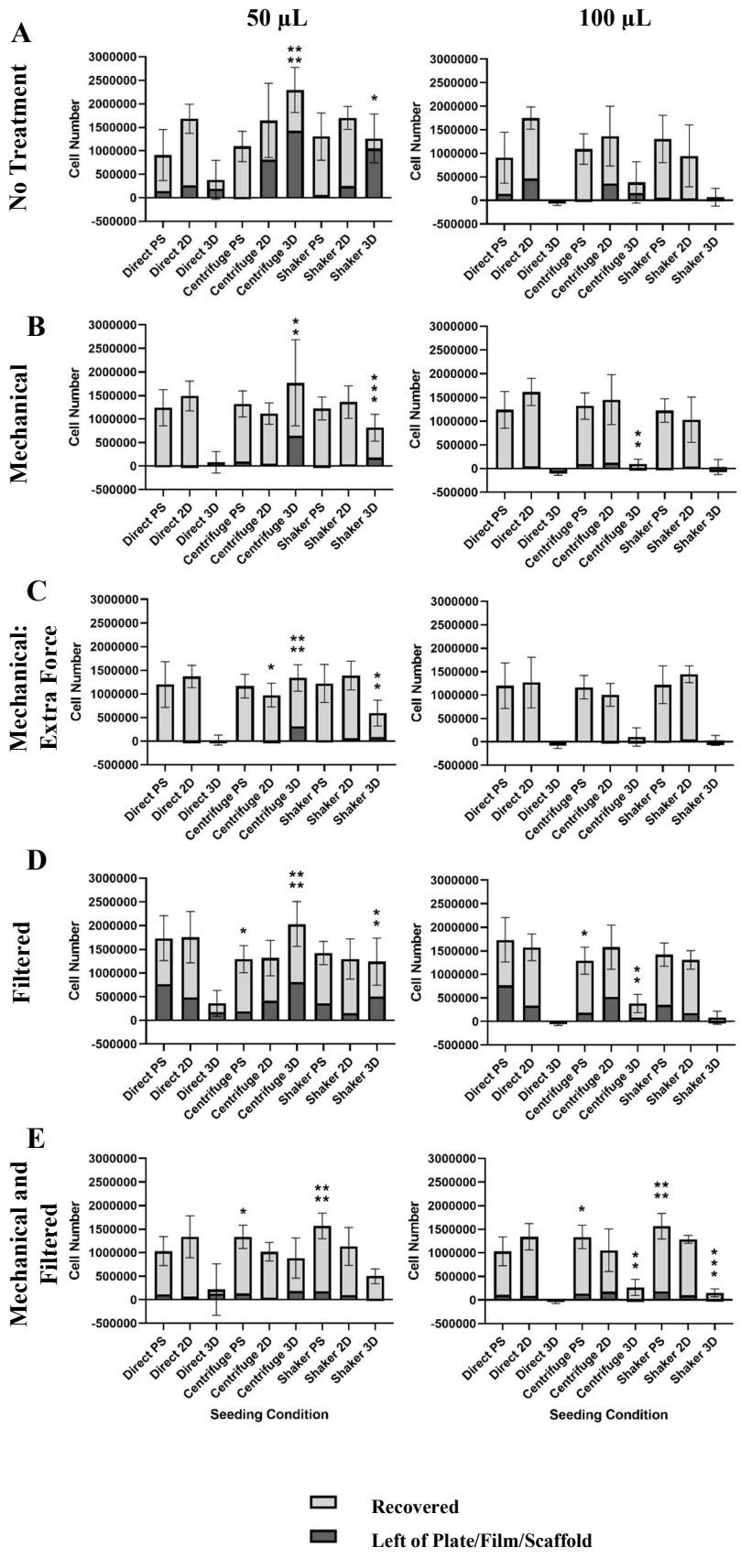

Figure 8. Evaluation of growth efficiency across various seeding methods on 2D Collagen Films and 3D Scaffolds. Evaluation of three seeding methods was carried out by comparing the expansion of cells withing three separate culture conditions: PS, 2D collagen films and 3D collagen scaffolds. The collagen conditions were further separated into structures made of 50 µL suspension aliquots (left) and 100 µL (right). The cells were seeded onto the scaffolds at 50,000 cells/well with one of three methods: static seeding, centrifugation at 1500 rpm for 10 seconds and application of an orbital shaker throughout incubation at 200 rpm. After incubation cells were recovered from the cultures through one of five recovery techniques and the recovered cells along with those left in the cultures were stained with Alamar Blue and fluorescent response was analyzed (Data reported as Mean ±SD, t-test two-tailed, (*) $p < 0.05$, (**) $p < 0.01$, (***) $p < 0.001$, (****) $p < 0.0001$). (**A**). Recovery was performed by direct transfer of cell suspension from each condition. (**B**). Prior to cell suspension transfer cells were agitated from the films and scaffolds by employ of a fabricated plunger with a set force. (**C**). Prior to cell suspension transfer cells were agitated from the films and scaffolds by employ of a fabricated plunger with a set force, doubled compared to the previous recovery technique. (**D**). Cell suspension was transferred from culture with engagement of a manufactured filtering system. (**E**). Cells were agitated, with the use of the previously mentioned plunger, in their respective culture conditions and transferred from culture through a filtering system.

recovery methods and each set were compared across a corresponding scaffold size. The total number of cells recorded consists of the cells recovered from the culture as well as those left over inside the collagen structures and polystyrene (Figure 4). All seeding methods are compared to their appropriate structure to demonstrate the significance of each seeding technique for a particular condition. A similar number of cells is left on the polystyrene structure across all conditions and the major variations come from the cells that have been harvested from the structures, except for the samples recovered with a "Filter" technique, where a large number of cells still remaining within the culture structures can be observed. For seeding on polystyrene, the different seeding techniques demonstrate small variation with a few exceptions. The orbital shaker seeding method causes a slight increase in the number of cells reported in Figure 8E (****$p<0.0001$) recovery method. A slight decrease can be observed in the centrifugal seeding as compared to static for filtered recovery (*$p<0.05$) (Figure 8D), however in combined mechanical and filtered treatment (Figure 8E) the same seeding method on polystyrene causes a slight increase in the number of cells recovered (*$p<0.05$). Assessment of seeding on two-dimensional collagen films does not yield a consistent trend across all recovery conditions. For the recovery treatments involving a filter, no significant variation is observed. For treatments involving mechanical recovery alone a slight decrease for centrifugal seeding was identified when compared to the static technique (*$p<0.05$), but only for the 50 µL samples. For 3D scaffolds, however, a more distinctive pattern emerges. Consistently across all recovery methods, centrifugation significantly increases the total number of cells in the sample for both scaffold sizes with a greater impact on smaller scaffold size, where the observed increase in cells recovered is almost 10-fold. Additionally, a significantly higher number of cells that remain within the scaffold structures was recorded for dynamic seeding techniques compared to static. The orbital shaker method also demonstrated a significant increase in total cell number compared to static seeding, with few exceptions, however not as drastic as that exhibited by the centrifugation technique. Overall, it was ascertained that the larger three-dimensional scaffolds are not as efficient for cell growth when compared to the control and the 2D films, however, the smaller scaffolds appear to outperform the other conditions when centrifugal seeding is employed.

After determining the optimal seeding technique, which would permeate the scaffold and deposit the cells deep within the structure, a recovery method must be developed in order to harvest the cells from the collagen structures so that they can be analyzed further. Five various recovery techniques were tested in order to determine which would demonstrate the highest yield of recovered cells (Figure 9). A significant increase in the cells recovered following mechanical agitation of the suspension (*$p<0.05$, **$p<0.01$) from polystyrene controls was observed (Figure 9A), however, it was not consistent with the results obtained from dynamic seeding techniques. For both centrifugation and orbital shaker seeding no significant

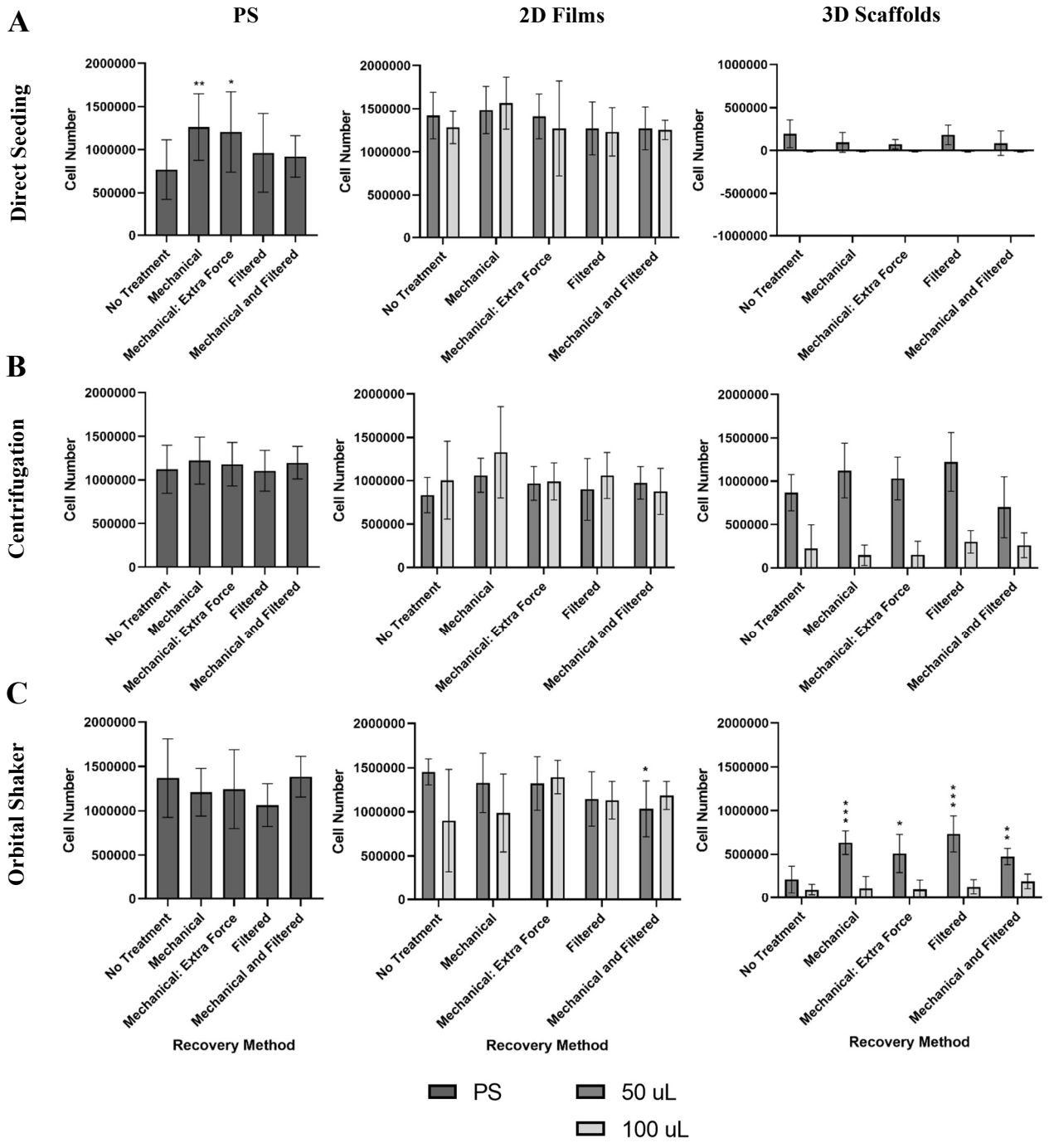

Figure 9. Cell recovery from cultures method evaluation. Five recovery methods were compared, and the number of cells retrieved from the various conditions was reported by staining the cells with Alamar Blue and analyzing the fluorescence values. Three culture systems were studied: 2D films, 3D scaffolds and polystyrene control, with the collagen containing samples further split into 50 µL and 100 µL size structures. Each recovery technique was evaluated across three separate seeding techniques. Cells were stained with Alamar Blue and fluorescent response was analyzed (Data reported as Mean ±SD, t-test two-tailed, (*) $p < 0.05$, (**) $p < 0.01$, (***) $p < 0.001$, (****) $p < 0.0001$). (**A**). Direct seeding was employed. (**B**). Dynamic seeding technique of centrifugation at 1500 rpm for 10 seconds was used. (**C**). Dynamic seeding technique of maintaining the cells on an orbital shaker throughout the incubation period was adopted.

difference was observed between various recovery methods (Figure 9B and 9C). For 2D films a slight decrease is identified for the mechanical and filtered treatment of 50 µL scaffolds in the orbital shaker seeding method (*$p<0.05$), however, no significant differences are observed for the 100 µL films. For 3D scaffolds a greater variation in number of cells recovered with the various methods is evident, however the results do not appear to be consistent across the seeding methods. For direct seeding and centrifugation techniques no statistically significant difference is observed between the recovery techniques (Figure 9A and 5B). For the orbital shaker seeding method it was observed that all recovery techniques significantly increase the cell number recovered from the 50 µL scaffolds, but not for the larger scaffold size (Figure 9C).

The number of cells recovered from the structures was also assessed with an application of HOECHST dye (See Appendix 2). The cell numbers reported were significantly lower due to the variation in analysis of soluble signal in Alamar Blue assay vs the HOECHST where the signal would be speckled throughout the suspension. Due to this difference in fluorescence signal, Alamar Blue was selected as the preferred method to generate more reliable data for our experimental purposes.

3.4 Survival of Cells in Various ECM Conditions

Assessment of survival of three leukemia cell lines was carried out on films and scaffolds composed of various combinations of ECM components. Films and scaffolds were prepared according to the protocols previously confirmed. Each cell line exhibited a unique preference for ECM combinations. The cells were recovered from the scaffolds and an assessment of both the number of cells recovered and left on the original plate was carried out to establish a total number of cells that grew in each condition.

3.4.1 AML OCI-2 Cell Survival in combination with ECM Components

AML OCI-2 cell line demonstrates an overall lower survival rate on films and scaffolds as compared to the polystyrene controls (Figure 10). Although some of the two-component films show a higher number of cells, they do not appear statistically significant (Figure 10A). For 3D scaffolds however, a noteworthy decrease in cell viability is observed with components other than collagen present in the formulation (Figure 10A). High concentrations of HA (0.7%) of both sizes (nano and micro) cause a significant drop in cell survival (**$p<0.01$) compared to the cell grow on the polystyrene control. Other concentrations of hydroxyapatite powders (0.3% and 0.5%) demonstrate a drastic decrease in cell survival as well. Scaffolds containing elastin fibers displayed a higher rate of survival when compared to hydroxyapatite-containing scaffolds, however, still exhibit a significantly lower growth than the 1% collagen scaffolds without other components (*$p<0.05$). Finally, cell growth on the 1% collagen scaffolds was not significantly different

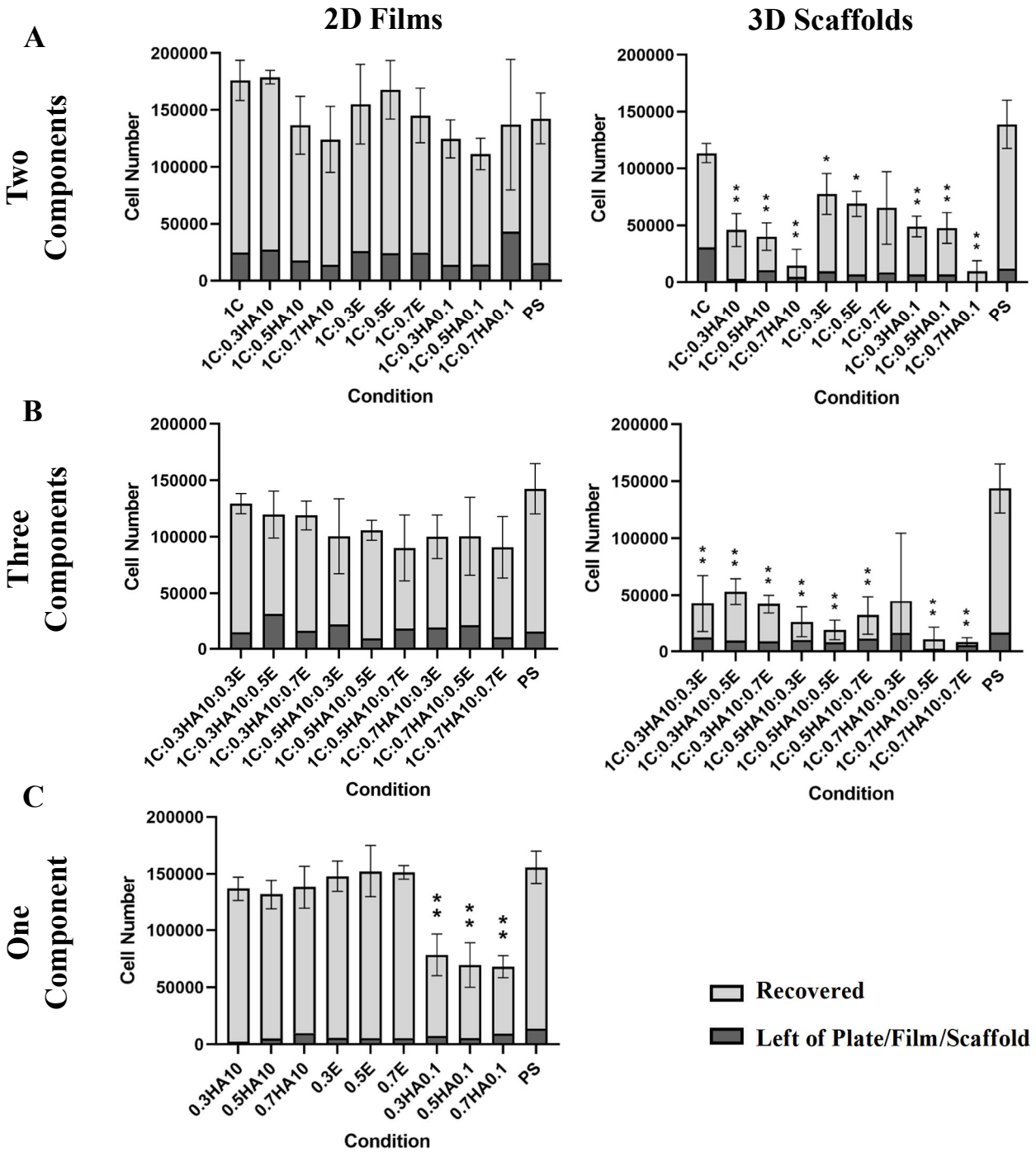

Figure 10. Examination of survival of AML OCI-2 cells in culture with various extracellular matrix component in suspension, on collagen films and in 3D scaffolds. Cells were seeded at 50,000 cells per condition and incubated for 72 hours at 37ºC with 5% CO_2. After incubation the cells were harvested and analyzed for metabolic activity with the Alamar Blue stain for both the recovered cells and those remaining in the original culture conditions (Data reported as Mean ±SD, t-test two-tailed, (*) $p < 0.05$, (**) $p < 0.01$, (***) $p < 0.001$). (**A**). 2D Films and 3D Scaffolds composed of collagen and one other extracellular matrix component at three different concentrations: hydroxyapatite 10 µm (HA10), hydroxyapatite nano powder (HA0.1) or elastin (E). (**B**). 2D Films and 3D Scaffolds composed of collagen (1%C) and various concentrations of hydroxyapatite 10 µm (HA10) and elastin (E). (**C**). Extracellular matrix components in media suspension.

from that of the polystyrene control. For films composed of three components an overall decrease in cell viability is observed compared to the polystyrene controls, however the results do fail to demonstrate a statistically significant decline in cell growth (Figure 10B). Three component 3D scaffolds demonstrate a significant decrease in cell survival as compared to the control (**$p<0.01$), with one exception present in the 1C:0.7HA10:0.3E sample, however a high standard deviation evident here can account for the lack of significance (Figure 10B). Testing of components in media solution without the collagen films and scaffolds reveals that presence of Hydroxyapatite nano powder (HA0.1) significantly decreases cell viability (**$p<0.01$) across all concentrations (Figure 10C). Elastin fibers do not alter cell growth compared to the polystyrene control and a slight decrease in cell growth can be observed in the presence of Hydroxyapatite 10 μm (HA10). Across all films and scaffolds a similar number of cells can be seen remaining in the scaffolds comparable to that of the polystyrene controls, with no statistical significance observed.

3.4.2 AML OCI-3 Cell Survival in combination with ECM Components

AML OCI-3 cell line demonstrates a different behaviour pattern (Figure 11). For two component formulations of the 2D films most combinations demonstrate a decrease in cell viability from the polystyrene control, apart from high concentration of Elastin (0.7% E) and low percentage of hydroxyapatite nano powder (0.3% HA0.1). The significant decrease in cell growth (*$p<0.05$) is observed in high Hydroxyapatite 10 μm (0.7%HA10) films and median concentration of nano powder hydroxyapatite (0.5%HA0.1) films (Figure 11A). For 3D scaffolds composed from two components the same two conditions exhibit the lowest reported cell numbers. Other conditions demonstrate a significant decrease in reported cell numbers; however, presence of elastin demonstrates a less drastic decrease, with the 0.5% Elastin Collagen Scaffold exhibiting the lowest drop in cell number compared to control across all scaffold conditions tested. The high concentration of nano powder Hydroxyapatite (0.7%HA0.1) shows the same significance, however a vast standard deviation can be observed here as well. Increased cell viability was not achieved in the 2D films composed of three components either (Figure 11B), where all conditions demonstrate a notable decrease in cell viability. For 3D scaffolds composed of three components a similar trend to the two components can be observed, where majority of conditions prove detrimental to cell survival (Figure 11B), with most conditions demonstrating a statistically significant drop in reported cell numbers compared with the control. Testing the components in the absence of the collagen films and scaffolds revealed some interesting trends (Figure 11C). In the presence of hydroxyapatite 10 μm (HA10) a slight decline in cell growth can be observed. Additionally, the presence of hydroxyapatite nano powder (HA0.1) appears to decrease cell viability with the 0.3% and 0.7% concentrations demonstrating noteworthy results. Finally, the presence of elastin in the cell media does not appear to interfere with cell growth as some reported values were higher than that of the control condition.

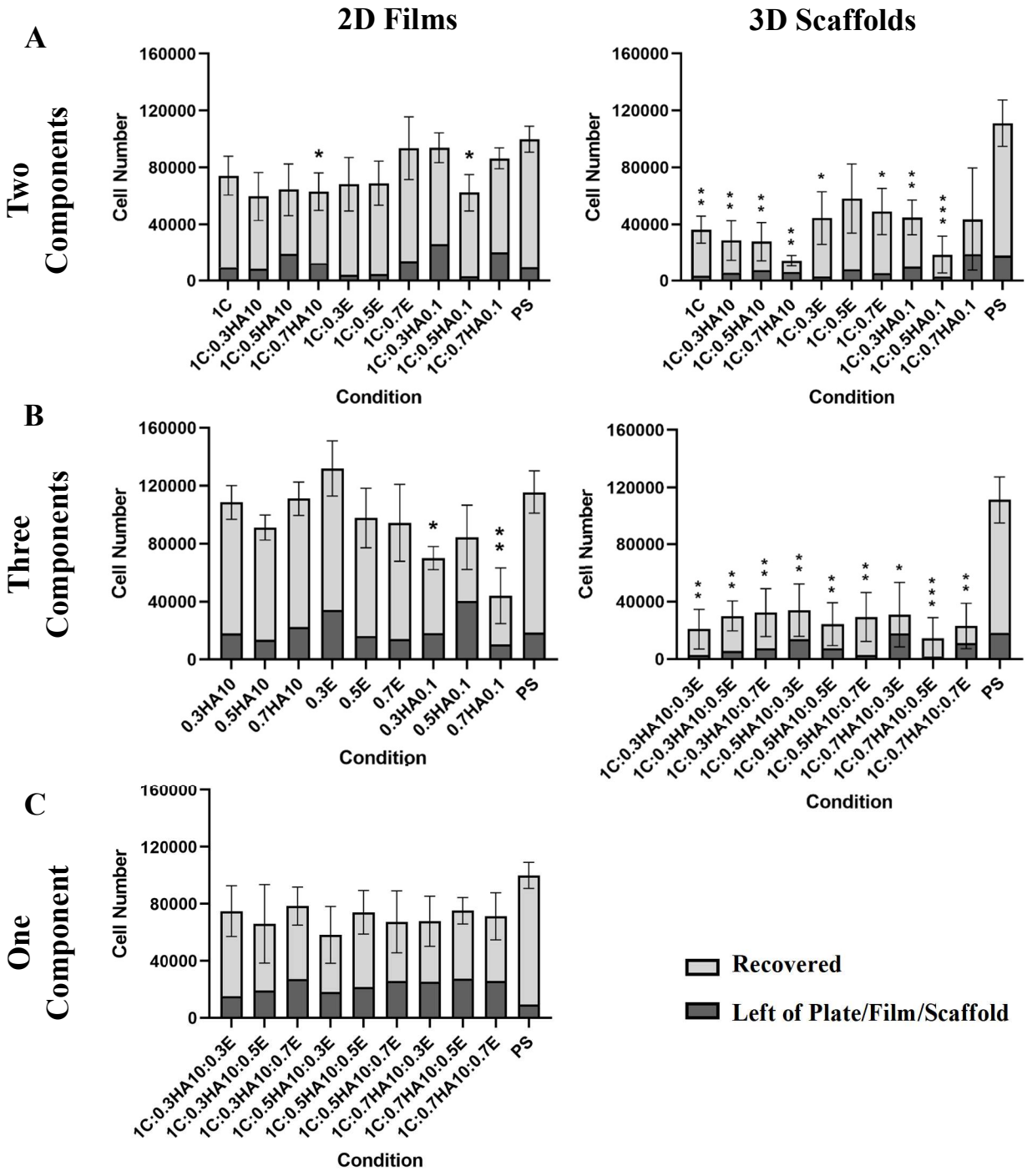

Figure 11. Examination of survival of AML OCI-3 cells in culture with various extracellular matrix component in suspension, on collagen films and in 3D scaffolds. Cells were seeded at 50,000 cells per condition and incubated for 72 hours at 37°C with 5% CO_2. After incubation the cells were harvested and analyzed for metabolic activity with the Alamar Blue stain for both the recovered cells and those remaining in the original culture conditions (Data reported as Mean ±SD, t-test two-tailed, (*) $p < 0.05$, (**) $p < 0.01$, (***) $p < 0.001$). (**A**). 2D Films and 3D Scaffolds composed of collagen and one other extracellular matrix component at three different concentrations: hydroxyapatite 10 µm (HA10), hydroxyapatite nano powder (HA0.1) or elastin (E). (**B**). 2D Films and 3D Scaffolds composed of collagen (1%C) and various concentrations of hydroxyapatite 10 µm (HA10) and elastin (E). (**C**). Extracellular matrix components in media suspension.

3.4.3 K-562-GFP Cell Survival in combination with ECM Components

Finally, the last cell line, K-562-GFP demonstrates a third growth pattern (Figure 12). For the 2D films composed of collagen and one other component an overall increase in cell growth can be seen compared to the polystyrene control (Figure 12A), with two conditions demonstrating statistical significance: the 1% collagen film, demonstrating the highest overall number of cells reported across all conditions tested as well as the 1% Collagen, 0.3% elastin condition. A slight linear correlation can also be seen between increasing concentrations of hydroxyapatite 10 μm (HA10) and decreasing cell growth. For 3D scaffolds composed of two components a similar correlation is observed, however it is much stronger with the 0.3% of Hydroxyapatite (HA10) demonstrating only a slight decline in reported cell number, followed by the 0.5% HA10 (*$p<0.05$) and finally the 0.7% HA10 demonstrating the largest drop in cell number (***$p<0.001$). Presence of hydroxyapatite in nano powder form also significantly decreases the number of cells observed, with the lower HA0.1 concentration 0.3% showing the most drastic drop (***$p<0.001$) followed by the 0.5% (**$p<0.01$) and a slightly larger cell number observed in 0.7% HA0.1, however a much larger standard deviation is observed here as well. The presence of elastin components does not significantly alter cell viability in culture as compared to the polystyrene control. For 2D films composed of three components no condition demonstrates a significant increase in cell survival rates as observed in the two component 2D films (Figure 12B). The presence of high concentrations of HA10 (0.7%) appears to decrease cell viability with lowest reported cell numbers in 1C:0.7HA:0.37 film condition. For the 3D scaffolds again, a considerable decrease in cell number accompanying the high HA10 concentrations (***$p<0.001$) can be detected and lower concentration of hydroxyapatite also demonstrate a notable decrease in cell number with variable significance. Additionally, higher concentration of Elastin (0.7%) combined with hydroxyapatite demonstrate a marginally higher cell number compared to those exhibited by lower elastin concentrations. The number of cells remaining on the films and scaffolds does not appear to be remarkably different from that of the control sample set. Finally, the assessment of the components without the presence of collagen films and scaffolds reveals some other noteworthy trends (Figure 12C). Unlike the collagen containing samples, here the presence of Hydroxyapatite 10 μm (HA10) appears to increase the number of cells observed, with the highest 0.7% HA10 concentration demonstrating the largest reported number of cells in absence of collagen. The presence of nano powder hydroxyapatite appears to decrease cell viability across all concentrations. Elastin does not appear to substantially alter the reported cell numbers.

Overall, it became evident that the growth patterns varied widely across all the different growth environments tested due to the differences in physical and chemical properties of each of the different cell lines. No one single condition has proven to be favorable for cell growth for all three cell lines tested. The

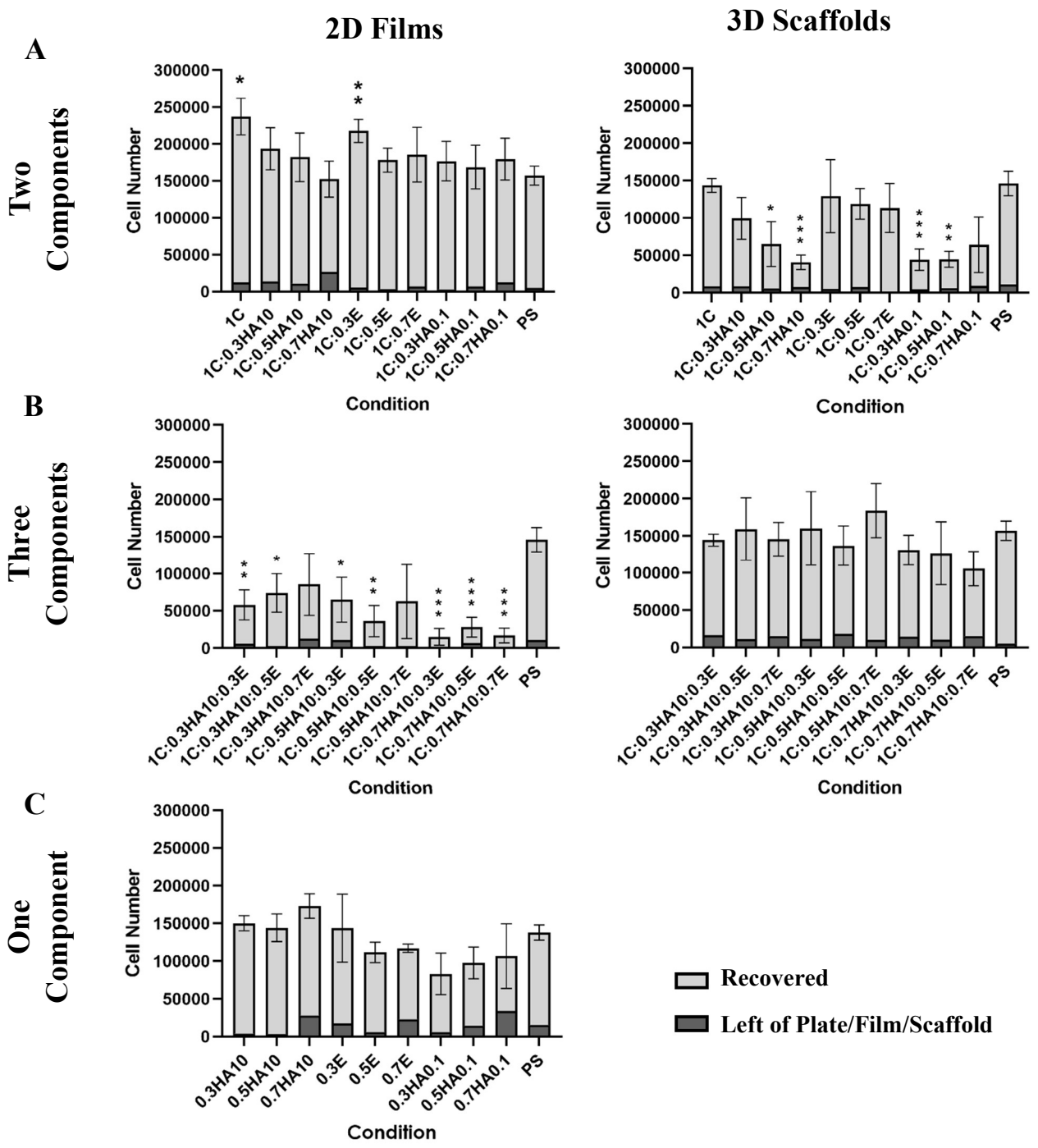

Figure 12. Examination of survival of K-562-GFP cells in culture with various extracellular matrix component in suspension, on collagen films and in 3D scaffolds. Cells were seeded at 50,000 cells per condition and incubated for 72 hours at 37ºC with 5% CO_2. After incubation the cells were harvested and analyzed for metabolic activity with the Alamar Blue stain for both the recovered cells and those remaining in the original culture conditions (Data reported as Mean ±SD, t-test two-tailed, (*) $p < 0.05$, (**) $p < 0.01$, (***) $p < 0.001$, (****) $p < 0.0001$). (**A**). 2D Films and 3D Scaffolds composed of collagen and one other extracellular matrix component at three different concentrations: hydroxyapatite 10 µm (HA10), hydroxyapatite nano powder (HA0.1) or elastin (E). (**B**). 2D Films and 3D Scaffolds composed of collagen (1%C) and various concentrations of hydroxyapatite 10 µm (HA10) and elastin (E). (**C**). Extracellular matrix components in media suspension.

condition that leads to the highest expansion rates of the AML OCI-2 cells is a 2D film (1%C:0.3%HA10). For AML OCI-3 no condition improves cell survival rates compared to the polystyrene control, however several conditions appear on par with it. For the K-562-GFP cells the 2D 1% Collagen matrix represents the optimal environment for cell growth. 3D scaffolds do not appear to increase cell growth across and conditions; however, the 1% collagen has demonstrated survival rates similar to the control data, with the exception of AML OCI-3 cell line.

3.5 AML OCI-2 Response to Treatment with Antileukemic Agents Across Various ECM Conditions

Testing of the AML OCI-2 cell line in with three different chemical compounds demonstrated variation between the different ECM compositions of films and scaffolds. The three compounds tested were DMSO – serving as the control, 10 μM Thioridazine in DMSO (Cat.# T9025, Sigma-Aldrich Co. Ltd., UK) and 10 μM Cytarabine in DMSO (Cat.# 147-94-4, Sigma-Aldrich Co. Ltd., UK). The compounds were analyzed within the same combination of conditions as seen in Figures 10-12; however the cells were not recovered from the scaffold structures after incubation and the films and scaffolds were stained directly for analysis.

For 2D films, analogous patterns can be observed as those seen in the absence of DMSO when cells are recovered from the films (Figure 10). Most conditions demonstrate a growth pattern similar to the polystyrene control with a few exhibiting a slight decrease in cell number (Figure 13A and 12C). The highest decrease is seen in the 1% Collagen and 0.7% Hydroxyapatite 10 μm condition. Assessing response of cells to thioridazine, for the two component films, similar conditions that exhibited a significant decrease in cell survival in the control demonstrate a drop in cell number when treated with the drug. Cellular response to cytarabine shows that the drug was successful in drastically reducing cell growth across all conditions, one condition does present a result that's notably different from the polystyrene control – the 1% Collagen and 0.7% Hydroxyapatite 10 μm condition, where the number of cells present in solution is drastically smaller than in the polystyrene control ($*p<0.05$). For three component films, however, more conditions demonstrate a higher cell number than the polystyrene control when treated with DMSO, especially those containing higher concentrations of hydroxyapatite, which in the absence of elastin demonstrated a decrease in cell survival. Cellular response to treatment with both anti-leukemic agents displays a decrease in cell number when compared to the response seen in polystyrene, however these reductions are not substantial enough to establish significance.

For 3D scaffolds an overall decrease in cell number is seen across all conditions compared to the polystyrene control (Figure 13B and 13D), with several conditions exhibiting statistically significant decline in cell number. Two-component scaffolds that incorporate Hydroxyapatite 10 μm (HA10) in their matrix do not significantly alter the reported cell numbers when treated with DMSO and compared to the

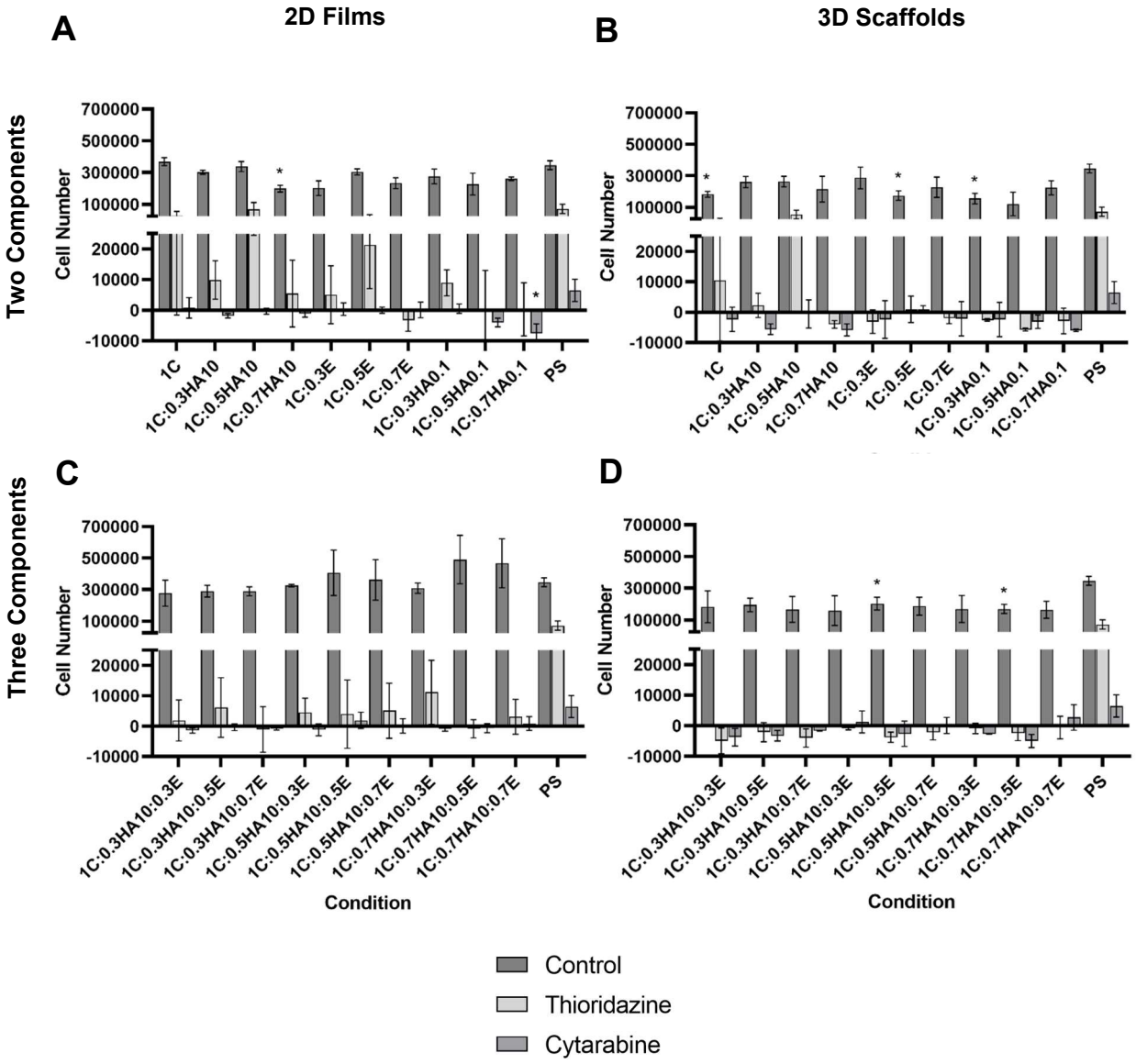

Figure 13. Drug response variation across various ECM conditions. Three chemical compounds were evaluated for divergent response across the distinct matrices mimicking ECM (C-collagen, E – elastin, HA10 – Micro Hydroxyapatite <200nm, HA0.1 – Nano Hydroxyapatite ~10 µm). Cells were seeded at 50,000 cells per condition and one of the three selected chemical compounds was added at concentration of 10 µM. The cells were then incubated for 72 hours at 37ºC with 5% CO_2. After incubation the cells were analyzed for metabolic activity with the Alamar Blue stain by directly staining the cells within their growth medium and evaluating solution fluorescence (Data reported as Mean ±SD, Welch Anova multiple comparison test, (*) $p < 0.05$, (**) $p < 0.01$). (**A**). 2D films composed of collagen matrix and one additional component (Elastin, Hydroxyapatite 10 µm or Hydroxyapatite nano powder) at three different concentrations – 0.3%, 0.5% and 0.7%, compared to the polystyrene controls. (**B**). 3D scaffolds composed of collagen matrix and one additional component (Elastin, Hydroxyapatite 10 µm or Hydroxyapatite nano powder) at three different concentrations – 0.3%, 0.5% and 0.7%, compared to the polystyrene controls. (**C**). 2D films composed of collagen matrix and two additional components (Elastin and Hydroxyapatite 10 µm) at three different concentrations – 0.3%, 0.5% and 0.7%, compared to the polystyrene controls. (**D**). 3D scaffolds composed of collagen matrix and two additional components (Elastin and Hydroxyapatite 10 µm) at three different concentrations – 0.3%, 0.5% and 0.7%, compared to the polystyrene controls.

polystyrene control, however other components at certain concentrations appear to significantly decrease cell survival. When examining the data from the three-component assay an overall decrease in cell number can also be seen with the conditions containing higher Hydroxyapatite 10 μm (HA10) concentrations and 0.5% Elastin exhibiting a statistically significant cell number reduction. Presence of thioridazine substantially decreases the amount of cells reported in the polystyrene condition, however, in the 3D scaffold conditions the decrease in cell number is more drastic, with lower reported cell numbers observed compared to the polystyrene control across all but one condition: the scaffold composed of 1% Collagen and 0.5% Hydroxyapatite, where the resulting cell number is on par with the control, indicating the condition does not provoke an altered response to the chemical agent. Interestingly, the same matrix composition tested in the presence of varying concentrations of elastin in the three-component assay (Figure 13D) demonstrates a reduction in cell numbers compared to control, indicating that elastin in combination with hydroxyapatite in 3D scaffolds can cause enhanced drug response. Cellular response to cytarabine in the scaffolds is similar to the polystyrene condition, here no condition exhibits an increase in cell number, with most demonstrating a higher reduction in the reported cell numbers.

3.6 High-throughput drug screening assay

The various testing conditions optimized throughout this manuscript were employed in order to conduct a high-throughput drug screening evaluation of the variation in drug response in the two novel collagen culturing systems: the two-dimensional films and the three-dimensional scaffolds. Both of these structures were prepared using slurry volume of 100 μL per well and the composition of the structure was chosen to be 1% collagen, without any additional ECM components. From the Tocris Mini 2.0 Compound Library, consisting of 1250 compounds, 157 compounds were randomly selected, and three additional chemical compounds were added for a total screen consisting of 160 chemical agents. The three components that were added were: DMSO, ara-C and TDZ. For the full list of chemical agents screened and brief summary of their target and effect see Appendix 3.

Evaluating cellular response to the chemical agents in the traditional polystyrene condition (Figure 14A), of the 160 compounds tested 60 (38%) drugs exhibit an increase in cell number of greater than 125% of the DMSO control sample, indicating a favorable effect on the growth of the AML OCI-2 cells. 26 compounds (16%) demonstrate a significant reduction of cell number below 25%, this is indicative of a total cell number that is below the 50,000 cells seeded onto each testing condition. 19 compounds (12%) demonstrate a reduction of the final reported cell numbers to the 25-75% of the DMSO control. And finally, the remaining 54 compounds (34%) exhibit cell numbers comparable to the control sample, with the average cell numbers of 75-125% of the DMSO control.

A drastic difference is observed when the same compounds are evaluated on the 2D collagen film culture (Figure 14B). First, only 1 (>1%) compound was able to cause an increase of cell number above 125% of the DMSO control. A similar number of compounds 23 (14%) as seen in the PS assay decreased cell number below 25% of the DMSO control condition. 61 (38%) chemical agents caused a reduction in cell number to 25-75% of the control. And a larger number 75 (47%) drugs demonstrated a final cell number similar to the control, indicating a lack of effect on cell survival. Finally, evaluation of the response of these 160 compounds on the 3D collagen scaffolds reveals a third pattern (Figure 14C). Surprisingly a higher number of compounds – 7 (4%), increase the amount of cells present to above 125% of the DMSO control condition, than we observed in the 2D culture. Next, 43 compounds (27%) demonstrate a decrease below the threshold of cells that were initially seeded >25% of the control (less than 50,000 cells), which is the highest number of compounds among the three tested conditions. 61 compounds (38%) demonstrate a cell number reduction to 25-75% of the DMSO control and finally, 49 compounds (31%) exhibit cell numbers comparable to the DMSO control (75-125%).

To summarize the variation of response to each of the drug a quantitative venn diagram was constructed (Figure 14D) using eulerAPE[233]. Each circle represents the response of the cells to the 160 screened agents in the appropriate culture condition. The overlap shown in the center, between all three culture systems, encompasses 30 various compounds and implies that these drugs cause a similar effect in all three conditions, such as a reduction or increase of cell number (ara-C is an example of a compound that reduces cell number below 25% in all three conditions and would fall into this category). The overlap observed between PS and 2D Films demonstrates that on top of the 30 compounds that behave similarly in all conditions an additional 31 compounds exhibit an analogous response to the drugs amongst the two culture conditions (Autophinib is a compounds that exhibits a similar response in the PS and 2D culture system of an increased average cell number, however in the 3D culture system it demonstrates a decrease in cell number below 50%) and 99 compounds diverge in their response between the two culture systems. The overlap seen between the traditional PS system and the 3D collagen scaffolds is smaller with only 13 compounds exhibiting similar responses, however as expected the overlap between 2D collagen films and 3D collagen scaffolds is the largest with 43 compounds exhibiting similar response (BRD 73954 is a compound that demonstrates a reduction in cell number in the collagen containing systems to approximately 65% of the control, whereas in the PS system the compounds indicates a benefit to cell growth with the average reported cell amount of 140% of the DMSO control).

In Figure 14E, the 160 compounds are arranged into six categories based on their targets: Enzymes, Nuclear Receptors, 7-TM Receptors, Ion Channels, Transporters and Cell Biology. Each category is further subdivided based on primary action (inhibitor, activator etc) and further arranged based on cellular response

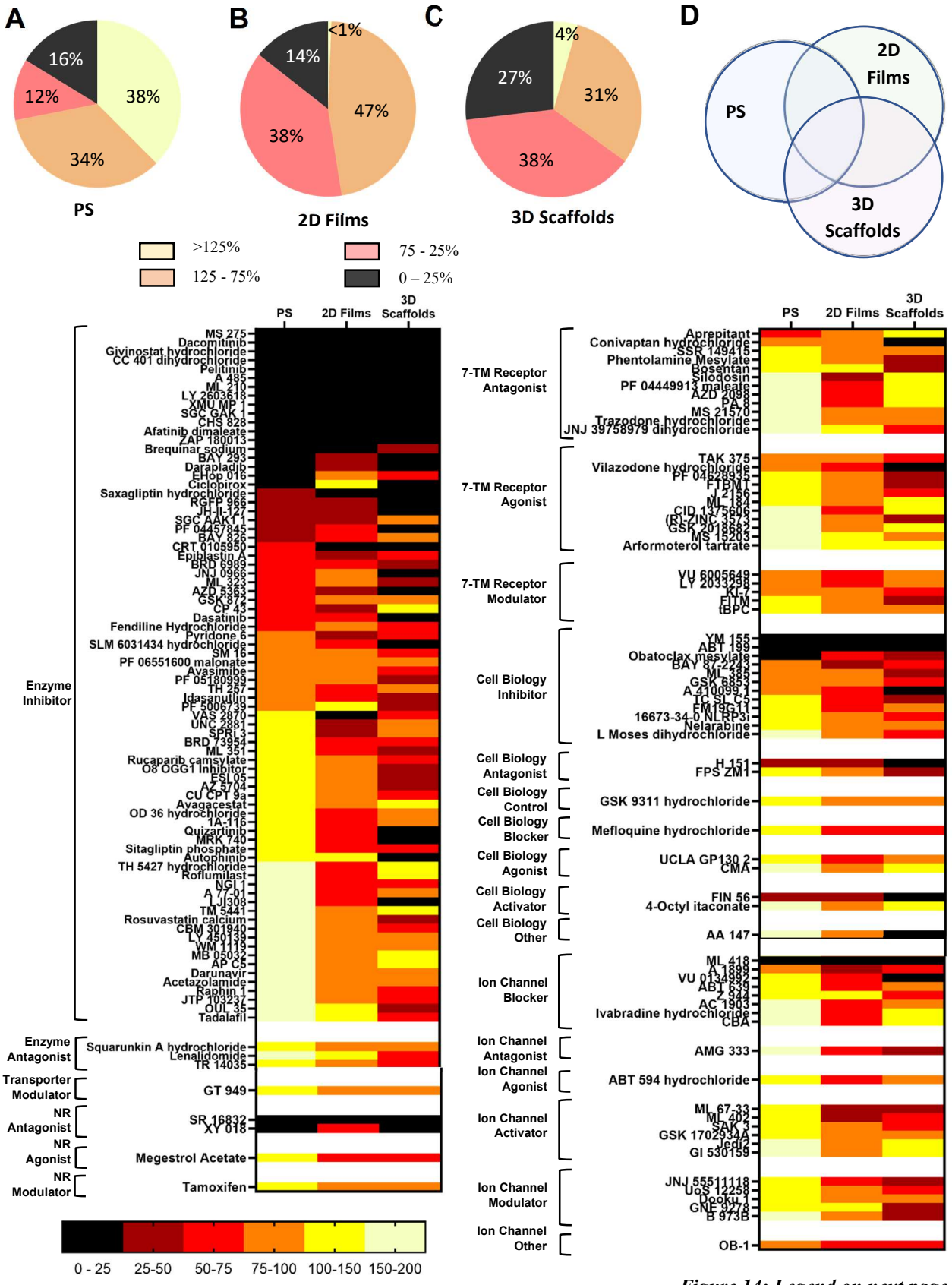

Figure 14: Legend on next page

in the PS condition (from the lowest to highest observed numbers). In this heatmap some trends become evident, the majority of conditions exhibiting drastic decrease in cell numbers act as enzyme inhibitors, with 13 drugs demonstrating cell number reduction below 25% of the DMS0 Control out of a total of 17. Although a large portion of Enzyme Inhibitors also demonstrated an increase in cell numbers in the PS matrix, in the collagen containing assay these conditions fail to effectively increase cell numbers, where a chemical that demonstrates an increase in PS and 2D films, still demonstrates a significant decrease in cell number in the 3D scaffolds (OUL 35 and Tadalafil). The chemical agent modulating a cell transporter – GT 949 demonstrates a final resulting cell number comparable to control across all three conditions tested. The drugs that act as nuclear receptor antagonists - SR16832 and XY018 – demonstrate a significant decrease in cell number across all conditions, however the chemical agents that act as an agonist – Megestrol Acetate or modulator – Tamoxifen of nuclear receptors demonstrate only a small reduction in cell number in the collagen containing conditions as compared to PS. The chemical agents targeting the 7-TM Receptors overall show an increase in the number of reported cells regardless of the action of the drug. Aprepitant presents the one exception, where the cell number is significantly reduced in the PS condition, however the cell numbers reported in the collagen containing assays are similar to the DMSO control. The drugs targeting cellular biology range in their response in the PS condition, however all of them exhibit a decrease of cell number below the control when tested in the presence of collagen matrices. Noteworthy is a drug that acts as an ER proteostasis regulator – AA 147 demonstrates a significant increase in cell number in the PS condition, but an almost complete abatement of cells in the 3D scaffolds. Finally, the chemical agents targeting Ion Channels demonstrate and overall increase in cell numbers in the PS conditions, while slightly decreasing the average cell numbers observed in the collagen matrices. One exception is a potassium channel blocker - ML 418, which reduced cell numbers below 25% in all conditions. Another two exemptions come in the form of a two-potassium channel blocker – A1899 and stomatin-like protein-3 oligomerization inhibitor – OB-1, which demonstrate a reduction in cell number compared to DMSO control across all three conditions tested. Overall, it is evident that the three culture conditions exhibit unique patterns of response to the various chemical compounds tested in our assay.

Figure 14. Summary of the Results from the Drug Screening of TOCRIS Chemical Compound Library. A total of 160 compounds from the chemical library were screened to monitor the effect on growth of AML OCI-2 cells in different matrix conditions (PS, 2D films, 3D scaffolds) after allowing the cells to grow for 72 hours at 37ºC with 5% CO_2 in the presence of chemical agents the cell numbers were assessed via direct staining with Alamar Blue. Fluorescence was evaluated with a microplate reader and the resulting values were normalized to the DMSO control of the appropriate matrix condition. (**A-C**) Pie charts summarizing the number of responses seen with the 160 defined compounds (**D**). Summary of the compounds demonstrating the variation of response between the three culture conditions (response considered different if >25% difference is observed). (**E**) Heat map demonstrating patterns in cellular response to the screened chemical agents in three separate culture conditions. The results are organized based on target molecule, mechanism of action in order of increasing cell number observed in the PS condition (Data reported as normalized mean and color coded based on 6 categories, n=3).

A detailed examination of the patterns between the standard PS cultures and those containing collagen reveals several compounds of interest which exhibit statistically significant variation between the culture conditions (Figure 15). Examination of the patterns of behavior between two conditions reveals several compound behaviours: compounds that perform similarly between the two conditions, drugs that cause a reduction of cell number below 25% in both conditions and chemical agents that demonstrate a significantly higher amount of cells in one condition, which is further subdivided into groups based on degree of significance and which condition demonstrates a higher result. The summary of the results corresponding to compounds is detailed in Appendix 4.

Figure 15A demonstrates the variation in cellular response between the 2D cultures: PS and the 2D collagen films. Of the seven compounds that have a lower average cell number in PS, one of them demonstrates a $^{**}p<0.01$ value between the two conditions, an NK1 receptor antagonist – Aprepitant. However, as previously observed a higher number of compounds, 48, lead to significantly decreased growth in the 2D conditions rather than PS. From these 3 compounds indicate a $^{***}p<0.001$ significance between the two conditions: Jedi-2 – a Piezo1 channel activator, A-77-01 – a potent inhibitor of TGF-βRI and LY 450139 – γ-secretase pseudo-inhibitor. A total of 19 compounds signify a reduction in cell number to under 25% of the DMSO control in both conditions and finally 86 compounds show no significant deviation in the response to the drugs between the two culture conditions.

Although similar categories can be defined the drug response in PS versus 3D collagen scaffold cultures, different compounds of interest emerge (Figure 15B). A total of 22 compounds demonstrate a significant reduction in cell number in both conditions and an additional 95 compounds don't demonstrate any significant difference in response across the two culture systems. Only one compound demonstrated a significantly lower cell number in PS compared to the scaffold – Aprepitant, which appeared to exhibit a similar result in the collagen containing 2D film (Figure 15A). Finally, a total of 42 compounds exhibited significantly lower reported cell numbers in the 3D collagen scaffolds than PS, one of them showing a $^{***}p<0.001$ significance – the LY 450139, which is consistent with the findings from 2D films as well. The last comparison is drawn between the two culture systems developed and optimized in this manuscript: the 2D collagen films and 3D collagen scaffolds (Figure 15C). A larger number of compounds, 119, performed similarly in the two conditions without exhibiting any significance and only 20 chemicals caused a decline of cells to below 25% in both conditions. The difference in response was evident in 21 compounds, where 14 drugs have an increased cell number in the 2D culture compared to 3D and 7 exhibit an increased cell growth in the 3D scaffolds – one of these compounds demonstrates a statistical significance of $^{**}p<0.01$ – the serine/threonine-protein kinase inhibitor CP 43.

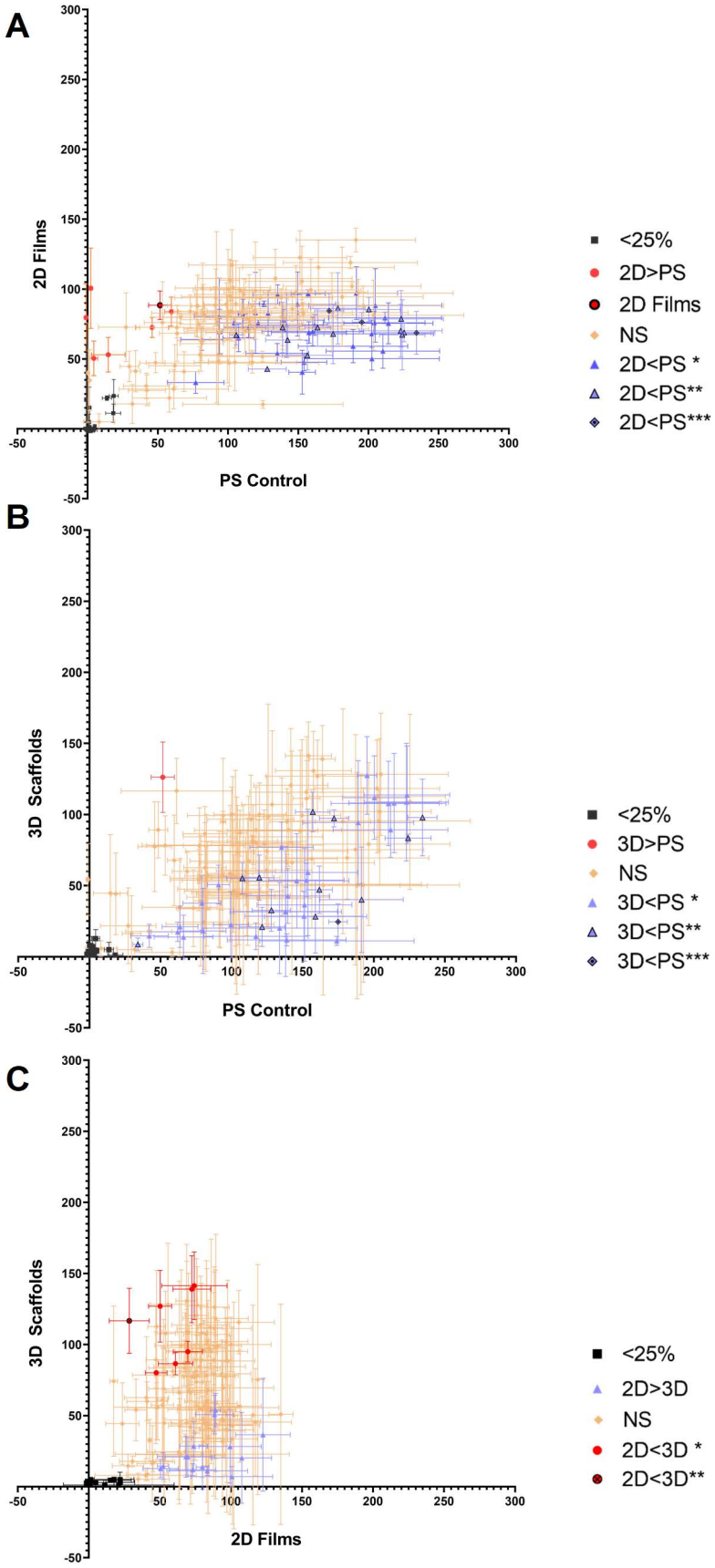

Figure 15. Chemical Screening of TOCRIS Chemical Compound Library for variation of response in different matrix conditions. Scatter plots showing correlation between the average normalized values of reported cell numbers of the AML OCI-2 cells cultivated in different matrix conditions in response to each of the 160 chemical compounds screened defined by reduction of fluorescence in Alamar Blue staining. (Data reported as normalized Mean ±SD, n=3, multiple unpaired t-test (*) $p < 0.05$, (**) $p < 0.01$. (**A**). Polystyrene plates – x-axis and two-dimensional 1% collagen films on the y-axis. (**B**). Polystyrene plates – x-axis and three-dimensional 1% collagen scaffolds on the y-axis. (**C**). Two-dimensional 1% collagen films on the x-axis and three-dimensional 1% collagen scaffolds on the y-axis.

The screening of the AML OCI-2 cells with 160 compounds from the Tocris Drug Library elucidated several compounds that demonstrate a variation in cell response due to the different culture conditions. The drug response between the standard PS culture and cells grown on 2D collagen films demonstrate a moderate correlation r=-61, $P<0.0001$. A slightly higher correlation of r=0.65, $P<0.0001$ is seen between the PS and 3D collagen scaffolds. The smallest correlation emerges between the two collagen containing culture systems – the 2D films and 3D scaffolds r=0.44, $P<0.0001$, however these correlation values are based on average cell numbers for each condition and do not take the standard deviation into account.

Chapter 4. Discussion

4.1 Collagen Suspension Formulation

The preparation of collagen films and scaffolds has been extensively characterized[220,228], however there is much variation for the diverse purposes that these structures are employed in. Therefore, it is important to derive a consistent method which is applicable to our specific goal of growing and studying leukemia cells on these fabricated films and scaffolds. Before the analysis of cell behavior on these structures can be undertaken, any variation that might occur during preparation of these fabricated extracellular matrices must be minimized, to ensure the future data acquired is properly controlled.

Upon rehydration of type I Collagen flakes with 0.05M acetic acid, the solution is homogenized by utilizing a conventional blender and the temperature is controlled by placing the beaker onto an ice bath. This results in the introduction of a significant number of bubbles into the suspension, which hinders the uniform dispensing of suspension into the casting wells. In order to remove the air bubbles, two separate procedures, that have been previously reported, were assessed. First procedure utilizes a vacuum pump, which removes air bubbles by applying a pressure reduction to the sample, causing the air bubbles to be lifted out of the viscous suspension[220,228.] Second method involves the use of a centrifuge, which causes the air bubbles to travel to the top of solution where they can be easily removed [146,204,214]. Although both methods were successful in significantly reducing both the amount and the size of air bubbles present in samples (Figure 5A and 5B), the centrifugation method was ultimately chosen due to several reasons listed below and centrifugation time was set at 4 minutes total. First, the centrifugation method is more efficient at removing bubbles than vacuum degassing (two tailed t-test between the two data sets demonstrates a $^{**}p<0.01$). Second, for centrifugation the temperature at which the samples are processed can be controlled, which is not possible for the vacuum method, this can lead to collagen fiber precipitation and solution instability. Third reason is efficiency, vacuum degassing is a procedure that takes 4 hours to conduct, and the centrifugation procedure only takes 1-10 minutes, making it a more sustainable and efficient choice. The centrifugation time was set to 4 minutes due to an observed increase in number of air bubbles present in samples that were centrifuged for longer than this period (two tailed t-test demonstrates a $^{**}p<0.01$ between centrifugation for 4 vs 10 minutes).

Introduction of other extracellular matrix components into the collagen suspension presented a new set of challenges. Of the three components that were tested hydroxyapatite in both nano and micro forms presented the biggest hurdle. The basic nature of Hydroxyapatite powder causes an increase in the pH of the collagen suspension (Figure 5C), which in turn leads to precipitation of collagen fibers from the solution, this not only alters the final concentration of collagen per film/scaffold, but it also causes precision

errors during dispensing and the final cast scaffolds appear to have an altered structure as a result. According to previous findings collagen exhibits highest solubility in acetic acid at pH 2.0, which decreases as the pH is raised[234,235]. It follows that as the pH increases with the addition of hydroxyapatite powders the collagen will begin to precipitate from solution. In order to prevent the pH increase of the solution accompanied by the addition of Hydroxyapatite powder the following procedure was developed: collagen suspension is prepared at a higher concentration than desired and diluted down with concentrated acetic acid, ≥99.7% (Sigma-Aldrich Co. Ltd., UK) as the appropriate amount of hydroxyapatite powder is slowly added to the mixture. As is evident from our results in Figure 5C this buffering effect prevents the solution from reaching the pH threshold of collagen precipitation when 4% of concentrated acetic acid is present for both nano and micro particles of hydroxyapatite.

Another property that was assessed upon addition of other ECM components was viscosity. Fluid flow is highly dependent on the viscosity of the solution making it an important factor for dispensing of the collagen suspension, specifically for 3D printing of scaffolds. Shear thinning is characteristic of some non-Newtonian fluids, and this behaviour is advantageous for dispensing – during distribution (high shear rate) the viscosity is low, promoting the flow of the material during casting operations[236–238]. After the material settles (zero shear rate) the viscosity is high promoting the stability of the shape of a uniform scaffold. Our collagen suspension continued to exhibit shear thinning behaviour even with addition of other ECM components (Figure 5D). The decrease in apparent viscosity with the presence of hydroxyapatite could be attributed to the presence of hydroxyapatite crystals in solution, or slight precipitation of collagen occurring due to pH increase associated with hydroxyapatite addition as observed in Figure 5C.

4.2 Optimization of Collagen Films and Scaffolds for Cell Culture

Collagen self-assembles into native-type fibrils in vitro under physiological conditions and these reconstituted fibrillar structures are used as scaffolds in tissue engineering because they mimic the extracellular matrix environment native to cells and offer a degree of natural biocompatibility[239–245]. Assembled collagen fibers form covalent cross-links, which provide it with high tensile strength and enzymatic resistance to degradation, however damage to the linkages upon handling of these fragile structures can cause these links to weaken over time. Additionally, sterilization of scaffolds involves the use of 25kGy gamma-irradiation, which has been shown to induce chain scission in dry collagen molecules causing decreased mechanical strength and increased susceptibility to enzymatic degradation[246–249]. In an effort to increase the mechanical strength of the assembled collagen structures and control the rate of degradation, introduction of additional cross-links within the structure is required[229,230]. This can be achieved with the use of a cross-linking agent by stimulating the formation of covalent bonds between the

amino and carboxyl groups of collagen molecules[231], which prevents the sliding of individual collagen fibers[240,250]. For our research purposes the 1-ethyl-3-(3-dimethylaminopropyl) carbodiimide (EDC) mixed with N-hydroxysuccinimide (NHS), have been chosen because it allows us to adjust the cross-linking concentration and exhibits lower cytotoxicity concerns[240,250]. The carbodiimide cross-links collagen without incorporating into the macromolecule via formation of iso-peptides, thus it can be easily removed after completion of reaction[251]. The by-product of this reaction is urea, which can also be extracted with a gentle rinse without having any negative impact on subsequent cell culture[218,251–257].

I demonstrated here that the cross-linking procedure increases the resistance of the scaffolds to shrinkage and deformation (Figure 6A and 6B) as the decreased concentration of cross-linker is directly related to the degree of scaffold deformation. Although scaffold shrinkage could only be evaluated in one plane, it was observed that the scaffolds shrink in all dimensions, as seen in Figure 6A scaffolds that were not cross-linked appear more transparent as they collapse on themselves no longer able to support the weight, whereas the cross-linked samples are able to hold their cylinder shape and therefore appears more solid. These samples are also able to reform upon deformation, such as depression with a centrifuge tip, the ethanol treated samples, however, do not return to their original shape upon deformation. The percentage of area shrinkage of samples cross-linked at different concentrations clearly shows a pattern of almost a linear correlation of increased scaffold stability as the cross-linker concentration is increased (Figure 6B). Overall, the cross-linking procedure allows us to increase the mechanical strength of our scaffolds and promote scaffold stability to degradation, therefore all scaffolds are cross-linked prior to cell seeding.

Preparation of three-dimensional collagen matrices requires a formation of an interconnected pore network within the structures, which would accommodate cell infiltration, attachment, and subsequent tissue growth. The size of the pores, the degree of interconnectivity as well as the surface area of the scaffolds are all integral parameters that need to be controlled when collagen lattices are employed in tissue engineering[258]. The scaffold pores must be large enough to accommodate cell migration, interconnected enough to provide nutrient and waste diffusion, but small enough to provide a sufficiently high surface area for cell adhesion[221,223]. The pore size and distribution can affect not only cell adhesion, but cell activity, morphology and phenotypic expression which has been a focus of several studies[27,198,208,222,259–262]. Therefore, when creating a porous biomaterial, it is crucial to control the pore structure and interconnectivity of the bioengineered scaffolds[197,221,263–265]. An investigation was conducted into the pore morphology of our composite scaffolds to assess whether addition of other ECM components as well as alterations to collagen scaffold preparation accompanying these components influences the resulting scaffold pores.

All scaffolds contained numerous transverse bridges that connected the pores. In the sample composed of collagen fibers alone, these bridges form longitudinal struts that span the scaffold giving rise to uniform

pore distribution and organized structure (Figure 6C). It is evident from our results, that incorporation of other ECM components causes significant changes in the scaffold structure (Figure 6C-F). Addition of elastin to the collagen slurry and its subsequent incorporation into the scaffold does not appear to significantly alter the pore organization or the number of pores observed in the sampled areas, however it does significantly reduce the average area of the reported pores ($p<0.001$). Elastin particles can be seen in the SEM image as the brighter spots as they accumulate charge extremely quickly (For fiber reference images see Appendix 1). Hydroxyapatite powders of both nano (HA0.1) and micro (HA10) size cause a change in pore organization of the scaffold. The longitudinal struts that span the control collagen samples appear thin and rope-like in the HA-containing samples, causing the lattice to appear irregular and the pore network of dense small pores is observed instead. With the increase in hydroxyapatite particle size the number of pores reported increases and the average pore size shows an apparent decrease. The hydroxyapatite incorporation into the collagen slurry could influence formation of ice crystals, where the component particles can serve as nucleation centers resulting in the altered microstructure of the scaffold [225]. This decrease in scaffold pore size can account for the subsequently observed decrease in cell viability of hydroxyapatite-containing 3D scaffolds as cell infiltration of the scaffold would be hindered.

Type I Collagen employed for the manufacture of films and scaffolds is known to be pH dependent: it's more soluble in acidic conditions and pH increase can lead to self-assembly of collagen molecules into fiber structures which results in a less homogeneous distribution of collagen in the suspension and the resulting structures [266–268]. Although the films and scaffolds must be prepared in acidic conditions, they must be suitable for cell culture experiments upon manufacture. Therefore, I sought to evaluate whether the pH of the resulting structures falls in the physiological range of pH 7.2-7.4. The procedure for construction of 2D films and 3D scaffolds differs after the casting of the collagen suspension solution into appropriate vessels (Figure 1). For preparation of the film coating the aliquoted suspension is allowed to evaporate leaving a layer of collagen film coating in the casting vessel, whereas preparation on 3D scaffolds involves lyophilization of the collagen suspension. This method requires formation of ice crystals within the structure by freezing of the aliquoted collagen suspension. The frozen samples are then lyophilized to produce a pore negative network. This process allows for quick evaporation of acid and causes minimal harm to the collagen protein [269,270]. Therefore, it could account for the overall lower residual acid content observed in all 3D scaffold samples when compared to their 2D film counterparts (Figure 7). Here a clear linear trend between increased percentage of concentrated acetic acid in the formulation and the resulting pH for the 2D films was observed, however the same is not true for the 3D scaffolds. These differences in pH can introduce a variable into the cell culture studies and should be minimized. A wash step appears to play a critical role in normalizing the pH of these structures to the physiological range. For 2D films a significant increase (~0.4) in system pH following a single wash with PBS for 30 minutes can be observed, it is possible

that with additional washes even the high acid content formulations can be brought up to the 7.2-7.4 range. For 3D scaffolds an increase in pH following a wash step can also be detected, however not as drastic (~0.2). For our formulation of interest (1% Collagen Suspension) a single PBS wash is sufficient in restoring the collagen structure environment to the physiological pH range for both scaffold sizes evaluated.

It is clear from the results that the size of the collagen structure plays a role in the final pH value as a larger volume of suspension aliquoted equates to a larger content of acid present in the structure that must undergo evaporation. I therefore sought to evaluate further the effect that the size of the structure ultimately has on the final pH by evaluating structures of 4 different sizes: 25 µL, 50 µL, 100 µL and 150 µL (Figure 7B). Across all sizes the wash step was successful in significantly altering the system pH (t-test, $p<0.0001$), however for the larger sizes evaluated (100 and 150 µL) the pH was not restored to the physiological range, meaning that as scaffold formulation size increases alternative methods need to be explored prior to cell culture in order to control the pH of the formulation. Scaffolds of 50 and 100 µL are used in the current study, therefore an alternative method to adjust the pH of the 3D scaffolds to the appropriate range must be evaluated. Therefore, an evaluation of the wash time as a variable affecting the final pH of the structures was conducted. It is evident that wash time does not appear to significantly affect the final pH as the 24-hour wash time appears to exhibit the lowest pH increase for most conditions tested (Figure 7C). Although the 100 µL 3D scaffolds are outside the physiological range, the utility of sodium bicarbonate in the media can further provide the buffering effect required for cell culture. However, to minimize the variation present across all conditions an alternative technique of increasing the number of washes, rather than the time was evaluated (Figure 7D).

Addition of other extracellular components into the collagen formulation alters the protocol for the collagen suspension preparation, therefore an investigation into how these deviations might affect the subsequent pH of our films and scaffolds was conducted (Figure 7C). Addition of hydroxyapatite powder (both HA10 and HA0.1) leads to a higher pH of structures as compared to our 1% collagen control, however when these were prepared according to the updated protocol with the addition of 4% of concentrated acetic acid, the pH of resulting structures becomes significantly lower than that of the control. Both, however, can be restored to the physiological range to be utilized for cell culture experiments. Overall, addition of concentrated acetic acid into the collagen suspension appears to have a significant effect on the resulting pH of the structures after evaporation/lyophilization, although the original pH of the component suspension is equivalent to that of the control 1% collagen formulation (Figure 5C) due to the balanced pH increase provided by hydroxyapatite powder. This significant pH difference observed in the films and scaffolds does not appear to restore to the physiological pH with the single 1-hour wash, however, the procedure followed post cross-linking of the scaffolds involves three 30-minute washes. It is evident here that the procedure is

sufficient in restoring the pH of all 2D films and 3D scaffolds of both sizes of interest (50 µL and 100 µL) to the physiological range. Therefore, the procedure will remain as described in Figure 1, where following the evaporation/lyophilization step, the structures are then γ-irradiated, cross-linked with EDC-NHS and washed three times for 30 minutes, not only to wash away the cross-linking chemicals and by-products, but also to restore the pH of the structures to the physiological range for cell culture experiments.

4.3 Cell Seeding and Recovery from Collagen Structures

Cell seeding is a critical step in three-dimensional (3D) cell cultures and tissue engineering. It represents the first step to the integration of the cells into the scaffold pores influencing cell density, retention, and spatial distribution within the scaffold, which can have drastic effects on cell growth and differentiation[271,272]. Therefore, the performance of the cell within the scaffolds is determined by the initial seeding efficiency. Effective seeding of cells onto the 3D lattices presents challenges when compared to simple two-dimensional cultures. The optimal seeding technique for cells, would enhance the performance of the tissue engineered scaffolds and would have to satisfy the following criteria: 1) generate spatially uniform dispersion of cells throughout the scaffold, providing basis for uniform tissue regeneration[273], 2) minimize damage to the cells, and 3) demonstrate time and cost efficiency and ease of use[271,274]. Efficient seeding techniques are especially important when scarce patient samples are involved, as the number of cells available for seeding is likely to be very small. It is crucial that the spatial distribution is homogenous and cellular phenotype is maintained by minimizing cell manipulation[275]. A variety of methods have been developed that seek to optimize cellular penetration and distribution within the scaffold structures, which can all be categorized as static and dynamic seeding.

It is worth noting that during the experimental procedure the cells were stained with both the metabolic Alamar Blue stain as well as the Hoechst stain for live cells, both stains were optimized for the application. Alamar Blue has been widely used in cell viability studies for over 50 years and monitors the reducing environment of living cells [276]. The active ingredient – resazurin, is a water-soluble, non-toxic, membrane permeable compound that is stable in culture media. As the indicator dye accepts electrons it changes from the oxidized, non-fluorescent blue form to a reduced, pink state, this allows for measurement of fluorescence as well as colorimetry, however fluorescence is considered more sensitive with readings taken at 530 nm for excitation and 590 nm for emission [277]. The resazurin reduction to resorufin occurs in the mitochondria of cells in response to cellular metabolism [276]. The Hoechst 33342 (2'-[4-ethoxyphenyl]-5-[4-methyl-1-piperazinyl]-2,5'-bi-1H-benzimidazole trihydrochloride trihydrate) dye is a water-soluble, cell permeable, nucleic acid stain composed of a bisbenzimidazole derivative, which binds the minor groove of the double stranded DNA molecule and is used for staining of live cells [278]. Upon binding the dye has an emission signal at 361 nm and excitation at 497 nm [278]. The fluorescent signal of the two dyes do not

interfere and optimization assays were conducted to confirm prior to the experiment. Overall, the Hoechst stain provides the staining of individual cells in assay, whereas Alamar Blue stain changes the overall fluorescence of the solution based on the metabolic activity of the cells within. Therefore, evaluation of cell number with Alamar Blue stain in the given assay would provide a more accurate result, as the individual cell signals provided by the Hoechst stain might be lost within the culture structures decreasing the strength of the fluorescent signal acquired. The results obtained from the analysis of Hoechst fluorescence are provided in Appendix 2.

In my experiments I compared three different seeding methods across a variety of collagen lattice conditions. The first seeding method evaluated was static seeding, which is the most frequently used as it is easy to conduct and does not expose cells to potentially damaging forces[274], however, they have been shown to demonstrate low scaffold penetration, high cell sedimentation and non-uniform distribution throughout the scaffold[279,280]. Our results confer with these findings where for 3D scaffolds the direct seeding technique (Direct 3D) comprised of pipetting the cell suspension directly onto the scaffolds yields the lowest number of cells present across both scaffold sizes tested (Figure 8A). This is not the case for our polystyrene control or the 2D films, as these conditions do not require infiltration of cells into a three-dimensional lattice. The presence of the 2D films appears to be beneficial for cell growth as a higher cell number can be detected in the direct 2D conditions vs direct polystyrene. The second type of seeding methods evaluated was dynamic seeding, this involves application of an external force to enable the cells to infiltrate the lattice structure[272]. Dynamic seeding has been previously reported to exhibit better cell coverage and subsequent growth when compared with static methods[281–283]. Although there is a large variety of dynamic seeding methods that have been extensively studied for a wide range of cell and scaffold types, such as application of vacuum[279], centrifugation[271,284], oscillating perfusion[285], application of low pressure[286] and the use of an orbital shaker[281]. These methods often demonstrate a higher yield number of cells throughout the scaffold, however they also have drawbacks, such as growing complexity and prolonged seeding time, which can result in alterations to normal cell behavior[274,279]. Two of the techniques listed, however, appear to have minimal drawbacks when applied to the purpose of the present study, namely centrifugation and employ of an orbital shaker. Centrifugal seeding is one of the most efficient dynamic seeding methods and the external force applied on the cells by centrifugation did not appear to cause cell damage[271]. It has been demonstrated that a higher centrifugal force causes cells to travel through a three-dimensional lattice faster, hence as the force increases, the time required for seeding should decrese[271]. It is evident from the results that centrifugation was indeed the most efficient seeding method for 3D scaffolds as a significantly higher cell number for the centrifuged samples was detected compared to the direct seeding method across both sample sizes, where in some conditions the cell number increased 10-fold. Although larger scaffold sizes did not perform as well in increasing the cell number as the smaller size

tested, this can be attributed to formation of necrotic cores within larger scaffolds as nutrients aren't able to penetrate the larger structures in order to sustain the cells deep within. For the smaller scaffold sizes, however the total number of cells reported (averaged for all recovery techniques) is higher than that of polystyrene and 2D films, meaning the environment is more favorable for cell growth. It is also reported that a higher number of cells remain trapped in the scaffolds and are not recovered compared to other seeding conditions, which could indicate deeper penetration of the scaffold structures by the cells and therefore a more uniform dispersion. For the polystyrene control the introduction of the centrifugation step does not cause significant changes to the cell number present, with the exception of the recovery methods involving the use of a filter, however these discrepancies can be attributed to the recovery methods rather than the seeding technique. For the 2D films, centrifugation does appear to cause a slight decrease in cell number across some recovery conditions (mechanical and mechanical extra force) for the 50 µL film size, however as it is inconsistent across all conditions the effect is negligible. The last seeding method tested involved the use of an orbital shaker, which provides a continuous perfusion of cells and media through the around the films and scaffolds[281,287,288]. This would provide not only a homogenous distribution of cells throughout the film and scaffold structures, but also increase access to nutrients within deeper areas of the 3D scaffolds[289]. Although a significant increase in the number of cells present in the 3D scaffolds seeded with the orbital shaker is observed when compared to direct seeding method, it is not as significant as the increase accompanying the centrifugation method. Additionally, just as in the centrifugation methods a higher cell number for the smaller scaffold structures 50 µL vs 100 µL scaffolds is seen across all recovery methods, indicating that higher scaffold size is not able to support the number of cells seeded. For the polystyrene control samples, across some recovery methods the introduction of this dynamic seeding technique causes an increase in the number of cells present in the samples. However, for the 2D film samples this particular seeding-/ method does not elicit any changes in cell number recovered compared to the static seeding technique across both film sizes tested. Since the orbital shaker method does not appear as efficient in increasing the number of cells present in the 3D scaffold structures and causes minor inconsistencies in our control and film structures, the seeding method of choice for the cell culture experiments was determined to be centrifugation at 1500 rpm for 10 seconds.

After the cells have been successfully seeded onto the collagen structures and have grown sufficiently, they must be recovered in order for cell analysis to take place, as the expansion and harvest of cells is critical for tissue engineering, especially in the case of patient samples. Several methods have been evaluated, such as enzymatic treatment or use of a bioreactor and filters[209,290]. However, these are not suitable for the intended research purposes as enzymatic degradation of scaffolds would take a considerable amount of time, since the collagen structures have undergone a crosslinking procedure making them more resistant to enzymatic degradation. Additionally, prolonged exposure of the cells to the enzyme while the scaffolds are

slowly being degraded can cause behavioral changes to the cells, with research previously demonstrating it can cause lineage differentiation in certain cell types[290]. Instead, an alternative method of mechanical extraction of cells from the three-dimensional scaffolds was developed, which involves rapid depression of the scaffold structure, presumably causing the cells to be expelled from within the porous structures into the media suspension, which is then collected, and the cells are harvested. A plunger was manufactured consisting of a silicone suction cup made from a 1-mL syringe and a pipette tip for easier handling (Figure 3), the technique chosen involves depression of the structures a set number of times, however, since this is done at a large scale, a control for human error is required, since the application could get inconsistent with time. Therefore, in addition to testing the standard "Mechanical" treatment the effect that the doubling of procedure would cause on cell recovery was evaluated and the "Mechanical: Extra Force" treatment was introduced. It was also observed that during pipetting of cell suspension collagen residue would interfere with pipetting as well as absorb a large portion of the media. In an attempt to prevent potential variations in cell number this may cause, a filter was introduced, which would simultaneously depress the scaffold, preventing media absorption, and prevent uptake of collagen fibers, increasing the efficiency of cell recovery. Finally, a combination of mechanical treatment and the filtration system was also evaluated.

Overall, the results do not demonstrate a clear correlation of a specific recovery method and high yield of harvested cells (Figure 9). Interestingly, for the polystyrene control an increase in recovered cell number across all of our treatments can be observed when compared to a no treatment control, with the mechanical extraction exhibiting a statistically significant increase. However, this trend is not consistent across all seeding methods tested. The 2D films demonstrate a similar behavior to the polystyrene control, and overall show consistent cell numbers recovered across all recovery treatments. With one exception present in the orbital shaker seeding method, where treatments involving the use of a combination of mechanical force and filter show a slight decrease in the number of recovered cells, although high standard deviation of samples is observed here and the same trends aren't present for the 100 µL scaffolds. Finally, for our 3D scaffolds an overall higher number of cells harvested with one of the four recovery treatments when compared to control can be seen, with significantly higher numbers for our smaller scaffold size tested. For the samples seeded onto the 3D scaffolds with the static method the number of cells present is lower than the amount that was initially seeded onto the scaffold (Figure 9A) and is too low for accurate quantitation with our method, which can account for the lack of statistical significance in this data set. However, when the data from the dynamic seeding methods is analyzed, a higher cell yield is observed with the use of a filter as compared to the no treatment control. A higher number of statistically significant results in the orbital shaker seeding method data can be detected across all the recovery treatments, however, this is attributed to the no treatment sample exhibiting a significantly lower cell yield than the one observed in the centrifugation seeding method. After assessment of the results, the recovery method that combines filtration

of samples with mechanical agitation was chosen as default for future experiments as it might play a more significant role in recovery of samples from the multiple component scaffolds.

4.4 Defining the Optimal ECM Condition for Acute Myeloid Leukemia

The bone marrow microenvironment is a complex three-dimensional structure composed of many cell types, abundant ECM proteins and other secreted and mineralized components [291,292]. These various structures do not just form inert scaffolding but play an active role in compartmentalization and presentation of cytokines, cell adhesion and migration and either directly or indirectly promote survival of certain cell types [82,196,292–295]. It has been previously reported that these microenvironmental elements not only affect leukaemia growth but can also protect the leukemic stem cells from effective treatment, however these ECM-cell interactions are difficult to investigate [21,296,297]. As a result, the precise location of these ECM constituents and their regulatory roles in various cell populations remain poorly understood [291]. Evaluation of the components contributing to the optimal cell niche for acute myeloid leukemia cells can provide a functional study model which would demonstrate the interactions the malignant cells have with their surroundings and its effect on disease initiation, progression, and treatment. The definition of an optimal leukemia cell niche would provide a new diagnostic tool for evaluating disease progression as well as provide prognosis for treatment outcomes. A define recipe of ECM components with appropriate proportions and concentration could provide a culture system capable of sustaining leukemia stem cell growth, which would not only allow for further studies of cell behaviour, but also provide ideal conditions for drug screening analysis to identify new therapeutic targets. In this research a vast number of ECM conditions were tested composed of combinations of four ECM components: collagen, hydroxyapatite 10 µm, hydroxyapatite nano powder and elastin. The number of components involved, the combinations, concentrations as well as dimensions were varied.

The first and the most critical component involved in the assay is type I collagen, which constitutes 20% and represents the main organic phase of the bone microenvironment[213]. Collagens serve as extracellular matrix molecules for many soft and hard connective tissue, although more than 20 human collagens have been identified, type I collagen is considered the most abundant protein in the human body and is responsible for the structural integrity of connective tissues[213,298]. In the bone marrow type I collagen is localized in a delicate meshwork throughout the bone, particularly concentrated near the large blood vessels and in the trabeculae [299]. It forms the structural framework of the bone marrow stroma and provides anchorage for other EMC components [299] and has been previously implicated in hematopoiesis, guiding HSC cell differentiation [300]. In this assay type I collagen is employed not only as a spatial regulator, providing the structural framework in the form of a two-dimensional film coating or a three-dimensional

scaffold, but also as a meshwork for attachments of other ECM components. Next component – hydroxyapatite, is the main inorganic constituent of the bone, amounting to approximately 70% of the bone, which can easily form direct chemical bonds with living tissues [301,302]. It also offers excellent biocompatibility, bioaffinity, biodegradability and is able to support attachment of osteoprogenitor cells, supporting osteoblastic cell adhesion, growth, and differentiation [74,301]. The hydroxyapatite particles are regularly aligned along collagen particles to form fibrils and facilitate cell attachment, however size and shape of the particles seem to play a critical role in cell fate decisions of the cells [74,301,303]. It is due to this variation that two different sizes of hydroxyapatite powder are examined in this assay, where hydroxyapatite particles provide a representation of the endosteal niche of the bone marrow. The next component, Elastin is a key protein of the ECM and is present in most connective tissues, it is an insoluble polymer composed of a monomeric precursor – tropoelastin [304]. These fibers contribute to the structural integrity and biomechanics of tissues by providing flexibility of stretch and relaxation without energy input [305]. Additionally, elastin sequences interact with multiple proteins found in or around microfibrils, and bind to elastogenic cell surface receptors of a variety of cell types [295,304]. Within the bone marrow elastin fibers are most commonly found in the vascular niche and play a key role in attachment of mesenchymal stem cells and their differentiation as a result of compressive elasticity of the tissue [82,294,295]. Therefore, elastin provides a characteristic of the vascular niche of the bone marrow in the current assay.

Three cell line were investigated OCI/AML-2 (acute myeloid leukemia), OCI/AML-3 (acute myeloid leukemia) and K-462-GFP (erythroleukaemia). Testing of these separate AML cell lines was conducted in order to account for differences in the growth patterns of the different AML subtypes as well as assist in the development of a 3D *ex vivo* disease model. Defining a scaffold that demonstrates growth of all three AML lines, would provide a suitable growth environment for the culture of primary AML cells. However, it became evident that the growth patterns varied widely across all the different growth environments tested due to the differences in physical and chemical properties of each cell line.

For the AML OCI-2 cell line several of the 2D films composed on two components were able to increase the cell number yield after expansion, however, these results failed to establish a statistically meaningful result. Interestingly, higher concentrations of hydroxyapatite 10 μm (HA10) appear to decrease cell viability, this is especially evident in the three component scaffolds (Figure 10B) where the 0.5% and the 0.7% conditions demonstrate a significant drop in cell number. In the absence of the collagen matrix, however, this component does not appear to decrease cell survival (Figure 10C), therefore the trend on decreasing cell viability with increasing concentration of HA10 is only evident in the presence of a collagen matrix.

3D Scaffold appear to have a negative effect on the overall cell growth of the AML OCI-2 cells, with all scaffolds composed of two components exhibiting a significant decrease in cell survival. Nearly all scaffolds composed with HA10 demonstrate a decrease in the reported cell number compared to the initial amount of cells seeded (50,000 cells), indicating that cells fail to establish, and their numbers begins to decline at the time of seeding or they lose their proliferation potential (Figure 10A-6B). This can be attributed to several factors, the hydroxyapatite particles themselves or the alterations they provide to the collagen matrix upon incorporation could be responsible for the reported cell number decrease, although the latter appears more likely as the decrease in cell number reported in the absence of collagen matrix with the various concentrations of HA10 is not as drastic (Figure 10C). The decreased pore size observed in the three-dimensional collagen lattices that incorporate hydroxyapatite crystals demonstrates one such potential alteration (Figure 6C). Scaffolds containing elastin as the only component other than the collagen matrix demonstrate a slight decrease in the reported cell numbers across all the concentrations tested, however a decrease in cell survival is not observed for the same conditions in the 2D films or when elastin is tested in the absence of collagen. Additionally, when compared to the 3D scaffolds composed of collagen fibers only, there is a significant drop in cell number across all three elastin concentrations. All these findings would lead to the conclusion that the elastin fibers within the 3D collagen scaffolds cause a change in structure of the scaffold lattice, which is not beneficial for the survival of the AML OCI-2 cells.

The second cell line tested was AML OCI-3, the cell line demonstrated an overall lower growth rate and none of the conditions tested were able to increase cell growth beyond that reported in the polystyrene control. Unlike the AML OCI-2 cells where the majority of 2D films reported cell numbers similar to the polystyrene control for the AML OCI-3 cell line the 2D collagen films appear to have an overall negative effect on cell growth.

Similarly to the previous cell line, the presence of hydroxyapatite 10 μm decreased the reported cell numbers across all 3D conditions. However, unlike the AML OCI-2 cells here the presence of elastin increased cell viability when compared to the 1% collagen matrix without other components. This combined with a slight increase in reported cell numbers in the elastin conditions where the collagen matrix was absent (Figure 11C) can suggest a significant role of the cell-elastin interaction in the growth rate for this cell line.

Presence of nano powder hydroxyapatite in media suspension has a detrimental effect on survival of both AML cell lines, where the cells barely expand past the seeded amount (50,000 cells). Hydroxyapatite nano particles have been shown to have a cytotoxic effect on some cells in the past[306], however this effect is highly dependent on size, structure and shape of the hydroxyapatite form[307]. The same cytotoxic effect exhibited by the nano powder present in the cell media (Figure 10C and Figure 11C), is not as evident in

the films and scaffolds containing the various concentrations of nano powder hydroxyapatite (Figure 10A and Figure 11A), which could signify that once this component is incorporated into the collagen matrix it no longer presents as toxic to these cells.

Finally, the last cell line, K-562, are chronic myelogenous leukemia cells, which exhibited growth patterns in some ways analogous to the AML cell lines. Similarly to the AML OCI-2 cell line, several 2D film conditions demonstrated a significant increase in the number of cells reported, indicating a favorable environment (Figure 12A). Additionally, the presence of HA10 in the films appears to have an inimical effect on the cells, as the conditions containing HA10 demonstrate a decrease in cell survival compared to the collagen films alone, although not statistically significant (Figure 12A and 12B) and the increased concentration of HA10 in 2D films demonstrates a linear decrease in cell viability. When these conditions are compared to the 1% collagen films without additional components a statistically significant decrease in cell yield is observed with increasing HA10 concentration: *$p<0.05$ for 1%:0.5%HA10 and **$p<0.01$ for 1%C:0.7%HA10. Additionally, when examining the results for the same conditions in the 3D scaffold a similar pattern emerges where overall cell survival in all conditions containing hydroxyapatite 10 μm (HA10) is decreased with a clear linear decline corresponding to the increasing HA10 concentrations in the two-component assay (Figure 12A). Altogether these findings might indicate a cytotoxic effect of hydroxyapatite 10 μm (HA10) on the cells, when tested in the absence of collagen, the ECM component appears to have the opposing effect – increasing cell yield at higher HA10 concentrations (Figure 12C). Therefore, hydroxyapatite 10 μm (HA10) particles alone do not produce a cytotoxic effect in the cells, but in combination with collagen they cause alterations to the protein matrix that appear deleterious to survival of K-562 cells.

Nano powder hydroxyapatite (HA0.1) does not exhibit a uniform trend across all conditions as seen with HA10. In 2D films presence of HA0.1 slightly decreases cell survival as compared to the collagen matrix alone (*$p<0.05$), however in 3D scaffolds the decrease in survival is quite striking (Figure 12A), overall, it does appear to be independent of the concentration of HA0.1 present in the structure. Additionally, the nano powder hydroxyapatite tested in the absence of collagen components also demonstrates a decrease in cell survival (Figure 12C), although not as drastic as the one observed in the 3D scaffolds. This is similar to the patterns observed with the AML cell lines and leading to the conclusion that the nano powder hydroxyapatite particles exhibit a cytotoxic effect on all cell lines tested with varying degrees.

Elastin fibers appear to exhibit different effects on the survival of K-562 cells conditional on the presence of other components. When elastin is incorporated into the 2D collagen films an overall increase in the reported cell number is observed compared to the polystyrene control, however this number is still lower

than that observed in the film in the absence of elastin (Figure 12A). This trend is reflected in the 3D scaffolds, however no discernible increase in cell survival is observed in the scaffold conditions, and scaffolds composed with elastin demonstrate cell growth comparable to the polystyrene control and marginally smaller than the collagen scaffolds without elastin (Figure 12A). However, when the effect of elastin on cell survival is assessed in the absence of a collagen matrix a decline in cell viability can be seen (Figure 12C). This indicates that elastin fibers in media suspension have a negative effect on the growth of K-562 cells, which is somewhat diminished when the fibers are incorporated into a collagen matrix.

Although a single condition favorable among all the cell lines could not be definitively established with different conditions exhibiting improved cell growth for the different cell lines, the films and scaffolds composed of 1% collagen without any other additional ECM components have demonstrated consistent growth patterns across all the cell lines tested. This matrix was therefore utilized for the subsequent high-throughput drug screening analysis in order to minimize the inconsistencies between the different structure compositions and evaluate the response to the matrices themselves.

4.5 Cellular Response to Drug Treatment Across a Variety of ECM Compositions

In the pharmaceutical industry, 2D cancer culture of leukemia cell lines is the most commonly used method for drug screening, due to its simplicity and efficient growth rates[308]. However, the 2D polystyrene-based cultures alter cell behaviour and induce different characteristics from that of the disease cells growing in vivo[308–310], therefore these screening assays do not offer an accurate disease model. Mounting evidence has demonstrated that the bone marrow niche provides the cells with microenvironmental clues that may contribute to the maintenance and survival of leukemia initiating cells (LIC) not only during disease initiation, but also after treatment with chemotherapeutic agents[133,311–315]. The absence of surrounding cells and extracellular matrix in these 2D screening assays may provide one explanation for the high attrition rate of potential drugs as they transition into clinical testing [316]. These assays fail to reproduce the cellular heterogeneity, the complex architecture and the key interactions that occur within the tumour microenvironment in vivo [316]. The ECM is a detrimental feature of the bone marrow microenvironment, which has been shown to foster resistance to therapy and subsequently survival of leukemic clones [110,142] it is, therefore, crucial to incorporate ECM features into the drug screening assays. Here I investigated whether the presence of several components native to the bone marrow in the culture system would influence outcomes of treatment with three different chemical compounds. First compound screened is Dimethyl sulfoxide (DMSO) the organosulfur compound is employed as the control [317]. The compound has been used in high throughput drug assays in the past as it is able to dissolve both polar and non-polar compounds and is also readily miscible with water and cell culture media [318]. Second compound analyzed

was thioridazine (TDZ), a dopamine receptor D2 (DRD2) antagonist, that has been shown to harbor potent antileukemic properties[319] and is currently undergoing clinical trials as an antileukemic agent[320]. Additionally, thioridazine demonstrated selective targeting of cancer cells as healthy primitive cell output was not affected after exposure to TDZ at optimal concentrations in vitro[319]. The last compound tested was cytarabine also known as cytosine arabinoside (ara-C) – a chemotherapeutic compound widely utilized for treatment of leukemia, specifically acute myeloid leukemia (AML)[321]. The tests were conducted with the AML OCI-2 cell line as it demonstrated the highest growth and survival rates on the combination scaffolds (Figure 10), the same set of conditions was analyzed, however now in the presence of one of the three chemical compounds.

Overall, there is an evident increase in cell number in our control DMSO treatment (Figure 13) as compared to the tests conducted in the absence of chemical agents (Figure 10). It has been previously demonstrated that at low concentration levels of DMSO can improve cell growth and enhance proliferation in vitro[322,323]. However, the effects of DMSO in collagen-based matrices have not been investigated. In 2D films in the absence of DMSO the two component conditions exhibited a slight increase in cell numbers compared to the polystyrene control (Figure 10A), however with the chemical agent present the same conditions demonstrate a decrease in cell numbers relative to the control (Figure 13A). For three component films, however, the relative reported values are higher than those demonstrated in the absence of DMSO where several combinations of conditions report higher cell numbers than in the polystyrene control.

For 3D scaffolds an overall increase in cell number is observed in the control treatment as well as across all conditions tested (both two-components and three-components). Whereas in the absence of DMSO an almost 3-fold decrease in cell number can be seen in the scaffolds compared to polystyrene control (Figure 10A and 10B), with addition of DMSO to the assay the reported cell numbers are twice as high with even the lowest reported conditions demonstrating only a 2-fold decrease when compared to the polystyrene control (Figure 13B and 13D). Overall, there is a slight increase in the cell numbers observed after treatment with DMSO across all conditions in both films and scaffolds as well as polystyrene, which could indicate that the enhanced cell growth perpetrated by the DMSO compound in the polystyrene assays that has been previously demonstrated [322,323] can also be evident in the presence of a collagen matrix.

Thioridazine exerts its anti-leukemic activity via antagonism of D2-family dopamine receptors which are differentially expressed on neoplastic cells [319]. Although the exact mechanisms of action of the drug on leukemia cells remain unclear, there are current efforts to elucidate the underlying molecular mechanisms of TRZ-induced cell death. A recent study reported a potential mechanism of TRZ via inhibition of proliferation and induced apoptosis through the inhibition of the PI3K/AKT/mTOR and

Ras/Raf/MEK/ERK signaling pathway in acute lymphoblastic leukemia cells[324]. Treatment of the AML OCI-2 cell line with thioridazine resulted in a significant decrease in cell number across all conditions tested (Figure 13). Although the overall number of cells appears lower than the polystyrene control, for most conditions the decrease is comparable to that observed in treatment with DMSO and is due to the cellular response to the matrix rather than the drug. There are several exceptions, where the levels of cells reported were on par with the polystyrene control, which could indicate that ECM composition can play a role in the cellular response to TRZ treatment, but these will need to be investigated further.

Cytosine Arabinoside is a combination of a cytosine base and an arabinose sugar, and acts as an antimetabolic agent. It is similar enough to a human deoxy cytosine that it is incorporated into the cell DNA interfering with DNA synthesis and causing subsequent cell arrest and death. Therefore, it is most effective in rapidly dividing cells, however it does not provide targeted response to neoplastic cells and destroys both healthy and malignant cells[321,325,326] thus alternative drug therapies are being sought out. Overall, the cytotoxic effect of cytarabine is evident in all conditions tested with the variation being proportional to what we observe in the DMSO treated samples (i.e., an average of 2-fold decrease). The strong cytotoxic effect of the chemotherapy drug makes it difficult to accurately quantify lower cell numbers in the present assay, which explains the high standard deviation of the obtained results. However, the strong decline in average cell numbers is very clear (Figure 13) and indicates, as expected, that the ECM components tested do not provide any protection to the cells from the activity of this therapeutic. Cytarabine is employed as a negative control in our subsequent high-throughput drug screen as it demonstrated significant reduction in cell numbers across all conditions tested.

Although the results do not readily identify statistically significant differences in drug receptivity in regard to variation of matrix conditions it does demonstrate that some fluctuation exists. Herein a functional assay is developed, and several amendments can be explored to improve the resolution of the results in future screening experiments. One such modification can involve improving the resolution of the calibration curve in the lower region, which would improve the accuracy of the obtained results and decrease the standard deviation rates. Additionally, adjusting the concentration of the chemical agents can also lead to a higher resolution of the obtained values and provide further insight into the cooperation between cells and the surrounding matrix composition. Finally, adjustment of the protocol to allow time for the cells to establish on the matrix prior to treatment with pharmaceutical may establish more significant variation in responsiveness to chemical agents and lend more insight into the functionalities of the culture system in acting as a barrier to cancer treatment.

4.6 High Throughput drug screening

Therapeutic outcomes and treatment options for AML have not significantly improved over the past 20 years and drug resistance remains an important determinant of treatment failure[327–329]. Although new promising drug targets have been identified, inhibitors against these targets have shown limited clinical efficacy, with 1—100-fold decrease in sensitivity, as drug response is altered in the conventional *in vitro* culture conditions [211,316,330,331]. In the past traditional 2D static cultures have been adopted as a screening culture for AML cell lines and these have helped clarify key molecular mechanisms of the disease as well as elucidate potential new therapeutics[332]. However, these lack the complexity of the bone marrow niche that may enhance leukemia growth or protect the leukemic blast from therapy, leading to failure to translate these pre-clinical findings to successful clinical therapies, causing great loss of time, cost, and research[308–310,316]. Cultivation of primary leukemic cells in vitro is extremely difficult to accomplish, with cells rapidly differentiating and undergoing apoptosis in in vitro cultures without the BM support[110,329], although some attempts have been made to optimize the media and growth factors that are able to sustain the cells [21,333–335], they fail to promote leukemic stem cell expansion, hampering cancer research efforts. Additionally, leukemia cells have demonstrated an ability to modify endothelial cell behaviour altering composition of their microenvironment to promote disease progression while suppressing normal hematopoiesis[126,336,337], thus establishing a connection between the malignant cells and their niche in disease progression. Although, tissue engineering offers opportunities for leukemia cell research, enabling researchers to create alternative culturing methods in order to mimic the native cell niche and investigate the fundamental disease drives, it's application to the manufacture of viable bone marrow niche environments in vitro has remained challenging[329]. The tissue complexity of the bone marrow involves not only the spatial organization, but the matrix components, topology, the cellular diversity and nutrition – all must be precisely defined, as the variation in each factor causes changes in cell behaviour [26,142,147,198,262,290,338]. Although several of these models are under investigation to replace the 2D polystyrene cultures, each possess drawbacks and limitations.

Three-dimensional (3D) culture methods address the lack of spatial architecture in standard assays and provide a dock for cells to arrange and aggregate [21,339]. These structures whether synthetic or natural must possess a pore distribution and framework similar to the bone marrow niche and a high degree of porosity must be observed to allow for cell infiltration, movement, communication, and nutrient supply [221,223]. It has been previously established that cells grown in three-dimensional assays demonstrate a high degree of similarity to cells grown in vivo in terms of cellular metabolism, gene expression signaling and cellular topology [29,340–344]. However, employment of 3D culturing methods has proven to be technically challenging and labour intensive, especially when considering high-throughput, multi-well multi-plate experiments and

retrieval of cells from these structures after drug treatment are relatively complicated [329]. In addition to spatial considerations, these structures must provide the cells with biorecognition signals and employ the native extracellular compounds and proteins and provide the cell-matrix interactions crucial in both normal tissue homeostasis and disease progression[311]. ECM has a capacity to not only influence cancer initiation at early stages[345–348] but drive disease progression and dictate treatment outcomes as it has shown to mediate resistance of malignant cells to chemotherapeutics [133,312–315,349]. Although these have been limited to in vivo studies a functional culture system that employs ECM components can provide a more time and cost-efficient study model to understand these underlying mechanisms and ultimately help with efforts to combat the disease. Finally, co-culturing of the malignant cells alongside other constituents of the stroma, such as healthy HSCs and stromal cells, would enhance the culture model and provide further insight into the cell-cell interactions and contribution to disease initiation, progression and treatment outcomes [200,201,211,350]. Over the course of this thesis, an efficient, low-cost, and straightforward method for developing biodegradable 3D scaffolds was demonstrated. These structures are comprised of a native ECM protein and can be supplemented with other components for optimal cell growth of specific cell types. Additionally, a method for assessing cell numbers without disturbing the cells and scaffolds was provided, and a technique of recovering the cells from the structures for other analysis was optimized, allowing the cellular morphology to be assessed further. Although not included in the scope of this research, the developed culture systems can also be adopted for co-culturing with other cells to provide an optimal environment to establish the necessary cellular interactions. Additionally, the developed screening system is suitable for automation with liquid handlers and can accommodate high-throughput assays, establishing a low-cost, simple and efficient screening assay. As a proof-of-concept I have employed these culture systems for a chemical library screening on an established leukemia cell line to evaluate the impact of the matrix on cell growth and drug sensitivity. The novel ex vivo assay provides a high-throughput screening platform for identification of compounds that are stable and active in the presence of ECM components in 2D and 3D spatial arrangements. A total of 160 compounds were screened with the AML OCI-2 cell line and a significant number of drugs were identified as compounds of interest, providing unique response patterns across the different culture conditions. With some compounds eliciting characteristics of promising drug leads that may be overlooked in the traditional cultures but prove significant in the bone marrow environment.

Tocris Mini 2.0 Drug Library was employed for the screen and of the 1280 chemical agents, 157 compounds were randomly selected (See Appendix 3 for comprehensive list of compounds), and an additional three compounds were added to the assay for a total screen of 160 therapeutics. The three additional components were: 1) DMSO, serving as the control due to all chemical agents in the Tocris Library being suspended in

DMSO; 2) Cytarabine, which acted as a negative control as it previously demonstrated it's efficiency in significantly reducing the number of metabolically active cells in the assay with equal efficiency across all three culture systems (Figure 14); 3) thioridazine – a compound previously identified in a similar screen, which is currently undergoing clinical trials for treatment of AML[319,320]. Each of the 160 compounds were evaluated in triplicate in each culture condition resulting in a screening of 18 x 96-well plates as well as additional plates used for calibration of fluorescence signal. AML OCI-2 cell line was chosen for the screen as its key gene expression signatures are comparable with primary AML cells [351] and it has demonstrated the optimal growth rate in the previous assay (Figure 10) in contrast with the other available leukemia cell lines.

The results of the drug screening demonstrate a significant variation in the response to the chemical compounds across the different culture conditions (Figure 14). Of the 60 compounds that exhibited a positive effect on cell growth in the PS culture only one compound demonstrated a similar outcome in the 2D film cultures – Lenalidomide, and although it increased the final reported cell numbers in the 2D cultures, in the 3D scaffolds it caused a significant decrease in cell number to approximately 50% of the control, however the large standard deviation across all samples does not display any significance. Although the drug sensitivity for the compounds enhancing cell growth appears to diminish in the collagen film cultures, the effect is not as drastic in the 3D collagen scaffolds, where 7 compounds exhibited significant increase in cellular growth. One of these compounds demonstrates a significant increase in cell number in 3D collagen condition, which was not reflected in the PS cultures, where the reported cell number is significantly lower than the DMSO control – Aprepitant, a potent long-acting neuroleukin-1 antagonist.

The compounds demonstrating activity against leukemia cells respond differently in the presence of ECM compounds. In the PS assay 26 compounds exhibit potent anti-leukemic activity, decreasing cell numbers below 25% of the DMSO control condition, which indicates a decrease below the number of the cells initially seeded onto the plates. The majority of these compounds, 18, fall into the enzyme inhibitor category (Figure 14E). In the 2D film cultures only 23 compounds exhibit this drastic decrease, with 19 compounds falling into the enzyme inhibitor category. However, in the 3D scaffold conditions the number of chemical agents causing cell number to decrease below 25% of the control condition increases to 43, almost double of the other two conditions. One compound that strikes interest is LJI308, which demonstrates an average cell growth at 175% in the PS condition – a positive effect on cellular growth, however in the collagen containing assays it has the opposite effect, decreasing the cell numbers to 68% in the 2D culture and 25% in the 3D scaffolds, with the numbers exhibiting statistical significance (see Appendix 4). LJI308 is a potent ribosomal s6 kinase (RSK) inhibitor – a protein involved in signal transduction [352], which has been implicated as pivotal in the growth and proliferation of cancer stem cells in breast cancer [353,354]. RSK

knockout mice demonstrate that the protein does not interfere with normal hematopoietic cell development suggesting that RSK is uniquely linked to the cancer cell population [352,355]. The studies on the effect of LJI308 were conducted in vitro, using PS cultures with cell lines of epithelial cell type [356]. In contrast the present findings (Figure 14) indicate that in PS culture LJI308 has stimulating effect on cell growth, however in collagen containing cultures the cell numbers are reduced, specifically in 3D cultures. This may indicate that the cell-matrix interactions encourage susceptibility to LJI308 for leukemia cells.

Assessing cellular response across all conditions and to summarize the results seen in the heatmap portrayed in Figure 14E (standard deviation not accounted for), only 30 compounds behave similarly across all three conditions (within 25%) (Figure 14D). 17 of those represent compounds that prevent the establishment of the cells in the culture, demonstrated by a reported cell number below the number seeded. These findings signify that ECM plays a key role in drug response with 71% of chemical agents exhibiting divergent responses to the drugs in the three culture conditions. These patterns of response are directly associated with the cultures being assessed. The first two cultures, the traditional PS culture and the 2D collagen films, offer similar spatial arrangement, but differ in the availability of biological signals from the collagen protein, hence we observe a 38% overlap in the drug response between these two conditions. Next, the PS cultures and the 3D scaffolds demonstrate the greatest difference, this is expected as the two cultures differ not only in spatial arrangement, but also in the presence of the ECM protein, with only 28% of chemical agents demonstrating similar response between the two conditions. The two collagen containing cultures – 2D films and 3D scaffolds, differ only in spatial arrangement and exhibit the lowest difference with a 46% overlap in drug response between the two matrices. These findings highlight the inability of traditional PS cultures to sustain high-throughput drug screening efforts as it does not provide an accurate representation of how cells may respond to chemical agents in vivo, leading to discovery of false hits and wasted research efforts.

Shifting the discussion over to a more detailed overview of the response patterns observed in the assay, several categories emerge (Figure 15 and Appendix 4). First category represents the chemical agents that do not cause a significant difference in response across the culture conditions tested (indicated in cream color in scatter plots and table). These compounds demonstrate that their effect is universal despite the ECM conditions that the cells reside in and although their mechanisms vary, they do not indicate significance in the present assay, although further in-depth investigations of these compounds and their precise mechanism of action can be undertaken to identify pathways of leukemic cells.

The next category involves the drugs that cause a significant reduction in cell number across several conditions (indicated in grey color in scatter plots and table). These agents indicate potential new

therapeutics for the treatment of leukemia. One example is compound ML 418 – a Kir7.1 rectifier potassium channel inhibitor. The expression of the Kir 7.1 ion channel has been confirmed in several diverse structures such as the eye, brain, uterus, kidney, gut, and thyroid gland [357,358]. Alterations of the channel functionality have been linked to diverse pathologies [357], however a link between dysregulation of the ion channel and cancer has not previously been established. The results of the present screening (Figure 15) indicate a significant reduction in leukemia cell population due to addition of ML 418 – an inhibitor of Kir 7.1. This provides a new potential target for leukemia treatment as well as a new mechanism which the malignant cells may exploit to control their growth, survival and proliferation, opening an avenue for future research to be conducted. Potential future experiments should investigate whether these compounds are able to selectively target cancer cells while avoiding destruction of the healthy hematopoietic system. In the case of ML 418, expression of Kir 7.1 has not been confirmed in the healthy HSCs [357], therefore it could provide a potential candidate for targeted malignancy treatment. Compounds lacking this selectivity would be considered equivalent to chemotherapeutic compounds like cytarabine, and although could offer alternatives to standard treatment, are likely not to elevate the significant burden that standard chemotherapy takes on the human body.

The categories that warrant special interest are the ones where the response to the collagen matrices differs from the standard PS cultures. First, the compounds that exhibit higher growth rates in collagen containing cultures (indicated in red color in scatter plots and table) as well as higher growth rate in 3D vs 2D collagen matrix. This category presents only a few notable compounds: Aprepitant, Ciclopirox, XY 018, EHop 016, Obatoclax mesylate, BAY 826 and Fendiline Hydrochloride. A compound that appears to decrease the number of cells present in the traditional PS system could potentially be identified as a new therapeutic agent in a traditional drug screening assay. However, in the present screening several of these compounds demonstrate that in the presence of collagen drug sensitivity is decreased. To provide an example, EHop 016 – a Rac inhibitor, demonstrates a complete ablation of leukemia cells in the PS culture, however in the presence of collagen the number of cells is significantly larger, although reduced below that observed in the DMSO control. The Rac is a Rho family GTPase involved in regulation of actin cytoskeleton reorganization to form cell surface extensions required for cell migration and invasion during cancer metastasis[359,360]. Due to leukemia cells not exhibiting metastatic properties another mechanism of action must be affecting the cells. EHop 016 has also demonstrated inhibition to CDC42 at high concentrations such as those used in the present assay[359]. It has previously been demonstrated that high expression and activity of CDC42 is associated with transformation of HSC to AML cells and inhibition of protein in primary AML cells blocks leukemia progression in mice models [361]. Therefore, CDC42 has been identified as a potential target for treatment of AML [361]. EHop 016, would represent a new potential therapeutic,

however the results of the present assay indicate that the sensitivity of the drug decreases in the native cell conditions, namely presence of collagen, and potentially eliminates it as a candidate prior to undergoing expensive in vivo experiments. Another example is the previously mentioned Aprepitant compound, a potent long-acting neuroleukin-1 antagonist. The compound is presently sold as a medication to combat chemotherapy-induced and post-operative nausea[362]. Neuroleukin-1 has previously been identified as a target for treatment of cancer as data has shown that it exhibits an anti-apoptotic effect of malignant cells and favors angiogenesis in solid tumors[363–368]. In human AML cells the receptor is overexpressed on the cell surface and has been shown to mediate anti-leukemic action with antagonists, specifically the damage induced by Aprepitant in cancer cells was higher than that exerted in non-cancer cells[363,369]. Experiments in solid tumors have previously demonstrated that Aprepitant is able to decrease both tumor volume and cell proliferation in vivo[366–368,370]. In non-solid tumors, specifically an acute lymphoid leukemia cell line, the drug has demonstrated a cytotoxic and antiproliferative action when the experiments were undertaken in PS cultures in vitro[368,369]. In the present assay Aprepitant exhibits similar results in PS cultures with significant reduction in cell numbers, in contrast the culture system more representative of the native cell niche exhibits decreased drug sensitivity. In both compounds discussed above, the implication presents a potential early marker of drug failure prior to in vivo studies, as the drug efficacy is not translated to the marrow native cells outside the PS culture.

The last category demonstrates compounds that exhibit increased drug sensitivity in the presence of collagen (indicated in blue color in scatter plots and table) and includes 70 compounds. These results indicate potential leukemia therapeutics that may have been overlooked in a traditional PS assay, due to the decreased sensitivity in the absence of native conditions. This comprises almost 44% of potential chemical agents out of the 160 compounds that were screened in the present assay, indicating the significance of developing a screening assay with representative ECM conditions. One example is the chemical agent Rosuvastatin calcium, a Potent HMG-CoA reductase inhibitor, which is currently employed as a cholesterol modulating drug[371]. Statins have previously demonstrated toxicity towards malignancies such as AML as these exhibit higher low-density lipoprotein processing than normal blood cells, presumably requiring cholesterol for membrane synthesis[371,372]. Rosuvastatin calcium is currently undergoing an FDA Phase IV clinical trials for AML in adults[373,374]. Another example from this category is MRK 740, a potent PRDM9 (PR domain zinc finger protein 9) inhibitor. This protein expression is restricted to germ cells and there is growing evidence suggesting its aberrant expression may play a role in oncogenesis and genomic instability in cancer[375]. Previous studies have investigated the effect of MRK 740 on in vitro cell cultures of several cancer cell lines and have demonstrated that the drug did not have a significant effect on proliferation of any of the cell lines[376]. The study employed traditional polystyrene culture systems in their assay, similarly,

in the present analysis of PS cultures the drug exhibited slight elevation of cell number, however in the novel culture systems containing collagen, the response to the drug differed significantly. In the presence of collagen in 2D cultures the leukemia cell numbers are halved and when spatial arrangement is taken into consideration – the 3D collagen scaffolds, the decrease in cell number is more evident with cell numbers falling below the seeding threshold, indicating a strong cytotoxic effect of chemical agent. This highlights that potential new therapeutics can be overlooked in standard PS cultures, as they do not exhibit sensitivity to the drug in absence of ECM components native to their niche. Another compound worth mentioning is Quizartinib, a highly potent FLT3 inhibitor, currently undergoing multiple clinical trials on a fast-track status for targeted treatment of AML[377]. Surprisingly, the results of the screening indicate that the compound caused an increase in cell numbers in the PS cultures, however reduced cell numbers below the seeding threshold in the 3D cultures, indicating increasing drug sensitivity in native cell environment. Finally, a recently identified (R)-zinc 3573 a Mas related G-protein-coupled receptor member X2 (MRGPRX2) agonist, developed for treatment of allergic diseases, demonstrates potential of anti-leukemic activity in vivo based on the results of the ECM screening (Figure 14). MRGPRX2 is specifically expressed in mast cells, a cell of the myeloid lineage, and agonists cause cell degranulation – pseudo-allergic reaction[378], however it has not previously been investigated whether the protein is expressed in AML cells. The results of the high-throughput screening indicate that the agonist of MRGPRX2 induces reduction in cell numbers of AML cells in native cell conditions (Figure 15). This represents not only a novel mechanism potentially imperative in malignant cell survival in vivo, but a promising therapeutic target as well as a possible existing drug that can be utilized for treatment of the disease.

The niche-based quantitative biochemical screening developed in this work allows for the evaluation of the impact of matrix composition as well spatial arrangement on growth and drug sensitivity of human myeloid leukemia cells. Empirically, we detected significant differences in the drug activities of several individual compounds when leukemia cells were grown in standard cultures versus the collagen-containing matrix and further differences between two and three-dimensional spatial organization of the structures. The drug screening presented provides a proof-of-concept assay, that is efficient and simple and is capable of identifying not only potential new therapeutics and targets but can also identify compounds that demonstrate variations in drug activity and sensitivity in the presence of the native ECM matrix.

Several limitations of this assay warrant further comment. First, although specificity and toxicity of the selected drugs are beyond the scope of this work, the concentrations used for the assay – 10 μM – are considered relatively high. Next, the assay is not sufficient in addressing the issue of cell specificity and further toxicology studies and co-cultures must be conducted to define which compounds exhibit selectivity towards malignant cells. Moreover, safety and potential therapy application of these compounds must be

further assessed in other non-hematopoietic tissues prior to in vivo studies, although several of these compounds have already undergone such studies and are being used clinically. Subsequent mechanistic studies will need to be conducted on all compounds of interest to illuminate the pathway that is exploited within the cell during drug administration. Furthermore, the developed 2D films and 3D scaffolds do not fully reproduce the in vivo environment of the leukemia cells but represents a step in the direction of composing an efficient screening technique that is more closely representative of the native niche. Additionally, the screening involved a leukemia cell line, it is limited to the characteristics exhibited by the AML OCI-2 cells and is not fully representative of the behavior exhibited by primary AML cells, further studies on other human cell lines as well as primary samples would produce further evidence of the efficacy of this assay.

Chapter 5. Concluding Remarks

5.1 Conclusion

The bone marrow niche is an intricate complex system that must balance proliferation and differentiation of a variety of cells in order to maintain healthy hematopoiesis. A multitude of factors work in synergy to establish a microenvironment that is capable of supporting hematopoietic development. Acute myeloid leukemia hijacks these components in order to shift the niche towards support of malignant cells at the detriment of healthy HSCs. A crucial role of specific ECM modifications by AML is further highlighted by correlations of certain ECM signatures with disease prognosis.

In order to gain a deeper understanding of the biological processes and the physio-chemical conditions of the bone marrow niche, efforts have been made to recapitulate this complex system in vitro using existing biomaterial platforms. Although attempts have been made to cultivate AML cells in a variety of novel three-dimensional cultures, an assessment of cell survival in a synthesized type I collagen matrix has not been conducted. This research represents the first attempt at optimizing a collagen scaffold system for culturing of AML cells. Physical and chemical parameters of the scaffolds were investigated and additional ECM components that are believed to contribute to AML survival in vivo were incorporated into the culture system and assessed for their contribution to cell number expansion of several leukemia cell lines.

To establish the application potential of the developed culture system as a proof-of-concept a high throughput drug screening analysis was undertaken. This screening assay represents a first of its kind application of structural collagen fabricated scaffolds, without the use of synthetic materials, in a high-throughput screening of chemical agents. The data obtained confirmed that the system can be adapted to quantitative high-throughput screens and may improve disease relevance in contrast to standard polystyrene drug screening platforms. The conducted assay contradicts the previously held belief that multi-plate multi-well 3D assays are expensive and labor-intensive and creates a precedent for future application in drug screening. Automation of the assay is already underway with custom liquid handlers in development. Finally, the experiments demonstrated that the assay developed over the course of this thesis is capable of more accurately predicting drug efficacy by recapitulating tumor microenvironment with three-dimensional collagen scaffolds. The results of the initial screening underscore the importance of performing screens for new drugs using model systems that more faithfully recapitulate tissue architecture at the malignant site. Furthermore, these models can find application in personalized medicine approaches, due to therapeutic compound responses exhibiting correlation to specific cancer genotypes, which can greatly vary between individuals[379]. Primary patient-derived cells can be employed in a screening of established therapeutics to determine the ideal treatment for each patient, with not just the most favourable therapeutic, but

combinations of compounds as well as optimal concentrations, easing the disease treatment burden. In summary, our results imply that drug discovery employing a physiologically applicable organotypic model for human disease is efficient, and likely to identify effective compounds quicker and with a lower attrition rate than other traditional screening approaches.

5.2 Future Directions

The culture system developed here only represents a foundation for the development of an optimal AML scaffold. First, a multitude of additional components can be screened in order to perfect the scaffold 'recipe' and define an ideal signature of ECM constituents in vitro. Additionally varying the physical attributes of the scaffold such as the overall size of the structures as well as pore size and topography, induction of hypoxic conditions or incorporation of a profusion system can provide insight on how these variables are able to influence cell behavior. Studies of specific cell marker expressions induced by these variables, through flow cytometry, and assessment of cell protein expression patterns through qPCR, will further elucidate the molecular mechanisms involved in cellular response to the ECM components under investigation. Finally, screening of patient AML samples rather than cell lines, will ultimately provide a more reliable recapitulation of the ECM signature of AML and allow for the development of a functional culture system for leukemia stem cells, which continue to elude in depth investigations due to induced differentiation outside of native ECM. This in vitro system would then allow for investigations into ECM-mediated AML mechanisms that function in cell proliferation, differentiation, apoptosis, and matrix remodelling.

Efforts are currently underway to develop similar optimal scaffolds for cultivation of mesenchymal and hematopoietic stem cells. Once all three systems are established a comparison can be drawn and the differences investigated further. This will allow for co-culture studies to be conducted, furthering efforts to establish a niche-like culture in vitro. Additionally, analysis of the differences in ECM signature between healthy and malignant cells can provide insight into disease initiation and progression, which may represent a new early diagnostic tool for onset of hematopoietic malignancies or a potential therapeutic target to improve disease outcomes.

The conducted drug screening analysis revealed several compounds of interest that elicit further investigation of their therapeutic potential against leukemia cells in vivo. The screening can also be supplemented with a protein expression assay in order to gain insight into how certain therapeutics are able to elucidate a different response across various matrix conditions. Conducting the drug screening experiment with the employment of primary patient AML samples would be of utmost curiosity as it will provide insight into the therapeutic effect on LSCs such as cell survival, molecular mechanisms and

induction of proliferation and differentiation. This will allow us to identify compounds which can target the elusive cells, improving remission rates in AML patients. Additionally, it will provide insight into the role of genetic differences between different patients in therapeutic response to the chemical agents, providing a steppingstone towards developing a personalized medicine approach.

References

1. Ribatti, D. Editorial: Bone marrow vascular niche and the control of tumor growth in hematological malignancies. *Leukemia* vol. 24 1247–1248 (2010).

2. Till, J. E. & McCulloch, E. A. A Direct Measurement of the Radiation Sensitivity of Normal Mouse Bone Marrow Cells. *Radiation Research* (1961) doi:10.2307/3570892.

3. Mahla, R. S. Stem cells applications in regenerative medicine and disease therapeutics. *International Journal of Cell Biology* (2016) doi:10.1155/2016/6940283.

4. Schöler, H. R. The potential of stem cells: An inventory. *Bundesgesundheitsblatt - Gesundheitsforschung - Gesundheitsschutz* (2004) doi:10.1007/s00103-004-0818-3.

5. Walasek, M. A., van Os, R. & de Haan, G. Hematopoietic stem cell expansion: challenges and opportunities. *Ann N Y Acad Sci* **1266**, 138–150 (2012).

6. Osawa, M., Hanada, K. I., Hamada, H. & Nakauchi, H. Long-Term Lymphohematopoietic Reconstitution by a Single CD34-Low/Negative Hematopoietic Stem Cell. *Science (1979)* **273**, 242–245 (1996).

7. Pinho, S. & Frenette, P. S. Haematopoietic stem cell activity and interactions with the niche. *Nat Rev Mol Cell Biol* **20**, 303 (2019).

8. Crisan, M. *et al.* A perivascular origin for mesenchymal stem cells in multiple human organs. *Cell Stem Cell* **3**, 301–313 (2008).

9. Hwang, N. S., Zhang, C., Hwang, Y. S. & Varghese, S. Mesenchymal stem cell differentiation and roles in regenerative medicine. *Wiley Interdisciplinary Reviews: Systems Biology and Medicine* **1**, 97–106 (2009).

10. Nwajei, F. & Konopleva, M. The Bone Marrow Microenvironment as Niche Retreats for Hematopoietic and Leukemic Stem Cells. *Advances in Hematology* **2013**, (2013).

11. Konopleva, M., Tabe, Y., Zeng, Z. & Andreeff, M. Therapeutic targeting of microenvironmental interactions in leukemia: mechanisms and approaches. *Drug Resist Updat* **12**, 103–113 (2009).

12. Ding, L., Saunders, T. L., Enikolopov, G. & Morrison, S. J. Endothelial and perivascular cells maintain haematopoietic stem cells. *Nature* **481**, 457–462 (2012).

13. Méndez-Ferrer, S. *et al.* Mesenchymal and haematopoietic stem cells form a unique bone marrow niche. *Nature* **466**, 829–834 (2010).

14. Calvi, L. M. *et al.* Osteoblastic cells regulate the haematopoietic stem cell niche. *Nature* **425**, 841–846 (2003).

15. Naveiras, O. *et al.* Bone-marrow adipocytes as negative regulators of the haematopoietic microenvironment. *Nature* **460**, 259–263 (2009).

16. Yamazaki, S. *et al.* Nonmyelinating Schwann cells maintain hematopoietic stem cell hibernation in the bone marrow niche. *Cell* **147**, 1146–1158 (2011).

17. Lee-Thedieck, C., Schertl, P. & Klein, G. The extracellular matrix of hematopoietic stem cell niches. *Advanced Drug Delivery Reviews* **181**, None (2022).

18. Park, B., Yoo, K. H. & Kim, C. Hematopoietic stem cell expansion and generation: the ways to make a breakthrough. *Blood Res* **50**, 194 (2015).

19. Celso, C. lo & Scadden, D. T. The haematopoietic stem cell niche at a glance. *Journal of Cell Science* **124**, 3529–3535 (2011).

20. Perlin, J. R., Sporrij, A. & Zon, L. I. Blood on the tracks: hematopoietic stem cell-endothelial cell interactions in homing and engraftment. *J Mol Med (Berl)* **95**, 809–819 (2017).

21. Blanco, T. M., Mantalaris, A., Bismarck, A. & Panoskaltsis, N. The development of a three-dimensional scaffold for ex vivo biomimicry of human acute myeloid leukaemia. *Biomaterials* **31**, 2243–2251 (2010).

22. Chan, C. K. F. *et al.* Endochondral ossification is required for haematopoietic stem-cell niche formation. *Nature* **457**, 490–494 (2009).

23. Li, H. *et al.* Biomechanical cues as master regulators of hematopoietic stem cell fate. *Cellular and Molecular Life Sciences* **78**, 5881 (2021).

24. Zhang, P. *et al.* The physical microenvironment of hematopoietic stem cells and its emerging roles in engineering applications. *Stem Cell Res Ther* **10**, (2019).

25. Vining, K. H. & Mooney, D. J. Mechanical forces direct stem cell behaviour in development and regeneration. *Nat Rev Mol Cell Biol* **18**, 728–742 (2017).

26. Klamer, S. & Voermans, C. The role of novel and known extracellular matrix and adhesion molecules in the homeostatic and regenerative bone marrow microenvironment. *Cell Adhesion & Migration* **8**, 563 (2014).

27. Murphy, C. M., Haugh, M. G. & O'Brien, F. J. The effect of mean pore size on cell attachment, proliferation and migration in collagen–glycosaminoglycan scaffolds for bone tissue engineering. *Biomaterials* **31**, 461–466 (2010).

28. Hsu, S. H., Tsai, I. J., Lin, D. J. & Chen, D. C. The effect of dynamic culture conditions on endothelial cell seeding and retention on small diameter polyurethane vascular grafts. *Medical Engineering and Physics* **27**, 267–272 (2005).

29. Berthiaume, F., Moghe, P. v., Toner, M. & Yarmush, M. L. Effect of extracellular matrix topology on cell structure, function, and physiological responsiveness: hepatocytes cultured in a sandwich configuration. *FASEB J* **10**, 1471–1484 (1996).

30. Szade, K. *et al.* Where Hematopoietic Stem Cells Live: The Bone Marrow Niche. *Antioxidants & Redox Signaling* **29**, 191 (2018).

31. Visnjic, D. *et al.* Hematopoiesis is severely altered in mice with an induced osteoblast deficiency. *Blood* **103**, 3258–3264 (2004).

32. Ding, L. & Morrison, S. J. Haematopoietic stem cells and early lymphoid progenitors occupy distinct bone marrow niches. *Nature* **495**, 231 (2013).

33. Yu, V. W. C. & Scadden, D. T. Hematopoietic Stem Cell and Its Bone Marrow Niche. *Curr Top Dev Biol* **118**, 21 (2016).

34. Winkler, I. G. *et al.* Bone marrow macrophages maintain hematopoietic stem cell (HSC) niches and their depletion mobilizes HSCs. *Blood* **116**, 4815–4828 (2010).

35. Katayama, Y. *et al.* Signals from the Sympathetic Nervous System Regulate Hematopoietic Stem Cell Egress from Bone Marrow. *Cell* **124**, 407–421 (2006).

36. Testa, U., Labbaye, C., Castelli, G. & Pelosi, E. Oxidative stress and hypoxia in normal and leukemic stem cells. *Experimental Hematology* **44**, 540–560 (2016).

37. Wilson, A. & Trumpp, A. Bone-marrow haematopoietic-stem-cell niches. *Nature Reviews Immunology* vol. 6 93–106 (2006).

38. Huang, J. *et al.* Extracellular matrix and its therapeutic potential for cancer treatment. *Signal Transduction and Targeted Therapy 2021 6:1* **6**, 1–24 (2021).

39. Nicolas, J. *et al.* 3D Extracellular Matrix Mimics: Fundamental Concepts and Role of Materials Chemistry to Influence Stem Cell Fate. *Biomacromolecules* **21**, 1968–1994 (2020).

40. Prydz, K. Determinants of Glycosaminoglycan (GAG) Structure. *Biomolecules* **5**, 2003–2022 (2015).

41. Raman, R., Sasisekharan, V. & Sasisekharan, R. Structural insights into biological roles of protein-glycosaminoglycan interactions. *Chem Biol* **12**, 267–277 (2005).

42. Ricard-Blum, S. The Collagen Family. *Cold Spring Harbor Perspectives in Biology* **3**, 1–19 (2011).

43. Schlesinger, P. H. *et al.* Cellular and extracellular matrix of bone, with principles of synthesis and dependency of mineral deposition on cell membrane transport. *American Journal of Physiology - Cell Physiology* **318**, C111–C124 (2020).

44. Marinkovic, M. *et al.* Native extracellular matrix, synthesized ex vivo by bone marrow or adipose stromal cells, faithfully directs mesenchymal stem cell differentiation. *Matrix Biol Plus* **8**, (2020).

45. Çelebi, B., Pineault, N. & Mantovani, D. The Role of Collagen Type I on Hematopoietic and Mesenchymal Stem Cells Expansion and Differentiation. *Advanced Materials Research* **409**, 111–116 (2012).

46. Koenigsmann, M., Griffin, J. D., DiCarlo, J. & Cannistra, S. A. Myeloid and Erythroid Progenitor Cells From Normal Bone Marrow Adhere To Collagen Type I. *Blood* **79**, 657–665 (1992).

47. Pankov, R. & Yamada, K. M. Fibronectin at a glance. *Journal of Cell Science* **115**, 3861–3863 (2002).

48. George, E. L., Georges-Labouesse, E. N., Patel-King, R. S., Rayburn, H. & Hynes, R. O. Defects in mesoderm, neural tube and vascular development in mouse embryos lacking fibronectin. *Development* **119**, 1079–1091 (1993).

49. Weinstein, R. *et al.* Dual Role of Fibronectin in Hematopoietic Differentiation. *Blood* **73**, 111–116 (1989).

50. Tsai, S. *et al.* Differential Binding of Erythroid and Myeloid Progenitors to Fibroblasts and Fibronectin. *Blood* **69**, 1587–1594 (1987).

51. Durbeej, M. Laminins. *Cell and Tissue Research* **339**, 259–268 (2010).

52. Susek, K. H. *et al.* Bone marrow laminins influence hematopoietic stem and progenitor cell cycling and homing to the bone marrow. *Matrix Biol* **67**, 47 (2018).

53. Foster, J. A. Elastin. *Encyclopedia of Biological Chemistry: Second Edition* 192–193 (2013) doi:10.1016/B978-0-12-378630-2.00170-5.

54. (PDF) Clinical significance of elastin turnover--focus on diseases affecting elastic fibres. https://www.researchgate.net/publication/8100213_Clinical_significance_of_elastin_turnover--focus_on_diseases_affecting_elastic_fibres.

55. Elastin metabolism is disrupted in patients after allogeneic hematopoietic stem cell transplantation (alloHSCT) for acute and chronic myeloid leukemia. https://nauka-polska.pl/#/profile/publication?id=1835704&_k=ym124i.

56. Casale, J. & Crane, J. S. Biochemistry, Glycosaminoglycans. *StatPearls* (2021).

57. Kochlamazashvili, G. *et al.* The extracellular matrix molecule hyaluronic acid regulates hippocampal synaptic plasticity by modulating postsynaptic L-type Ca(2+) channels. *Neuron* **67**, 116–128 (2010).

58. Gerecht, S. *et al.* Hyaluronic acid hydrogel for controlled self-renewal and differentiation of human embryonic stem cells. *Proc Natl Acad Sci U S A* **104**, 11298–11303 (2007).

59. Ouasti, S. *et al.* Network connectivity, mechanical properties and cell adhesion for hyaluronic acid/PEG hydrogels. *Biomaterials* **32**, 6456–6470 (2011).

60. Monslow, J., Govindaraju, P. & Puré, E. Hyaluronan - a functional and structural sweet spot in the tissue microenvironment. *Front Immunol* **6**, (2015).

61. Yang, C. *et al.* The high and low molecular weight forms of hyaluronan have distinct effects on CD44 clustering. *J Biol Chem* **287**, 43094–43107 (2012).

62. Nilsson, S. K. *et al.* Hyaluronan is synthesized by primitive hemopoietic cells, participates in their lodgment at the endosteum following transplantation, and is involved in the regulation of their proliferation and differentiation in vitro. *Blood* **101**, 856–862 (2003).

63. Goncharova, V. *et al.* Hyaluronan Expressed by the Hematopoietic Microenvironment Is Required for Bone Marrow Hematopoiesis. *The Journal of Biological Chemistry* **287**, 25419 (2012).

64. Schraufstatter, I. *et al.* Hyaluronan Stimulates Mobilization of Mature Hematopoietic Cells but Not Hematopoietic Progenitors. *J Stem Cells* **4**, 191 (2009).

65. Lee-Sayer, S. S. M. *et al.* CD44-mediated hyaluronan binding marks proliferating hematopoietic progenitor cells and promotes bone marrow engraftment. *PLoS ONE* **13**, (2018).

66. Pilarski, L. M. *et al.* Potential Role for Hyaluronan and the Hyaluronan Receptor RHAMM in Mobilization and Trafficking of Hematopoietic Progenitor Cells. *Blood* **93**, 2918–2927 (1999).

67. Jadin, L. *et al.* Skeletal and hematological anomalies in HYAL2-deficient mice: a second type of mucopolysaccharidosis IX? *The FASEB Journal* **22**, 4316–4326 (2008).

68. Wu, L. N. Y. *et al.* Physicochemical Characterization of the Nucleational Core of Matrix Vesicles *. *Journal of Biological Chemistry* **272**, 4404–4411 (1997).

69. Ulian, G., Moro, D. & Valdrè, G. Hydroxylapatite and Related Minerals in Bone and Dental Tissues: Structural, Spectroscopic and Mechanical Properties from a Computational Perspective. *Biomolecules* **11**, (2021).

70. Lee-Thedieck, C. & Spatz, J. P. Biophysical regulation of hematopoietic stem cells. *Biomaterials Science* **2**, 1548–1561 (2014).

71. Chua, K. N. *et al.* Surface-aminated electrospun nanofibers enhance adhesion and expansion of human umbilical cord blood hematopoietic stem/progenitor cells. *Biomaterials* **27**, 6043–6051 (2006).

72. Choi, J. S. & Harley, B. A. C. The combined influence of substrate elasticity and ligand density on the viability and biophysical properties of hematopoietic stem and progenitor cells. *Biomaterials* **33**, 4460–4468 (2012).

73. Ha, S. W., Jang, H. L., Nam, K. T. & Beck, G. R. Nano-hydroxyapatite modulates osteoblast lineage commitment by stimulation of DNA methylation and regulation of gene expression. *Biomaterials* **65**, 32–42 (2015).

74. Yazid Bajuri, M. *et al.* Tissue-Engineered Hydroxyapatite Bone Scaffold Impregnated with Osteoprogenitor Cells Promotes Bone Regeneration in Sheep Model. doi:10.1007/s13770.

75. Ha, S. W., Park, J., Habib, M. M. & Beck, G. R. Nano-Hydroxyapatite Stimulation of Gene Expression Requires Fgf Receptor, Phosphate Transporter, and Erk1/2 Signaling. *ACS Applied Materials and Interfaces* **9**, 39185–39196 (2017).

76. Altrock, E., Muth, C. A., Klein, G., Spatz, J. P. & Lee-Thedieck, C. The significance of integrin ligand nanopatterning on lipid raft clustering in hematopoietic stem cells. *Biomaterials* **33**, 3107–3118 (2012).

77. Muth, C. A., Steinl, C., Klein, G. & Lee-Thedieck, C. Regulation of hematopoietic stem cell behavior by the nanostructured presentation of extracellular matrix components. *PLoS One* **8**, (2013).

78. Nies, C. & Gottwald, E. Artificial hematopoietic stem cell niches-dimensionality matters. *Advances in Tissue Engineering & Regenerative Medicine: Open Access* **Volume 2**, (2017).

79. Adamo, L. *et al.* Biomechanical forces promote embryonic haematopoiesis. *Nature* **459**, 1131–1135 (2009).

80. Kang, Y. G., Jeong, J. Y., Lee, T. H., Lee, H. S. & Shin, J. W. Synergistic Integration of Mesenchymal Stem Cells and Hydrostatic Pressure in the Expansion and Maintenance of Human Hematopoietic/Progenitor Cells. *Stem Cells International* **2018**, (2018).

81. Lee-Thedieck, C., Rauch, N., Fiammengo, R., Klein, G. & Spatz, J. P. Impact of substrate elasticity on human hematopoietic stem and progenitor cell adhesion and motility. *J Cell Sci* **125**, 3765–3775 (2012).

82. Holst, J. *et al.* Substrate elasticity provides mechanical signals for the expansion of hemopoietic stem and progenitor cells. *Nature Biotechnology 2010 28:10* **28**, 1123–1128 (2010).

83. Winer, J. P., Janmey, P. A., McCormick, M. E. & Funaki, M. Bone marrow-derived human mesenchymal stem cells become quiescent on soft substrates but remain responsive to chemical or mechanical stimuli. *Tissue Eng Part A* **15**, 147–154 (2009).

84. Asgari, M., Latifi, N., Heris, H. K., Vali, H. & Mongeau, L. In vitro fibrillogenesis of tropocollagen type III in collagen type I affects its relative fibrillar topology and mechanics. *Sci Rep* **7**, (2017).

85. Licup, A. J. *et al.* Stress controls the mechanics of collagen networks. *Proc Natl Acad Sci U S A* **112**, 9573–9578 (2015).

86. Mammoto, A. & Ingber, D. E. Cytoskeletal control of growth and cell fate switching. *Curr Opin Cell Biol* **21**, 864–870 (2009).

87. Vogel, V. & Sheetz, M. Local force and geometry sensing regulate cell functions. *Nat Rev Mol Cell Biol* **7**, 265–275 (2006).

88. Wirth, F., Lubosch, A., Hamelmann, S. & Nakchbandi, I. A. Fibronectin and Its Receptors in Hematopoiesis. *Cells* **9**, (2020).

89. Williams, D. A., Rios, M., Stephens, C. & Patel, V. P. Fibronectin and VLA-4 in haematopoietic stem cell-microenvironment interactions. *Nature* (1991) doi:10.1038/352438a0.

90. Notta, F. *et al.* Isolation of single human hematopoietic stem cells capable of long-term multilineage engraftment. *Science* **333**, 218–221 (2011).

91. Schreiber, T. D. *et al.* The integrin alpha9beta1 on hematopoietic stem and progenitor cells: involvement in cell adhesion, proliferation and differentiation. *Haematologica* **94**, 1493–1501 (2009).

92. Umemoto, T. *et al.* Expression of Integrin beta3 is correlated to the properties of quiescent hemopoietic stem cells possessing the side population phenotype. *J Immunol* **177**, 7733–7739 (2006).

93. Carafoli, F. & Hohenester, E. Collagen recognition and transmembrane signalling by discoidin domain receptors. *Biochim Biophys Acta* **1834**, 2187–2194 (2013).

94. Steidl, U. *et al.* Primary human CD34+ hematopoietic stem and progenitor cells express functionally active receptors of neuromediators. *Blood* **104**, 81–88 (2004).

95. Ponta, H., Sherman, L. & Herrlich, P. A. CD44: from adhesion molecules to signalling regulators. *Nat Rev Mol Cell Biol* **4**, 33–45 (2003).

96. Naor, D., Dransfield, I., Robson, T., Günthert, U. & Zöller, M. CD44, hyaluronan, the hematopoietic stem cell, and leukemia-initiating cells. *Front. Immunol* **6**, 235 (2015).

97. Hematopoietic Cancers. *Primer to the Immune Response* 553–585 (2014) doi:10.1016/B978-0-12-385245-8.00020-0.

98. Juo, P.-Show. Concise dictionary of biomedicine and molecular biology. 1154 (2002).

99. Chiba, S. Hematopoietic Stem Cells: The Paradigmatic Tissue-Specific Stem Cell. *The American Journal of Pathology* **169**, 338–346 (2006).

100. Vardiman, J. W. *et al.* The 2008 revision of the World Health Organization (WHO) classification of myeloid neoplasms and acute leukemia: rationale and important changes. *Blood* **114**, 937–951 (2009).

101. Siegel, R. L., Miller, K. D. & Jemal, A. Cancer statistics, 2015. *CA Cancer J Clin* **65**, 5–29 (2015).

102. Li, D. *et al.* A novel extracellular matrix-based leukemia model supports leukemia cells with stem cell-like characteristics. *Leukemia Research* (2018) doi:10.1016/j.leukres.2018.08.012.

103. Behrmann, L., Wellbrock, J. & Fiedler, W. Acute myeloid leukemia and the bone marrow niche - Take a closer look. *Frontiers in Oncology* (2018) doi:10.3389/fonc.2018.00444.

104. Sill, H., Olipitz, W., Zebisch, A., Schulz, E. & Wölfler, A. Therapy-related myeloid neoplasms: pathobiology and clinical characteristics. *Br J Pharmacol* **162**, 792–805 (2011).

105. Bonnet, D. & Dick, E. Human acute myeloid leukemia is organized as a hierarchy that originates from a primitive hematopoietic cell. (1997).

106. Jin, L., Hope, K. J., Zhai, Q., Smadja-Joffe, F. & Dick, J. E. Targeting of CD44 eradicates human acute myeloid leukemic stem cells. *Nature Medicine 2006 12:10* **12**, 1167–1174 (2006).

107. Ho, T. C. *et al.* Myeloid Neoplasia: Evolution of acute myelogenous leukemia stem cell properties after treatment and progression. *Blood* **128**, 1671 (2016).

108. Shlush, L. I. *et al.* Identification of pre-leukemic hematopoietic stem cells in acute leukemia. *Nature* **506**, 328 (2014).

109. Corces, M. R. *et al.* Lineage-specific and single cell chromatin accessibility charts human hematopoiesis and leukemia evolution. *Nat Genet* **48**, 1193 (2016).

110. Bruserud, Ø., Aasebø, E., Hernandez-Valladares, M., Tsykunova, G. & Reikvam, H. Therapeutic targeting of leukemic stem cells in acute myeloid leukemia – the biological background for possible strategies. *http://dx.doi.org/10.1080/17460441.2017.1356818* **12**, 1053–1065 (2017).

111. Krivtsov, A. v. *et al.* Transformation from committed progenitor to leukaemia stem cell initiated by MLL–AF9. *Nature 2006 442:7104* **442**, 818–822 (2006).

112. Jones, R. J. & Armstrong, S. A. Cancer Stem Cells in Hematopoietic Malignancies. *Biol Blood Marrow Transplant* **14**, 12 (2008).

113. Huntly, B. J. P. & Gilliland, D. G. Leukaemia stem cells and the evolution of cancer-stem-cell research. *Nature Reviews Cancer* (2005) doi:10.1038/nrc1592.

114. Ninomiya, M. *et al.* Homing, proliferation and survival sites of human leukemia cells in vivo in immunodeficient mice. *Leukemia* **21**, 136–142 (2007).

115. Lane, S. W., Scadden, D. T. & Gilliland, D. G. The leukemic stem cell niche: Current concepts and therapeutic opportunities. *Blood* (2009) doi:10.1182/blood-2009-01-202606.

116. Radisky, D., Muschler, J. & Bissell, M. J. Order and disorder: The role of extracellular matrix in epithelial cancer. in *Cancer Investigation* (2002). doi:10.1081/CNV-120000374.

117. Kumar, B. *et al.* Acute myeloid leukemia transforms the bone marrow niche into a leukemia-permissive microenvironment through exosome secretion. *Leukemia* **32**, 575–587 (2018).

118. Yao, Y., Li, F., Huang, J., Jin, J. & Wang, H. Leukemia stem cell-bone marrow microenvironment interplay in acute myeloid leukemia development. *Experimental Hematology & Oncology* **10**, (2021).

119. Brenner, A. K., Nepstad, I. & Bruserud, Ø. Mesenchymal stem cells support survival and proliferation of primary human acute myeloid leukemia cells through heterogeneous molecular mechanisms. *Frontiers in Immunology* **8**, (2017).

120. Ito, S. *et al.* Long Term Maintenance of Myeloid Leukemic Stem Cells Cultured with Unrelated Human Mesenchymal Stromal Cells. *Stem Cell Res* **14**, 95 (2015).

121. Diaz de la Guardia, R. *et al.* Detailed Characterization of Mesenchymal Stem/Stromal Cells from a Large Cohort of AML Patients Demonstrates a Definitive Link to Treatment Outcomes. *Stem Cell Reports* **8**, 1573–1586 (2017).

122. Hanoun, M. *et al.* Acute myelogenous leukemia-induced sympathetic neuropathy promotes malignancy in an altered hematopoietic stem cell niche. *Cell Stem Cell* **15**, 365–375 (2014).

123. Dias, S., Shmelkov, S. v., Lam, G. & Rafii, S. VEGF(165) promotes survival of leukemic cells by Hsp90-mediated induction of Bcl-2 expression and apoptosis inhibition. *Blood* **99**, 2532–2540 (2002).

124. Zhan, Q., Bieszczad, C. K., Bae, I., Fornace, A. J. & Craig, R. W. *Induction of BCL2 family member MCL1 as an early response to DNA damage*. (1997).

125. Hatfield, K., Ryningen, A., Corbascio, M. & Bruserud, Ø. Microvascular endothelial cells increase proliferation and inhibit apoptosis of native human acute myelogenous leukemia blasts. *Int J Cancer* **119**, 2313–2321 (2006).

126. Passaro, D. *et al.* Increased Vascular Permeability in the Bone Marrow Microenvironment Contributes to Disease Progression and Drug Response in Acute Myeloid Leukemia. *Cancer Cell* **32**, 324-341.e6 (2017).

127. Schliemann, C. *et al.* Circulating angiopoietin-2 is a strong prognostic factor in acute myeloid leukemia. *Leukemia 2007 21:9* **21**, 1901–1906 (2007).

128. Aguayo, A. *et al.* Plasma Vascular Endothelial Growth Factor Levels Have Prognostic Significance in Patients with Acute Myeloid Leukemia but Not in Patients with Myelodysplastic Syndromes. (2002) doi:10.1002/cncr.10900.

129. Tavor, S. *et al.* CXCR4 regulates migration and development of human acute myelogenous leukemia stem cells in transplanted NOD/SCID mice. *Cancer Res* **64**, 2817–2824 (2004).

130. Schelker, R. C. *et al.* TGF-β1 and CXCL12 modulate proliferation and chemotherapy sensitivity of acute myeloid leukemia cells co-cultured with multipotent mesenchymal stromal cells. *Hematology* **23**, 337–345 (2018).

131. Pitt, L. A. *et al.* CXCL12-Producing Vascular Endothelial Niches Control Acute T Cell Leukemia Maintenance. *Cancer Cell* **27**, 755–768 (2015).

132. Zeng, Z. *et al.* Targeting the leukemia microenvironment by CXCR4 inhibition overcomes resistance to kinase inhibitors and chemotherapy in AML. *Blood* **113**, 6215–6224 (2009).

133. Matsunaga, T. *et al.* Interaction between leukemic-cell VLA-4 and stromal fibronectin is a decisive factor for minimal residual disease of acute myelogenous leukemia. *Nat Med* **9**, 1158–1165 (2003).

134. Imai, Y., Shimaoka, M. & Kurokawa, M. Essential roles of VLA-4 in the hematopoietic system. *International Journal of Hematology* **91**, 569–575 (2010).

135. Battula, V. L. *et al.* AML-induced osteogenic differentiation in mesenchymal stromal cells supports leukemia growth. *JCI Insight* **2**, (2017).

136. Shafat, M. S. *et al.* Leukemic blasts program bone marrow adipocytes to generate a protumoral microenvironment. *Blood* **129**, 1320–1332 (2017).

137. Boyd, A. L. *et al.* Acute myeloid leukaemia disrupts endogenous myelo-erythropoiesis by compromising the adipocyte bone marrow niche. *Nature Cell Biology 2017 19:11* **19**, 1336–1347 (2017).

138. Hole, P. S. *et al.* Overproduction of NOX-derived ROS in AML promotes proliferation and is associated with defective oxidative stress signaling. *Blood* **122**, 3322–3330 (2013).

139. Aurelius, J. *et al.* Monocytic AML cells inactivate antileukemic lymphocytes: role of NADPH oxidase/gp91phox expression and the PARP-1/PAR pathway of apoptosis. *Blood* **119**, 5832–5837 (2012).

140. Rizo, A. *et al.* Repression of BMI1 in normal and leukemic human CD34+ cells impairs self-renewal and induces apoptosis. *Blood* **114**, 1498–1505 (2009).

141. Izzi, V. *et al.* An extracellular matrix signature in leukemia precursor cells and acute myeloid leukemia. *Haematologica* **102**, e245 (2017).

142. Izzi, V. *et al.* Expression of a specific extracellular matrix signature is a favorable prognostic factor in acute myeloid leukemia. *Leukemia Research Reports* **9**, 9–13 (2018).

143. Long, L. *et al.* Genetic biomarkers of drug resistance: A compass of prognosis and targeted therapy in acute myeloid leukemia. *Drug Resistance Updates* **52**, 100703 (2020).

144. Lee, M. W. *et al.* Mesenchymal stem cells in suppression or progression of hematologic malignancy: current status and challenges. *Leukemia 2019 33:3* **33**, 597–611 (2019).

145. Kamga, P. T. *et al.* Notch signalling drives bone marrow stromal cell-mediated chemoresistance in acute myeloid leukemia. *Oncotarget* **7**, 21713–21727 (2016).

146. Wang, Y. *et al.* A microengineered collagen scaffold for generating a polarized crypt-villus architecture of human small intestinal epithelium. *Biomaterials* **128**, 44 (2017).

147. Pickup, M. W., Mouw, J. K. & Weaver, V. M. The extracellular matrix modulates the hallmarks of cancer. *EMBO Rep* **15**, 1243–1253 (2014).

148. Wolf, D. M. C. & Langhans, S. A. Moving myeloid leukemia drug discovery into the third dimension. *Frontiers in Pediatrics* (2019) doi:10.3389/fped.2019.00314.

149. Kirkland, S. C. Type I collagen inhibits differentiation and promotes a stem cell-like phenotype in human colorectal carcinoma cells. *Br J Cancer* **101**, 320–326 (2009).

150. Motegi, H., Kamoshima, Y., Terasaka, S., Kobayashi, H. & Houkin, K. Type 1 collagen as a potential niche component for CD133-positive glioblastoma cells. *Neuropathology* **34**, 378–385 (2014).

151. Januchowski, R. *et al.* Increased Expression of Several Collagen Genes is Associated with Drug Resistance in Ovarian Cancer Cell Lines. *J Cancer* **7**, 1295 (2016).

152. Lim, Y. C., Oh, S. Y. & Kim, H. Cellular characteristics of head and neck cancer stem cells in type IV collagen-coated adherent cultures. *Experimental Cell Research* **318**, 1104–1111 (2012).

153. Wu, Y. H., Chang, T. H., Huang, Y. F., Chen, C. C. & Chou, C. Y. COL11A1 confers chemoresistance on ovarian cancer cells through the activation of Akt/c/EBPβ pathway and PDK1 stabilization. *Oncotarget* **6**, 23748–23763 (2015).

154. Rada, M. *et al.* Inhibitor of apoptosis proteins (IAPs) mediate collagen type XI alpha 1-driven cisplatin resistance in ovarian cancer. *Oncogene* **37**, 4809–4820 (2018).

155. Liu, C. C. *et al.* Collagen XVII/laminin-5 activates epithelial-to-mesenchymal transition and is associated with poor prognosis in lung cancer. *Oncotarget* **9**, 1656 (2018).

156. Naci, D., Berrazouane, S., Barabé, F. & Aoudjit, F. Cell adhesion to collagen promotes leukemia resistance to doxorubicin by reducing DNA damage through the inhibition of Rac1 activation. *Scientific Reports* **9**, (2019).

157. Naci, D. *et al.* α2β1 integrin promotes chemoresistance against doxorubicin in cancer cells through extracellular signal-regulated kinase (ERK). *J Biol Chem* **287**, 17065–17076 (2012).

158. Favreau, A. J., Vary, C. P. H., Brooks, P. C. & Sathyanarayana, P. Cryptic collagen IV promotes cell migration and adhesion in myeloid leukemia. *Cancer Medicine* **3**, 265 (2014).

159. Taylor, G. A. *et al.* Decreased fibronectin expression in Met/HGF-mediated tumorigenesis. *Oncogene* **17**, 1179–1183 (1998).

160. Illario, M. *et al.* Fibronectin-induced proliferation in thyroid cells is mediated by alphavbeta3 integrin through Ras/Raf-1/MEK/ERK and calcium/CaMKII signals. *J Clin Endocrinol Metab* **90**, 2865–2873 (2005).

161. Nicosia, R. F., Bonanno, E. & Smith, M. Fibronectin promotes the elongation of microvessels during angiogenesis in vitro. *J Cell Physiol* **154**, 654–661 (1993).

162. Astrof, S. & Hynes, R. O. Fibronectins in vascular morphogenesis. *Angiogenesis* **12**, 165–175 (2009).

163. Fernandez-Vidal, A. *et al.* Cell adhesion regulates CDC25A expression and proliferation in acute myeloid leukemia. *Cancer Res* **66**, 7128–7135 (2006).

164. Johansen, S., Brenner, A. K., Bartaula-Brevik, S., Reikvam, H. & Bruserud, Ø. The Possible Importance of β3 Integrins for Leukemogenesis and Chemoresistance in Acute Myeloid Leukemia. *International Journal of Molecular Sciences* **19**, (2018).

165. Nair, M. S. *et al.* Development and molecular characterization of polymeric micro-nanofibrous scaffold of a defined 3-D niche for in vitro chemosensitivity analysis against acute myeloid leukemia cells. *Int J Nanomedicine* **10**, 3603–3622 (2015).

166. Chang, C. *et al.* A laminin 511 matrix is regulated by TAZ and functions as the ligand for the α6Bβ1 integrin to sustain breast cancer stem cells. *Genes Dev* **29**, 1–6 (2015).

167. Rousselle, P. & Scoazec, J. Y. Laminin 332 in cancer: When the extracellular matrix turns signals from cell anchorage to cell movement. *Seminars in Cancer Biology* **62**, 149–165 (2020).

168. Liu, W. *et al.* Aberrant expression of laminin γ2 correlates with poor prognosis and promotes invasion in extrahepatic cholangiocarcinoma. *Journal of Surgical Research* **186**, 150–156 (2014).

169. Laminin-5 chains are expressed differentially in metastatic and nonmetastatic hepatocellular carcinoma - PubMed. https://pubmed.ncbi.nlm.nih.gov/14506159/.

170. Cai, H. *et al.* Critical Role of Lama4 for Hematopoiesis Regeneration and Acute Myeloid Leukemia Progression. *Blood* (2021) doi:10.1182/BLOOD.2021011510.

171. Kobayashi, N. *et al.* Integrin α7 and Extracellular Matrix Laminin 211 Interaction Promotes Proliferation of Acute Myeloid Leukemia Cells and Is Associated with Granulocytic Sarcoma. *Cancers (Basel)* **12**, (2020).

172. Ando, K. *et al.* Expression of 67-Kda Laminin Receptor (67LR) Relates to the Aggressiveness and Poor Prognosis of AML: Modulation of the Expression of GM-CSF Receptor by 67LR. *Blood* **112**, 926–926 (2008).

173. Timar, J. *et al.* Interaction between elastin and tumor cell lines with different metastatic potential; in vitro and in vivo studies. *Journal of Cancer Research and Clinical Oncology 1991 117:3* **117**, 232–238 (1991).

174. Netland, P. A. & Zetter, B. R. Melanoma cell adhesion to defined extracellular matrix components. *Biochemical and Biophysical Research Communications* **139**, 515–522 (1986).

175. Yamashita, J. I. *et al.* Tumor Neutrophil Elastase Is Closely Associated With the Direct Extension of Non-small Cell Lung Cancer Into the Aorta. *Chest* **111**, 885–890 (1997).

176. Blood, C. H. & Zetter, B. R. Membrane-bound Protein Kinase C Modulates Receptor Affinity and Chemotaetic Responsiveness of Lewis Lung Carcinoma Sublines to an Elastin-derived Peptide. *Journal of Biological Chemistry* **264**, 10614–10620 (1989).

177. Blood, C. H., Sasse, J., Brodt, P. & Zetter, B. R. Identification of a tumor cell receptor for VGVAPG, an elastin-derived chemotactic peptide. *J Cell Biol* **107**, 1987–1993 (1988).

178. Helbig G, Krzemień S, Francuz T, Wojnar J & Hołowiecki J. Elastin metabolism is disrupted in patients after allogeneic hematopoietic stem cell transplantation (alloHSCT) for acute and chronic myeloid leukemia - PubMed. *Med Sci Monit* **14**, (2008).

179. Bourguignon, L. Y. W., Peyrollier, K., Xia, W. & Gilad, E. Hyaluronan-CD44 Interaction Activates Stem Cell Marker Nanog, Stat-3-mediated MDR1 Gene Expression, and Ankyrin-regulated Multidrug Efflux in Breast and Ovarian Tumor Cells *. *Journal of Biological Chemistry* **283**, 17635–17651 (2008).

180. Chanmee, T. *et al.* Excessive hyaluronan production promotes acquisition of cancer stem cell signatures through the coordinated regulation of twist and the transforming growth factor β (TGF-β)-snail signaling axis. *Journal of Biological Chemistry* **289**, 26038–26056 (2014).

181. Okuda, H. *et al.* Hyaluronan synthase HAS2 promotes tumor progression in bone by stimulating the interaction of breast cancer stem-like cells with macrophages and stromal cells. *Cancer Research* **72**, 537–547 (2012).

182. Shiina, M. & Bourguignon, L. Y. W. Selective Activation of Cancer Stem Cells by Size-Specific Hyaluronan in Head and Neck Cancer. *International Journal of Cell Biology* **2015**, (2015).

183. Misra, S. *et al.* HA/CD44 interactions as potential targets for cancer therapy. *FEBS J* **278**, 1429 (2011).

184. Klingbeil, P. *et al.* CD44 variant isoforms promote metastasis formation by a tumor cell-matrix cross-talk that supports adhesion and apoptosis resistance. *Mol Cancer Res* **7**, 168–179 (2009).

185. Han, Y. *et al.* Different Inhibitory Effect and Mechanism of Hydroxyapatite Nanoparticles on Normal Cells and Cancer Cells In Vitro and In Vivo. *Scientific Reports 2014 4:1* **4**, 1–8 (2014).

186. Pathi, S. P. MINERALS AND METASTASIS: HYDROXYAPATITE PROMOTES BREAST CANCER COLONIZATION OF BONE. (2013).

187. Sonmez, E. *et al.* Toxicity assessment of hydroxyapatite nanoparticles in rat liver cell model in vitro. *Human and Experimental Toxicology* **35**, 1073–1083 (2016).

188. Reagan, M. R., Liaw, L., Rosen, C. J. & Ghobrial, I. M. Dynamic interplay between bone and multiple myeloma: emerging roles of the osteoblast. *Bone* **75**, 161–169 (2015).

189. Grasset, E. M. *et al.* Matrix Stiffening and EGFR cooperate to promote the collective invasion of cancer cells. *Cancer Research* **78**, 5229–5242 (2018).

190. Gkretsi, V. & Stylianopoulos, T. Cell Adhesion and Matrix Stiffness: Coordinating Cancer Cell Invasion and Metastasis. *Front Oncol* **8**, (2018).

191. Liu, Y. *et al.* Fibrin stiffness mediates dormancy of tumor-repopulating cells via a Cdc42-driven Tet2 epigenetic program. *Cancer Research* **78**, 3926–3937 (2018).

192. Shin, J. W. & Mooney, D. J. Extracellular matrix stiffness causes systematic variations in proliferation and chemosensitivity in myeloid leukemias. *Proc Natl Acad Sci U S A* **113**, 12126–12131 (2016).

193. Choi, J. S., Mahadik, B. P. & Harley, B. A. C. Engineering the hematopoietic stem cell niche: Frontiers in biomaterial science. *Biotechnol J* **10**, 1529–1545 (2015).

194. Teicher, B. A. In vivo/Ex vivo and in situ assays used in cancer research: A brief review. *Toxicologic Pathology* **37**, 114–122 (2009).

195. Rocha, L. B., Goissis, G. & Rossi, M. A. Biocompatibility of anionic collagen matrix as scaffold for bone healing. *Biomaterials* **23**, 449–456 (2002).

196. Habibovic, P. *et al.* 3D microenvironment as essential element for osteoinduction by biomaterials. *Biomaterials* **26**, 3565–3575 (2005).

197. Zhang, Q., Lu, H., Kawazoe, N. & Chen, G. Pore size effect of collagen scaffolds on cartilage regeneration. *Acta Biomaterialia* **10**, 2005–2013 (2014).

198. Nehrer, S. *et al.* Matrix collagen type and pore size influence behaviour of seeded canine chondrocytes. *Biomaterials* **18**, 769–776 (1997).

199. Cheon, D. J. & Orsulic, S. Mouse models of cancer. *Annu Rev Pathol* **6**, 95–119 (2011).

200. Dhami, S. P. S. *et al.* Ex Vivo Co-Culture of AML Blasts and Bone Marrow Mesenchymal Stromal Cells to Accurately Predict the Clinical Efficacy of Cytarabine-Daunorubicin Treatment. *Blood* **132**, 2636 (2018).

201. Leisten, I. *et al.* 3D co-culture of hematopoietic stem and progenitor cells and mesenchymal stem cells in collagen scaffolds as a model of the hematopoietic niche. *Biomaterials* **33**, 1736–1747 (2012).

202. R., M., K., T., J., J. & Jin, S. Electrospun Nanofibers in Tissue Engineering. *Nanofibers - Production, Properties and Functional Applications* (2011) doi:10.5772/24095.

203. Paim, Á., Tessaro, I. C., Cardozo, N. S. M. & Pranke, P. Mesenchymal stem cell cultivation in electrospun scaffolds: mechanistic modeling for tissue engineering. *Journal of Biological Physics* vol. 44 245–271 (2018).

204. Sun, W. *et al.* Improving the Cell Distribution in Collagen-Coated Poly-Caprolactone Knittings. *Tissue Engineering. Part C, Methods* **18**, 731 (2012).

205. Raic, A., Rödling, L., Kalbacher, H. & Lee-Thedieck, C. Biomimetic macroporous PEG hydrogels as 3D scaffolds for the multiplication of human hematopoietic stem and progenitor cells. *Biomaterials* **35**, 929–940 (2014).

206. Severn, C. E. *et al.* Polyurethane scaffolds seeded with CD34(+) cells maintain early stem cells whilst also facilitating prolonged egress of haematopoietic progenitors. *Sci Rep* **6**, (2016).

207. Aljitawi, O. S. *et al.* A Novel 3 Dimensional Stromal-based Model for In Vitro Chemotherapy Sensitivity Testing of Leukemia Cells. *Leuk Lymphoma* **55**, 378 (2014).

208. O'Brien, F. J. Biomaterials & scaffolds for tissue engineering. *Materials Today* **14**, 88–95 (2011).

209. Bianco, J. E. R. *et al.* Characterization of a novel decellularized bone marrow scaffold as an inductive environment for hematopoietic stem cells. *Biomaterials Science* **7**, 1516–1528 (2019).

210. Tan, J. *et al.* Maintenance and expansion of hematopoietic stem/progenitor cells in biomimetic osteoblast niche. *Cytotechnology* **62**, 439 (2010).

211. Berg, E. L., Hsu, Y. C. & Lee, J. A. Consideration of the cellular microenvironment: physiologically relevant co-culture systems in drug discovery. *Adv Drug Deliv Rev* **69–70**, 190–204 (2014).

212. Chen, Y. *et al.* Human extramedullary bone marrow in mice: a novel in vivo model of genetically controlled hematopoietic microenvironment. *Blood* **119**, 4971–4980 (2012).

213. Prockop, D. J. & Kivirikko, K. I. Collagens: molecular biology, diseases, and potentials for therapy. *Annu Rev Biochem* **64**, 403–434 (1995).

214. Offeddu, G. S., Ashworth, J. C., Cameron, R. E. & Oyen, M. L. Multi-scale mechanical response of freeze-dried collagen scaffolds for tissue engineering applications. *Journal of the Mechanical Behavior of Biomedical Materials* **42**, 19–25 (2015).

215. Bak, S. Y., Lee, S. W., Choi, C. H. & Kim, H. W. Assessment of the Influence of Acetic Acid Residue on Type I Collagen during Isolation and Characterization. *Materials* **11**, (2018).

216. Davidenko, N. *et al.* Optimisation of UV irradiation as a binding site conserving method for crosslinking collagen-based scaffolds. *Journal of Materials Science: Materials in Medicine* **27**, 1–17 (2016).

217. Nong, L.-M. *et al.* The effect of different cross-linking conditions of EDC/NHS on type II collagen scaffolds: an in vitro evaluation. *Cell and Tissue Banking 2019 20:4* **20**, 557–568 (2019).

218. B, H., K, G., HG, G., H, S. & N, P. Cross-linking by 1-ethyl-3- (3-dimethylaminopropyl)-carbodiimide (EDC) of a collagen/elastin membrane meant to be used as a dermal substitute: effects on physical, biochemical and biological features in vitro. *J Mater Sci Mater Med* **12**, 437–446 (2001).

219. Bi, L. *et al.* Effects of different cross-linking conditions on the properties of genipin-cross-linked chitosan/collagen scaffolds for cartilage tissue engineering. *Journal of Materials Science: Materials in Medicine* **22**, 51–62 (2011).

220. DA, W., E, S., C, L. & JT, C. Controlling the processing of collagen-hydroxyapatite scaffolds for bone tissue engineering. *J Mater Sci Mater Med* **18**, 201–209 (2007).

221. O'Brien, F. J., Harley, B. A., Yannas, I. v. & Gibson, L. J. The effect of pore size on cell adhesion in collagen-GAG scaffolds. *Biomaterials* **26**, 433–441 (2005).

222. Sobral, J. M., Caridade, S. G., Sousa, R. A., Mano, J. F. & Reis, R. L. Three-dimensional plotted scaffolds with controlled pore size gradients: Effect of scaffold geometry on mechanical performance and cell seeding efficiency. *Acta Biomaterialia* **7**, 1009–1018 (2011).

223. Loh, Q. L. & Choong, C. Three-Dimensional Scaffolds for Tissue Engineering Applications: Role of Porosity and Pore Size. *Tissue Engineering. Part B, Reviews* **19**, 485 (2013).

224. Sachlos, E., Wahl, D. A., Triffitt, J. T. & Czernuszka, J. T. The impact of critical point drying with liquid carbon dioxide on collagen-hydroxyapatite composite scaffolds. *Acta Biomaterialia* (2008) doi:10.1016/j.actbio.2008.03.016.

225. Liu, L., Zhang, L., Ren, B., Wang, F. & Zhang, Q. Preparation and characterization of collagen-hydroxyapatite composite used for bone tissue engineering scaffold. *Artif Cells Blood Substit Immobil Biotechnol* **31**, 435–448 (2003).

226. Kane, R. J. & Roeder, R. K. Effects of hydroxyapatite reinforcement on the architecture and mechanical properties of freeze-dried collagen scaffolds. *Journal of the Mechanical Behavior of Biomedical Materials* **7**, 41–49 (2012).

227. ImageJ. https://imagej.nih.gov/ij/.

228. Sachlos, E., Reis, N., Ainsley, C., Derby, B. & Czernuszka, J. T. Novel collagen scaffolds with predefined internal morphology made by solid freeform fabrication. *Biomaterials* (2003) doi:10.1016/S0142-9612(02)00528-8.

229. Chattopadhyay, S. & Raines, R. T. Collagen-Based Biomaterials for Wound Healing. *Biopolymers* **101**, 821 (2014).

230. [PDF] Effect of physical crosslinking methods on collagen-fiber durability in proteolytic solutions. | Semantic Scholar. https://www.semanticscholar.org/paper/Effect-of-physical-crosslinking-methods-on-in-Weadock-Miller/d792e7120a735b5fbfd369f11c5993083910db9a.

231. Davidenko, N. *et al.* Control of crosslinking for tailoring collagen-based scaffolds stability and mechanics. *Acta Biomaterialia* **25**, 131–142 (2015).

232. Nair, M., Johal, R. K., Hamaia, S. W., Best, S. M. & Cameron, R. E. Tunable bioactivity and mechanics of collagen-based tissue engineering constructs: A comparison of EDC-NHS, genipin and TG2 crosslinkers. *Biomaterials* **254**, (2020).

233. Micallef, L. & Rodgers, P. eulerAPE: Drawing Area-Proportional 3-Venn Diagrams Using Ellipses. *PLOS ONE* **9**, e101717 (2014).

234. Truong, T. M. T., Nguyen, V. M., Tran, T. T. & Le, T. M. T. Characterization of acid-soluble collagen from food processing by-products of snakehead fish (Channa striata). *Processes* **9**, (2021).

235. Wolf, K. L. & Sobral, P. J. A. Characterizations of Collagen Fibers for Biodegradable Films Production. doi:10.1051/IUFoST:20060929.

236. Guvendiren, M., Lu, H. D. & Burdick, J. A. Shear-thinning hydrogels for biomedical applications. doi:10.1039/c1sm06513k.

237. Zandi, N. *et al.* Nanoengineered shear-thinning and bioprintable hydrogel as a versatile platform for biomedical applications. *Biomaterials* **267**, 120476 (2021).

238. Suo, H., Zhang, J., Xu, M. & Wang, L. Low-temperature 3D printing of collagen and chitosan composite for tissue engineering. *Materials Science and Engineering: C* **123**, 111963 (2021).

239. Pins, G. D. & Silver, F. H. A self-assembled collagen scaffold suitable for use in soft and hard tissue replacement. *Materials Science and Engineering: C* **3**, 101–107 (1995).

240. Van Wachem, P. B. *et al.* In vivo biocompatibility of carbodiimide-crosslinked collagen matrices: Effects of crosslink density, heparin immobilization, and bFGF loading. (2001) doi:10.1002/1097-4636.

241. Stamov, D., Grimmer, M., Salchert, K., Pompe, T. & Werner, C. Heparin intercalation into reconstituted collagen I fibrils: Impact on growth kinetics and morphology. *Biomaterials* **29**, 1–14 (2008).

242. White, J. F. *et al.* Collagen Fibril Formation in a Wound Healing Model. *Journal of Structural Biology* **137**, 23–30 (2002).

243. Yunoki, S., Nagai, N., Suzuki, T. & Munekata, M. Novel biomaterial from reinforced salmon collagen gel prepared by fibril formation and cross-linking. *Journal of Bioscience and Bioengineering* **98**, 40–47 (2004).

244. Kim, H. W., Li, L. H., Lee, E. J., Lee, S. H. & Kim, H. E. Fibrillar assembly and stability of collagen coating on titanium for improved osteoblast responses. *Journal of Biomedical Materials Research - Part A* **75**, 629–638 (2005).

245. Usha, R., Sreeram, K. J. & Rajaram, A. Stabilization of collagen with EDC/NHS in the presence of l-lysine: A comprehensive study. *Colloids and Surfaces B: Biointerfaces* **90**, 83–90 (2012).

246. Salehpour, A. *et al.* Dose-dependent response of gamma irradiation on mechanical properties and related biochemical composition of goat bone-patellar tendon-bone allografts. *Journal of Orthopaedic Research* **13**, 898–906 (1995).

247. LH, O. D. *et al.* Influence of ethylene oxide gas treatment on the in vitro degradation behavior of dermal sheep collagen. *J Biomed Mater Res* **29**, 149–155 (1995).

248. Dai, Z., Ronholm, J., Tian, Y., Sethi, B. & Cao, X. Sterilization techniques for biodegradable scaffolds in tissue engineering applications. *J Tissue Eng* **7**, 2041731416648810 (2016).

249. Yunoki, S. *et al.* Influence of gamma Irradiation on the Mechanical Strength and In Vitro Biodegradation of Porous Hydroxyapatite/Collagen Composite. *Journal of the American Ceramic Society* **0**, 060623005134013-??? (2006).

250. Patel, J. M., Jackson, R. C., Schneider, G. L., Ghodbane, S. A. & Dunn, M. G. Carbodiimide cross-linking counteracts the detrimental effects of gamma irradiation on the physical properties of collagen-hyaluronan sponges. *Journal of Materials Science: Materials in Medicine 2018 29:6* **29**, 1–8 (2018).

251. N, N. & Y, I. Mechanism of amide formation by carbodiimide for bioconjugation in aqueous media. *Bioconjugate Chemistry* **6**, 123–130 (1995).

252. Nam, K., Kimura, T. & Kishida, A. Controlling Coupling Reaction of EDC and NHS for Preparation of Collagen Gels Using Ethanol/Water Co-Solvents. *Macromolecular Bioscience* **8**, 32–37 (2008).

253. Park, S. N., Park, J. C., Kim, H. O., Song, M. J. & Suh, H. Characterization of porous collagen/hyaluronic acid scaffold modified by 1-ethyl-3-(3-dimethylaminopropyl)carbodiimide cross-linking. *Biomaterials* **23**, 1205–1212 (2002).

254. (PDF) Control of pH alters the type of cross-linking produced by 1-ethyl-3-(3-dimethylaminopropyl)-carbodiimide (EDC) treatment of acellular matrix vascular grafts. https://www.researchgate.net/publication/227804298_Control_of_pH_alters_the_type_of_cross-linking_produced_by_1-ethyl-3-3-dimethylaminopropyl-carbodiimide_EDC_treatment_of_acellular_matrix_vascular_grafts.

255. SN, P., HJ, L., KH, L. & H, S. Biological characterization of EDC-crosslinked collagen-hyaluronic acid matrix in dermal tissue restoration. *Biomaterials* **24**, 1631–1641 (2003).

256. MA, G., AQ, H. & CL, B. Stability of water-soluble carbodiimides in aqueous solution. *Anal Biochem* **184**, 244–248 (1990).

257. HM, P. & ST, B. EDC cross-linking improves skin substitute strength and stability. *Biomaterials* **27**, 5821–5827 (2006).

258. Yang, S., Leong, K. F., Du, Z. & Chua, C. K. The design of scaffolds for use in tissue engineering. Part I. Traditional factors. *Tissue Eng* **7**, 679–689 (2001).

259. Ishaug-Riley, S. L., Crane-Kruger, G. M., Yaszemski, M. J. & Mikos, A. G. Three-dimensional culture of rat calvarial osteoblasts in porous biodegradable polymers. *Biomaterials* **19**, 1405–1412 (1998).

260. Yamane, S. *et al.* Effect of pore size on in vitro cartilage formation using chitosan-based hyaluronic acid hybrid polymer fibers. *Journal of Biomedical Materials Research Part A* **81A**, 586–593 (2007).

261. Oh, S. H., Park, I. K., Kim, J. M. & Lee, J. H. In vitro and in vivo characteristics of PCL scaffolds with pore size gradient fabricated by a centrifugation method. *Biomaterials* **28**, 1664–1671 (2007).

262. Nuernberger, S. *et al.* The influence of scaffold architecture on chondrocyte distribution and behavior in matrix-associated chondrocyte transplantation grafts. *Biomaterials* **32**, 1032–1040 (2011).

263. Woodfield, T. B. F. *et al.* Design of porous scaffolds for cartilage tissue engineering using a three-dimensional fiber-deposition technique. *Biomaterials* **25**, 4149–4161 (2004).

264. Silva, M. M. C. G. *et al.* The effect of anisotropic architecture on cell and tissue infiltration into tissue engineering scaffolds. *Biomaterials* **27**, 5909–5917 (2006).

265. Faraj, K. A., van Kuppevelt, T. H. & Daamen, W. F. Construction of Collagen Scaffolds That Mimic the Three-Dimensional Architecture of Specific Tissues. *https://home.liebertpub.com/ten* **13**, 2387–2394 (2007).

266. Stanton, A. E., Tong, X. & Yang, F. Varying solvent type modulates collagen coating and stem cell mechanotransduction on hydrogel substrates. *APL Bioengineering* **3**, 036108 (2019).

267. Lavagnino, M., Arnoczky, S. P., Frank, K. & Tian, T. Collagen fibril diameter distribution does not reflect changes in the mechanical properties of in vitro stress-deprived tendons. *Journal of Biomechanics* **38**, 69–75 (2005).

268. HAYASHI, T. & NAGAI, Y. Effect of pH on the Stability of Collagen Molecule in Solution. *The Journal of Biochemistry* **73**, 999–1006 (1973).

269. Deville, S. Freeze-Casting of Porous Ceramics: A Review of Current Achievements and Issues. *Advanced Engineering Materials* **10**, 155–169 (2008).

270. Wegst, U. G. K., Schecter, M., Donius, A. E. & Hunger, P. M. Biomaterials by freeze casting. *Philosophical Transactions of the Royal Society A: Mathematical, Physical and Engineering Sciences* **368**, 2099–2121 (2010).

271. Ng, R., Gurm, J. S. & Yang, S.-T. Centrifugal seeding of mammalian cells in nonwoven fibrous matrices. *Biotechnology Progress* **26**, n/a-n/a (2009).

272. Solchaga, L. A. *et al.* A rapid seeding technique for the assembly of large cell/scaffold composite construct. in *Tissue Engineering* vol. 12 1851–1863 (NIH Public Access, 2006).

273. Griffon, D. J., Abulencia, J. P., Ragetly, G. R., Fredericks, L. P. & Chaieb, S. A comparative study of seeding techniques and three-dimensional matrices for mesenchymal cell attachment. *Journal of Tissue Engineering and Regenerative Medicine* **5**, 169–179 (2011).

274. Buizer, A. T., Veldhuizen, A. G., Bulstra, S. K. & Kuijer, R. Static versus vacuum cell seeding on high and low porosity ceramic scaffolds. *Journal of Biomaterials Applications* **29**, 3–13 (2014).

275. Weinand, C., Xu, J. W., Peretti, G. M., Bonassar, L. J. & Gill, T. J. Conditions affecting cell seeding onto three-dimensional scaffolds for cellular-based biodegradable implants. *Journal of Biomedical Materials Research Part B: Applied Biomaterials* **91B**, 80–87 (2009).

276. Rampersad, S. N. Multiple applications of Alamar Blue as an indicator of metabolic function and cellular health in cell viability bioassays. *Sensors (Basel)* **12**, 12347–12360 (2012).

277. Page, B., Page, M. & Noel, C. A new fluorometric assay for cytotoxicity measurements in vitro. *International Journal of Oncology* **3**, 473–476 (1993).

278. Hoechst Stains.

279. L, T., Y, R. & R, K. A 1-min method for homogenous cell seeding in porous scaffolds. *J Biomater Appl* **26**, 877–889 (2012).

280. Cámara-Torres, M., Sinha, R., Mota, C. & Moroni, L. Improving cell distribution on 3D additive manufactured scaffolds through engineered seeding media density and viscosity. doi:10.1101/815621.

281. Thevenot, P., Nair, A., Dey, J., Yang, J. & Tang, L. Method to analyze three-dimensional cell distribution and infiltration in degradable scaffolds. *Tissue Engineering - Part C: Methods* **14**, 319–331 (2008).

282. J, van den D., PH, S. & JA, J. Evaluation of various seeding techniques for culturing osteogenic cells on titanium fiber mesh. *Tissue Eng* **9**, 315–325 (2003).

283. F, Z. & T, M. Perfusion bioreactor system for human mesenchymal stem cell tissue engineering: dynamic cell seeding and construct development. *Biotechnol Bioeng* **91**, 482–493 (2005).

284. Roh, J. D. *et al.* Centrifugal Seeding Increases Seeding Efficiency and Cellular Distribution of Bone Marrow Stromal Cells in Porous Biodegradable Scaffolds. *https://home-liebertpub-com.ezproxy.library.yorku.ca/ten* **13**, 2743–2749 (2007).

285. D, W., A, M., M, J., M, H. & I, M. Oscillating perfusion of cell suspensions through three-dimensional scaffolds enhances cell seeding efficiency and uniformity. *Biotechnol Bioeng* **84**, 205–214 (2003).

286. Yoshii, T. *et al.* Fresh bone marrow introduction into porous scaffolds using a simple low-pressure loading method for effective osteogenesis in a rabbit model. *Journal of Orthopaedic Research* **27**, 1–7 (2009).

287. Almarza, A. J. & Athanasiou, K. A. Seeding Techniques and Scaffolding Choice for Tissue Engineering of the Temporomandibular Joint Disk. *https://home.liebertpub.com/ten* **10**, 1787–1795 (2004).

288. K, Y., S, I. & Y, T. Influence of culture method on the proliferation and osteogenic differentiation of human adipo-stromal cells in nonwoven fabrics. *Tissue Eng* **10**, 1587–1596 (2004).

289. Melke, J., Zhao, F., Ito, K. & Hofmann, S. Orbital seeding of mesenchymal stromal cells increases osteogenic differentiation and bone-like tissue formation. *Journal of Orthopaedic Research* **38**, 1228 (2020).

290. Bourgine, P. E. *et al.* In vitro biomimetic engineering of a human hematopoietic niche with functional properties. *Proc Natl Acad Sci U S A* **115**, E5688 (2018).

291. Nilsson, S. K. *et al.* Immunofluorescence characterization of key extracellular matrix proteins in murine bone marrow in situ. *Journal of Histochemistry and Cytochemistry* **46**, 371–377 (1998).

292. Klein, G. *The extracellular matrix of the hematopoietic microenvironment*.

293. Haylock, D. N. & Nilsson, S. K. The role of hyaluronic acid in hemopoietic stem cell biology. *Regenerative medicine* (2006) doi:10.2217/17460751.1.4.437.

294. Wu, W., Allen, R., Gao, J. & Wang, Y. Artificial Niche Combining Elastomeric Substrate and Platelets Guides Vascular Differentiation of Bone Marrow Mononuclear Cells. *Tissue Engineering. Part A* **17**, 1979 (2011).

295. Jin, M. *et al.* Transplantation of bone marrow-derived mesenchymal stem cells expressing elastin alleviates pelvic floor dysfunction. *Stem Cell Research and Therapy* **7**, 1–10 (2016).

296. Panoskaltsis, N., Reid, C. D. L. & Knight, S. C. Quantification and cytokine production of circulating lymphoid and myeloid cells in acute myelogenous leukaemia. *Leukemia 2003 17:4* **17**, 716–730 (2003).

297. Panoskaltsis, N. Dendritic cells in MDS and AML – cause, effect or solution to the immune pathogenesis of disease? *Leukemia 2005 19:3* **19**, 354–357 (2005).

298. Palmer, L. C., Newcomb, C. J., Kaltz, S. R., Spoerke, E. D. & Stupp, S. I. Biomimetic Systems for Hydroxyapatite Mineralization Inspired By Bone and Enamel. *Chem Rev* **108**, 4754 (2008).

299. Hamilton, R. & Campbell, F. R. I m m u nochem ical Localization of Extracel l u lar Materials in Bone Marrow of Rats. 231218–224 (1991).

300. Zuckerman, K. S. *et al.* Inhibition of collagen deposition in the extracellular matrix prevents the establishment of a stroma supportive of hematopoiesis in long-term murine bone marrow cultures. *J Clin Invest* **75**, 970–975 (1985).

301. Kattimani, V. S., Kondaka, S. & Lingamaneni, K. P. Hydroxyapatite–-Past, Present, and Future in Bone Regeneration: *https://doi.org/10.4137/BTRI.S36138* **7**, BTRI.S36138 (2016).

302. Szcześ, A., Hołysz, L. & Chibowski, E. Synthesis of hydroxyapatite for biomedical applications. *Advances in Colloid and Interface Science* **249**, 321–330 (2017).

303. Ratnayake, J. T. B., Mucalo, M. & Dias, G. J. Substituted hydroxyapatites for bone regeneration: A review of current trends. *Journal of Biomedical Materials Research Part B: Applied Biomaterials* **105**, 1285–1299 (2017).

304. Mithieux, S. M. & Weiss, A. S. Elastin. *Advances in Protein Chemistry* **70**, 437–461 (2005).

305. Kristensen, J. H. & Karsdal, M. A. Elastin. *Biochemistry of Collagens, Laminins and Elastin: Structure, Function and Biomarkers* 197–201 (2016) doi:10.1016/B978-0-12-809847-9.00030-1.

306. M, M. *et al.* Hydroxyapatite nano and microparticles: correlation of particle properties with cytotoxicity and biostability. *Biomaterials* **30**, 3307–3317 (2009).

307. Zhao, X. *et al.* Cytotoxicity of hydroxyapatite nanoparticles is shape and cell dependent. *Archives of Toxicology 2012 87:6* **87**, 1037–1052 (2012).

308. Yoshii, Y. *et al.* High-throughput screening with nanoimprinting 3D culture for efficient drug development by mimicking the tumor environment. *Biomaterials* **51**, 278–289 (2015).

309. Mizushima, H., Wang, X., Miyamoto, S. & Mekada, E. Integrin signal masks growth-promotion activity of HB-EGF in monolayer cell cultures. *Journal of Cell Science* **122**, 4277–4286 (2009).

310. Cukierman, E., Pankov, R., Stevens, D. R. & Yamada, K. M. Taking Cell-Matrix Adhesions to the Third Dimension. *Science (1979)* **294**, 1708–1712 (2001).

311. Poulos, M. G. *et al.* Activation of the vascular niche supports leukemic progression and resistance to chemotherapy. *Exp Hematol* **42**, 976 (2014).

312. Pezeshkian, B., Donnelly, C., Tamburo, K., Geddes, T. & Madlambayan, G. J. Leukemia Mediated Endothelial Cell Activation Modulates Leukemia Cell Susceptibility to Chemotherapy through a Positive Feedback Loop Mechanism. *PLoS One* **8**, (2013).

313. Cogle, C. R. *et al.* Functional integration of acute myeloid leukemia into the vascular niche. *Leukemia* **28**, 1978–1987 (2014).

314. Iwamoto, S., Mihara, K., Downing, J. R., Pui, C. H. & Campana, D. Mesenchymal cells regulate the response of acute lymphoblastic leukemia cells to asparaginase. *J Clin Invest* **117**, 1049–1057 (2007).

315. Ishikawa, F. *et al.* Chemotherapy-resistant human AML stem cells home to and engraft within the bone-marrow endosteal region. *Nat Biotechnol* **25**, 1315–1321 (2007).

316. Kenny, H. A. *et al.* Quantitative high throughput screening using a primary human three-dimensional organotypic culture predicts in vivo efficacy. *Nat Commun* **6**, 6220 (2015).

317. Ilouga, P. E., Winkler, D., Kirchhoff, C., Schierholz, B. & Wölcke, J. Investigation of 3 Industry-Wide Applied Storage Conditions for Compound Libraries: *http://dx.doi.org.ezproxy.library.yorku.ca/10.1177/1087057106295507* **12**, 21–32 (2006).

318. Cushnie, T. P. T. *et al.* Bioprospecting for Antibacterial Drugs: a Multidisciplinary Perspective on Natural Product Source Material, Bioassay Selection and Avoidable Pitfalls. *Pharmaceutical Research 2020 37:7* **37**, 1–24 (2020).

319. Sachlos, E. *et al.* Identification of Drugs Including a Dopamine Receptor Antagonist that Selectively Target Cancer Stem Cells. *Cell* **149**, 1284–1297 (2012).

320. Aslostovar, L. *et al.* A phase 1 trial evaluating thioridazine in combination with cytarabine in patients with acute myeloid leukemia. *Blood Advances* **2**, 1935 (2018).

321. Faruqi, A. & Tadi, P. Cytarabine. *xPharm: The Comprehensive Pharmacology Reference* 1–5 (2021).

322. Wen, J., Tong, Y. & Zu, Y. Low Concentration DMSO Stimulates Cell Growth and In vitro Transformation of Human Multiple Myeloma Cells. *Journal of Advances in Medicine and Medical Research* **5**, 65–74 (2015).

323. Tunçer, S. *et al.* Low dose dimethyl sulfoxide driven gross molecular changes have the potential to interfere with various cellular processes. *Scientific Reports 2018 8:1* **8**, 1–15 (2018).

324. Colturato-Kido, C. *et al.* Inhibition of autophagy enhances the antitumor effect of thioridazine in acute lymphoblastic leukemia cells. *Life* **11**, (2021).

325. Fischer, J. & Ganellin, C. R. (C. R. Analogue-based drug discovery. 575 (2006).

326. BS, C. & K, P. Development of cytarabine prodrugs and delivery systems for leukemia treatment. *Expert Opin Drug Deliv* **7**, 1399–1414 (2010).

327. Murphy, T. & Yee, K. W. L. Cytarabine and daunorubicin for the treatment of acute myeloid leukemia. *http://dx.doi.org/10.1080/14656566.2017.1391216* **18**, 1765–1780 (2017).

328. Briot, T., Roger, E., Thépot, S. & Lagarce, F. Advances in treatment formulations for acute myeloid leukemia. *Drug Discovery Today* **23**, 1936–1949 (2018).

329. Cucchi, D. G. J., Groen, R. W. J., Janssen, J. J. W. M. & Cloos, J. Ex vivo cultures and drug testing of primary acute myeloid leukemia samples: Current techniques and implications for experimental design and outcome. *Drug Resistance Updates* **53**, 100730 (2020).

330. Thoma, C. R. *et al.* A high-throughput-compatible 3D microtissue co-culture system for phenotypic RNAi screening applications. *J Biomol Screen* **18**, 1330–1337 (2013).

331. Vörsmann, H. *et al.* Development of a human three-dimensional organotypic skin-melanoma spheroid model for in vitro drug testing. *Cell Death Dis* **4**, (2013).

332. Perez, D. R. *et al.* High throughput flow cytometry identifies small molecule inhibitors for drug repurposing in T-ALL. *SLAS Discov* **23**, 732 (2018).

333. Sutherland, H. J., Blair, A. & Zapf, R. W. Characterization of a Hierarchy in Human Acute Myeloid Leukemia Progenitor Cells. *Blood* **87**, 4754–4761 (1996).

334. Minden, M. D., Buick, R. N. & McCulloch, E. A. Separation of Blast Cell and T-Lymphocyte Progenitors in the Blood of Patients With Acute Myeloblastic Leukemia. *Blood* **54**, 186–195 (1979).

335. Bradley, T. R. & Metcalf, D. The growth of mouse bone marrow cells in vitro. *Aust J Exp Biol Med Sci* **44**, 287–299 (1966).

336. Frisch, B. J. *et al.* Functional inhibition of osteoblastic cells in an in vivo mouse model of myeloid leukemia. *Blood* **119**, 540–550 (2012).

337. Krause, D. S. *et al.* Differential regulation of myeloid leukemias by the bone marrow microenvironment. *Nat Med* **19**, 1513–1517 (2013).

338. Halper, J. & Kjaer, M. Basic Components of Connective Tissues and Extracellular Matrix: Elastin, Fibrillin, Fibulins, Fibrinogen, Fibronectin, Laminin, Tenascins and Thrombospondins. 31–47 (2014) doi:10.1007/978-94-007-7893-1_3.

339. Kolenda, T. *et al.* State of the art paper 2D and 3D cell cultures-a comparison of different types of cancer cell cultures. (2016) doi:10.5114/aoms.2016.63743.

340. Marushima, H. *et al.* Three-dimensional culture promotes reconstitution of the tumor-specific hypoxic microenvironment under TGFβ stimulation. *Int J Oncol* **39**, 1327–1336 (2011).

341. Frieboes, H. B. *et al.* An Integrated Computational/Experimental Model of Lymphoma Growth. *PLoS Computational Biology* **9**, (2013).

342. Powers, M. J. *et al.* Functional behavior of primary rat liver cells in a three-dimensional perfused microarray bioreactor. *Tissue Eng* **8**, 499–513 (2002).

343. Semino, C. E., Merok, J. R., Crane, G. G., Panagiotakos, G. & Zhang, S. Functional differentiation of hepatocyte-like spheroid structures from putative liver progenitor cells in three-dimensional peptide scaffolds. *Differentiation* **71**, 262–270 (2003).

344. Ghosh, S. *et al.* Three-dimensional culture of melanoma cells profoundly affects gene expression profile: a high density oligonucleotide array study. *J Cell Physiol* **204**, 522–531 (2005).

345. Walkley, C. R. *et al.* A microenvironment-induced myeloproliferative syndrome caused by retinoic acid receptor gamma deficiency. *Cell* **129**, 1097–1110 (2007).

346. Walkley, C. R., Shea, J. M., Sims, N. A., Purton, L. E. & Orkin, S. H. Rb regulates interactions between hematopoietic stem cells and their bone marrow microenvironment. *Cell* **129**, 1081–1095 (2007).

347. Raaijmakers, M. H. G. P. *et al.* Bone progenitor dysfunction induces myelodysplasia and secondary leukaemia. *Nature* **464**, 852–857 (2010).

348. Kode, A. *et al.* Leukaemogenesis induced by an activating β-catenin mutation in osteoblasts. *Nature* **506**, 240–244 (2014).

349. Bergamaschi, A. *et al.* Extracellular matrix signature identifies breast cancer subgroups with different clinical outcome. *J Pathol* **214**, 357–367 (2008).

350. Dhami, S. P. S., Kappala, S. S., Thompson, A. & Szegezdi, E. Three-dimensional ex vivo co-culture models of the leukaemic bone marrow niche for functional drug testing. *Drug Discovery Today* **21**, 1464–1471 (2016).

351. Rücker, F. G. *et al.* Molecular profiling reveals myeloid leukemia cell lines to be faithful model systems characterized by distinct genomic aberrations. *Leukemia 2006 20:6* **20**, 994–1001 (2006).

352. Davies, A. H. *et al.* Inhibition of RSK with the novel small-molecule inhibitor LJI308 overcomes chemoresistance by eliminating cancer stem cells. *Oncotarget* **6**, 20570 (2015).

353. Speers, C. *et al.* Identification of novel kinase targets for the treatment of estrogen receptor-negative breast cancer. *Clin Cancer Res* **15**, 6327–6340 (2009).

354. Brough, R. *et al.* Functional viability profiles of breast cancer. *Cancer Discov* **1**, 260–273 (2011).

355. Kang, S. *et al.* Fibroblast growth factor receptor 3 associates with and tyrosine phosphorylates p90 RSK2, leading to RSK2 activation that mediates hematopoietic transformation. *Mol Cell Biol* **29**, 2105–2117 (2009).

356. Aronchik, I. *et al.* Novel potent and selective inhibitors of p90 ribosomal S6 kinase reveal the heterogeneity of RSK function in MAPK-driven cancers. *Molecular Cancer Research* **12**, 803–812 (2014).

357. Kumar, M. & Pattnaik, B. R. Focus on Kir7.1: physiology and channelopathy. *Channels* **8**, 488 (2014).

358. Swale, D. R. *et al.* ML418: The first selective, sub-micromolar pore blocker of Kir7.1 potassium channels. *ACS Chem Neurosci* **7**, 1013 (2016).

359. Montalvo-Ortiz, B. L. *et al.* Characterization of EHop-016, Novel Small Molecule Inhibitor of Rac GTPase. *The Journal of Biological Chemistry* **287**, 13228 (2012).

360. Dharmawardhane, S., Hernandez, E. & Vlaar, C. Development of EHop-016: a small molecule inhibitor of Rac. *Enzymes* **33 Pt A**, 117–146 (2013).

361. Mizukawa, B. *et al.* The cell polarity determinant CDC42 controls division symmetry to block leukemia cell differentiation. *Blood* **130**, 1336–1346 (2017).

362. Brandwein, J. M. *et al.* A phase II open-label study of aprepitant as anti-emetic prophylaxis in patients with acute myeloid leukemia (AML) undergoing induction chemotherapy. *Supportive Care in Cancer* **27**, 2295–2300 (2019).

363. Muñoz, M. & Coveñas, R. The Neurokinin-1 Receptor Antagonist Aprepitant, a New Drug for the Treatment of Hematological Malignancies: Focus on Acute Myeloid Leukemia. *Journal of Clinical Medicine* **9**, (2020).

364. Ziche, M. *et al.* Substance P stimulates neovascularization in vivo and proliferation of cultured endothelial cells. *Microvasc Res* **40**, 264–278 (1990).

365. Muñoz, M. & Coveñas, R. Involvement of substance P and the NK-1 receptor in cancer progression. *Peptides (N.Y.)* **48**, 1–9 (2013).

366. Muñoz, M. & Coveñas, R. Glioma and Neurokinin-1 Receptor Antagonists: A New Therapeutic Approach. *Anticancer Agents Med Chem* **19**, 92–100 (2019).

367. Javid, H., Mohammadi, F., Zahiri, E. & Hashemy, S. I. The emerging role of substance P/neurokinin-1 receptor signaling pathways in growth and development of tumor cells. *J Physiol Biochem* **75**, 415–421 (2019).

368. Muñoz, M., González-Ortega, A. & Coveñas, R. The NK-1 receptor is expressed in human leukemia and is involved in the antitumor action of aprepitant and other NK-1 receptor antagonists on acute lymphoblastic leukemia cell lines. *Invest New Drugs* **30**, 529–540 (2012).

369. Molinos-Quintana, A. *et al.* Human acute myeloid leukemia cells express Neurokinin-1 receptor, which is involved in the antileukemic effect of Neurokinin-1 receptor antagonists. *Investigational New Drugs* **37**, 17–26 (2019).

370. Song, H. *et al.* Hemokinins modulate endothelium function and promote angiogenesis through neurokinin-1 receptor. *Int J Biochem Cell Biol* **44**, 1410–1421 (2012).

371. Li, H. Y., Appelbaum, F. R., Willman, C. L., Zager, R. A. & Banker, D. E. Cholesterol-modulating agents kill acute myeloid leukemia cells and sensitize them to therapeutics by blocking adaptive cholesterol responses. *Blood* **101**, 3628–3634 (2003).

372. Clutterbuck, R. D. *et al.* Inhibitory effect of simvastatin on the proliferation of human myeloid leukaemia cells in severe combined immunodeficient (SCID) mice. *British Journal of Haematology* **102**, 522–527 (1998).

373. Crestor and Acute myelogenous leukemia (aml) - adult, a phase IV clinical study of FDA data - eHealthMe. https://www.ehealthme.com/ds/crestor/acute-myelogenous-leukemia-aml-adult/.

374. Chen, F. *et al.* Classic and targeted anti-leukaemic agents interfere with the cholesterol biogenesis metagene in acute myeloid leukaemia: Therapeutic implications. *Journal of Cellular and Molecular Medicine* **24**, 7378–7392 (2020).

375. Monaghan, L. *et al.* The Emerging Role of H3K9me3 as a Potential Therapeutic Target in Acute Myeloid Leukemia. *Frontiers in Oncology* **9**, 705 (2019).

376. Allali-Hassani, A. *et al.* Discovery of a chemical probe for PRDM9. *Nature Communications* **10**, (2019).

377. Zhou, F., Ge, Z. & Chen, B. Quizartinib (AC220): a promising option for acute myeloid leukemia. *Drug Design, Development and Therapy* **13**, 1117 (2019).

378. Hou, Y. *et al.* Design and synthesis of first environment-sensitive coumarin fluorescent agonists for MrgX2. *International Journal of Biological Macromolecules* **203**, 481–491 (2022).

379. Kim, N. *et al.* Systematic analysis of genotype-specific drug responses in cancer. *Int J Cancer* **131**, 2456–2464 (2012).

Appendices

Appendix 1. SEM Images of ECM Components Employed in Preparation of Composite Scaffolds

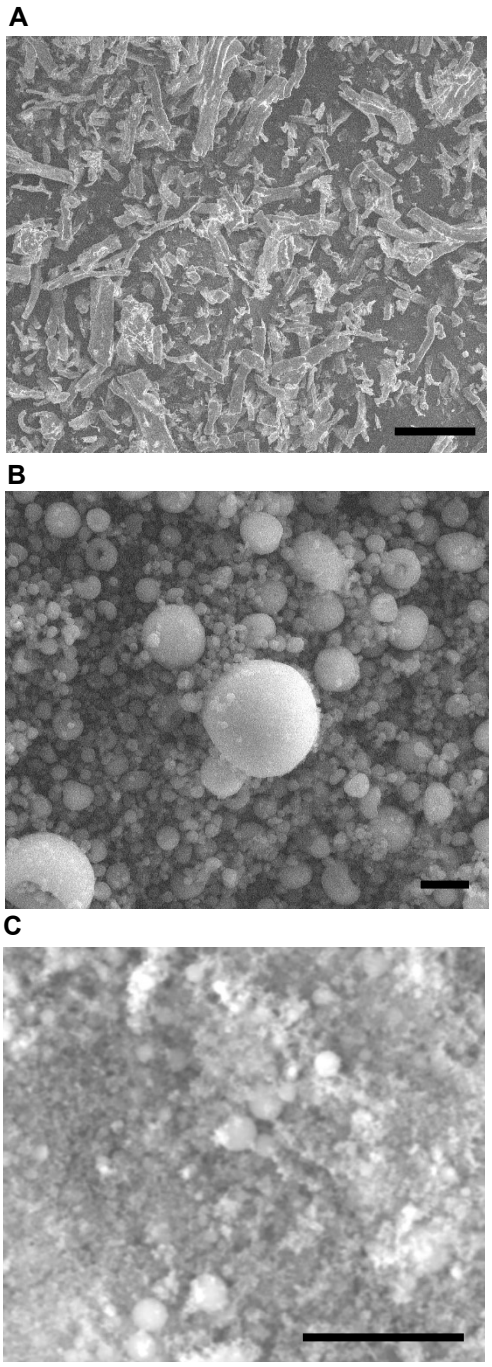

Supplemental Figure 2. Representative SEM Images of ECM Components (**A**) Elastin fibers, scale bar represents 100 µm. (**B**). Micro Hydroxyapatite powder 10 µm, scale bar represents 10 µm. (**C**). Nano Hydroxyapatite powder 10 µm, scale bar represents 5 µm.

Appendix 2. Cell Recovery from Collagen Structures Analysis with HOECHST dye

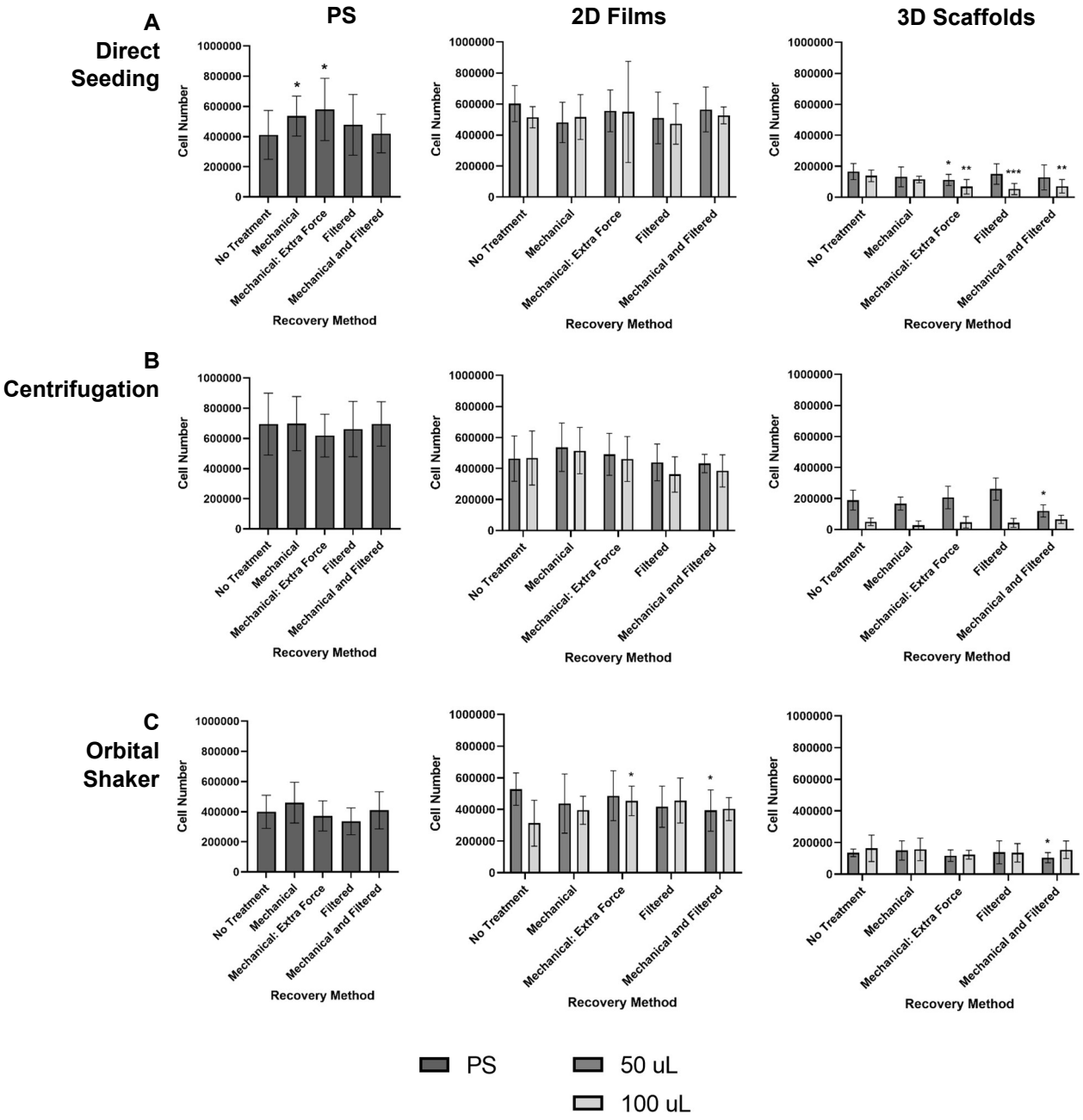

Supplemental Figure 3. Measuring of efficacy of different seeding and recovery methods for 2D collagen films and 3D scaffolds. Five recovery methods were compared, and the number of cells retrieved from the various conditions was reported by analyzing the reported HOECHST signal. Three culture systems were studied: 2D films, 3D scaffolds and polystyrene control, with the collagen containing samples further split into 50 µL and 100 µL size structures. Each recovery technique was evaluated across three separate seeding techniques Cells were stained with Alamar Blue and fluorescent response was analyzed (Data reported as Mean ±SD, t-test two-tailed, (*) $p < 0.05$, (**) $p < 0.01$, (***) $p < 0.001$). (**A**). Direct seeding was employed. (**B**). Dynamic seeding technique of centrifugation at 1500 rpm for 10 seconds was used. (**C**). Dynamic seeding technique of maintaining the cells on an orbital shaker throughout the incubation period was adopted.

Appendix 3. List of Compounds Employed in the Drug Screening Assay

Table 1. Description of the chemical agents utilized in the high-throughput screen, adopted from the Tocris Chemical Library.

Compound Name	Target Class	Action	Primary Target	Brief Description
TM 5441	Enzyme	Inhibitor	Plasminogen Activator Inhibitor 1	Plasminogen activator inhibitor-1 (PAI-1) inhibitor
Brequinar sodium			Dihyroorotate Dehydrogenase	Potent and selective DHODH inhibitor
MS 275			Class I HDACs	HDAC (Class I) inhibitor
Rucaparib camsylate			Poly(ADP-ribose) Polymerase	PARP inhibitor
Dacomitinib			EGFR	Potent irreversible pan ErbB inhibitor
O8 OGG1 Inhibitor			Glycosylases	Potent and selective 8-oxoguanine DNA glycosylase 1 (OGG1) inhibitor
SM 16			TGF-beta Receptors	Potent TGF-βRI inhibitor; orally bioavailable
EHop 016			Rho	Rac inhibitor
Givinostat hydrochloride			Non-selective HDACs	Histone deacetylase inhibitor
CC 401 dihydrochloride			JNK/c-jun	High affinity JNK inhibitor; also inhibits HCMV replication
CRT 0105950			LIMK	Potent LIMK1/2 inhibitor
SLM 6031434 hydrochloride			Sphingosine Kinase	Selective sphingosine kinase 2 (Sphk2) inhibitor
BRD 73954			Class II HDACs	Dual histone deacetylase (HDAC) 6/8 inhibitor
JH-II-127			LRRK2	Potent and selective LRRK2 inhibitor
Tadalafil			Phosphodiesterases	Potent and highly selective PDE5 inhibitor; orally bioavailable
CBM 301940			Decarboxylases	Potent malonyl-CoA decarboxylase inhibitor; orally bioavailable
ESI 05			EPAC	Epac2 inhibitor
Autophinib			PI 3-Kinase	Potent VPS34 inhibitor

Compound Name	Target Class	Action	Primary Target	Brief Description
AZ 5704	Enzyme	Inhibitor	ATM & ATR Kinase	Potent and selective ATM kinase inhibitor; orally bioavailable
Epiblastin A			Casein Kinase 1	CK1 inhibitor; converts epiblast stem cells to ESCs and promotes ESC self-renewal
Rosuvastatin calcium			HMG-CoA Reductase	Potent HMG-CoA reductase inhibitor
OUL 35			Poly(ADP-ribose) Polymerase	Selective PARP-10 inhibitor
PF 5006739			Casein Kinase 1	Potent CK1δ/ε inhibitor
Pelitinib			EGFR	Potent and irreversible EGFR inhibitor; orally bioavailable
Avagacestat			Gamma-Secretase	Highly potent γ-secretase inhibitor; orally bioavailable
PF 04457845			Fatty Acid Amide Hydrolase (FAAH)	Potent and selective irreversible FAAH inhibitor
Ciclopirox			Histone Demethylases	Pan-histone demethylase inhibitor
A 485			Histone Acetyltransferases	Potent and selective p300/CBP inhibitor; orally bioavailable
PF 05180999			Phosphodiesterases	Potent and selective PDE2A inhibitor
Fendiline Hydrochloride			Ras GTPases	Inhibits KRas localization to the plasma membrane; also L-type calcium channel blocker
ML 210			Ras GTPases	Selectively kills mutant HRAS-expressing cells; glutathione peroxidase inhibitor; induces ferroptosis
ML 323			Deubiquitinating Enzymes	Potent and selective USP1-UAF1 allosteric inhibitor

Compound Name	Target Class	Action	Primary Target	Brief Description
BRD 6989	Enzyme	Inhibitor	Cyclin-dependent Kinase	Cdk8 inhibitor; enhances IL-10 production
JNJ 0966			Matrix Metalloprotease	Pro-MMP9 activation inhibitor
ML 351			Lipoxygenase	Selective 12/15 LOX inhibitor; active in vivo
LY 2603618			Checkpoint Kinases	Potent and selective Chk1 inhibitor
CU CPT 9a			Toll-like Receptors	Highly potent TLR8 inhibitor
XMU MP 1			Other Kinases	Potent and selective MST1/2 inhibitor; orally bioavailable
GSK'872			RIP Kinases	Potent and selective RIP3 kinase inhibitor
Avasimibe			Acyl-CoA:Cholesterol Acyltransferase	ACAT inhibitor
PF 06551600 malonate			JAK Kinase	Potent and selective JAK3 inhibitor
Saxagliptin hydrochloride			Dipeptidyl Peptidase IV (DPP-IV)	High affinity DPP-IV inhibitor; active in vivo
SGC AAK1 1			Other Kinases	AAK1 and BMP2K inhibitor; activates Wnt signaling
TH 5427 hydrochloride			Other Hydrolases	Potent NUDT5 inhibitor
UNC 2881			Other RTKs	Potent Mer kinase inhibitor
CP 43			Other Kinases	Potent TAOK inhibitor
LY 450139			Gamma-Secretase	γ-secretase pseudo-inhibitor
SGC GAK 1			Other Kinases	High affinity cyclin G associated kinase (GAK) inhibitor
Pyridone 6			JAK Kinase	Potent pan-JAK inhibitor; induces intermediate mesoderm; cell-permeable

Compound Name	Target Class	Action	Primary Target	Brief Description
BAY 826	Enzyme	Inhibitor	Other RTKs	Potent Tie2 inhibitor
SPRi 3			Other Reductase	Potent sepiapterin reductase (SPR) inhibitor; attenuates proliferation of CD4+ T cells
OD 36 hydrochloride			RIP Kinases	Potent RIP2 kinase inhibitor
WM 1119			Histone Acetyltransferases	High affinity KAT6A (MOZ) competitive inhibitor
1A-116			Rho	Rac1 inhibitor; blocks Rac1-P-Rex1 interaction
MB 05032			Other Transferases	Potent FBPase inhibitor; promotes HSC expansion
AP C5			Protein Kinase G	Potent and selective PKG2 inhibitor
Roflumilast			Phosphodiesterases	Potent and selective PDE4 inhibitor
NGI 1			Other Transferases	Oligosaccharyltransferase (OST) inhibitor; anti-flaviviral
VAS 2870			NADPH Oxidase	NADPH oxidase (Nox) inhibitor
Darunavir			Other Proteases	Highly potent HIV protease inhibitor
A 77-01			TGF-beta Receptors	Potent inhibitor of TGF-βRI
RGFP 966			Class I HDACs	Potent and selective HDAC3 inhibitor
Acetazolamide			Carbonic anhydrases	Carbonic anhydrase inhibitor
CHS 828			NAMPT	NAMPT inhibitor; active in vivo and cytotoxic
LJI308			RSK	Potent pan-RSK inhibitor
Darapladib			Phospholipases	Potent lp-PLA2 inhibitor
Raphin 1			Protein Ser/Thr Phosphatases	Inhibitor of the regulatory subunit PPP1R15B of protein phosphatase 1; orally bioavailable and brain penetrant

Compound Name	Target Class	Action	Primary Target	Brief Description
JTP 103237	Enzyme	Inhibitor	Other Transferases	Potent and selective monoacyglycerol acyltransferase 2 (MOGAT2) inhibitor
Quizartinib			FLT3	Highly potent FLT3 inhibitor
Dasatinib			Src Kinases	Highly potent pan-Src/Bcr-Abl inhibitor
MRK 740			Other Lysine Methyltransferases	Potent PRDM9 inhibitor
Afatinib dimaleate			EGFR	Potent dual specificity EGFR/HER2 inhibitor; active in vivo
Sitagliptin phosphate			Dipeptidyl Peptidase IV (DPP-IV)	Potent and selective DPP IV inhibitor
ZAP 180013			Other RTKs	Zap70 inhibitor; inhibits interaction with ITAMs
BAY 293			Ras GTPases	Potent KRas/SOS1 interaction inhibitor
TH 257			LIMK	Potent and selective allosteric LIMK 1/2 inhibitor
Idasanutlin			Ubiquitin E3 Ligases	Potent MDM2 inhibitor; inhibits MDM2-p53 interaction
AZD 5363			Akt (Protein Kinase B)	Potent pan-AKT inhibitor
Cytarabine			DNA Polymerase Inhibitor	Pyrimidine analog, competes with cytidine to incorporate itself in the DNA ceasing DNA replication
TR 14035		Antagonist	Integrins	Potent integrin α4β7 and α4β1 (VLA-4) antagonist; orally bioavailable
Squarunkin A hydrochloride		Other	Src Kinases	UNC119 chaperone-cargo interaction inhibitor; disrupts Src activation
Lenalidomide			Ubiquitin E3 Ligases	Cereblon binder; induces ubiquitination and degradation of CK1α by E3 ubiquitin ligase
SSR 149415	7-TM Receptors	Antagonist	Vasopressin Receptors	Potent and selective vasopressin V1B antagonist
Bosentan			Non-selective Endothelin	High affinity dual ETA and ETB receptor antagonist;orally bioavailable

Compound Name	Target Class	Action	Primary Target	Brief Description
JNJ 39758979 dihydrochloride	7-TM Receptors	Antagonist	Histamine H4 Receptors	High affinity and selective histamine H4 antagonist; orally bioavailable
MS 21570			GPR171	GPR171 antagonist
Trazodone hydrochloride			5-HT2A Receptors	5-HT2A and α1 adrenoceptor antagonist; also enhances neural differentiation; antidepressant and neuroprotectant
Phentolamine Mesylate			Non-selective Adrenergic Alpha Receptors	Adrenergic α receptor antagonist; antihypertensive
Aprepitant			NK1 Receptor	Potent long-acting hNK1 antagonist
PF 04449913 maleate			Smoothened Receptors	Potent Smo antagonist
AZD 2098			Chemokine CC Receptors	Potent and selective CCR4 antagonist
PA 8			PACAP Receptors	PAC1 receptor antagonist
Silodosin			Adrenergic Alpha-1 Receptors	Selective α1A antagonist
Conivaptan hydrochloride			Vasopressin Receptors	Very high affinity vasopressin V1A and V2 antagonist; orally bioavailable
Thioridazine			Dopamine Receptor 2	Antipsychotic, DR antagonist of the phenothiazine group
J 2156		Agonist	Somatostatin Receptors	Selective high affinity human sst4 agonist
Vilazodone hydrochloride			5-HT1A Receptors	Potent 5-HT1A partial agonist and SSRI; antidepressant
Arformoterol tartrate			Adrenergic Beta-2 Receptors	Long-acting β2 agonist (LABA)
MS 15203			GPR171	Potent and selective GPR171 partial agonist
PF 04628935			Ghrelin Receptors	Potent ghrelin receptor inverse agonist

Compound Name	Target Class	Action	Primary Target	Brief Description
(R)-ZINC 3573	7-TM Receptors	Agonist	Mas-related G Protein-Coupled Receptors	MRGPRX2 agonist
CID 1375606			Orphan 7-TM Receptors	GPR27 agonist
ML 184			GPR55	Selective GPR55 agonist; also promotes NSC proliferation and differentiation
GSK 2018682			Sphingosine-1-phosphate Receptors	S1P1 and S1P5 agonist
TAK 375			Melatonin (MT) Receptors	Very high affinity and selective melatonin receptor agonist
FTBMT			Orphan 7-TM Receptors	Potent and selective GPR52 agonist; orally bioavailable and BBB permeable
tBPC		Modulator	NPY Receptors	Positive allosteric modulator of NPY Y4 receptor
KI-7			Adenosine A2B Receptors	Positive allosteric modulator of A2B receptors
FITM			Glutamate (Metabotropic) Group I Receptors	Potent and selective negative allosteric modulator of mGlu1 receptors
VU 6005649			Glutamate (Metabotropic) Group III Receptors	Positive allosteric modulators of mGlu7 and mGlu8 receptors; also NK1 antagonist; brain penetrant
LY 2033298			M4 Receptors	Selective positive allosteric modulator of M4 receptors; active in vivo; antipsychotic
GSK 6853	Cell Biology	Inhibitor	Bromodomains	Potent and selective BRPF1 inhibitor
ML 385			Nrf2	Nrf2 inhibitor; phenotypically lethal
L Moses dihydrochloride			Bromodomains	High affinity and selective PCAF bromodomain inhibitor
Nelarabine			DNA, RNA and Protein Synthesis	Purine nuceloside analog; inhibits DNA synthesis

Compound Name	Target Class	Action	Primary Target	Brief Description
A 410099.1	Cell Biology	Inhibitor	Inhibitor of Apoptosis (IAP)	High affinity XIAP antagonist; active in vivo
YM 155			Inhibitor of Apoptosis (IAP)	Survivin suppressor
FM19G11			Hypoxia Inducible Factors	HIF α-subunit inhibitor
Obatoclax mesylate			Bcl-2 Family	Inhibitor of Bcl-2 family members; antiapoptotic
16673-34-0 NLRP3i			Inflammasomes	NLRP3 inflammasome inhibitor
TC SL C5			DNA, RNA and Protein Synthesis	Metastasis-associated lung adenocarcinoma transcript 1 (Malat1) RNA inhibitor
ABT 199			Bcl-2 Family	Selective, high affinity Bcl-2 inhibitor; orally bioavailable
BAY 87-2243			Oxidative Phosphorylation	Mitochondrial complex I inhibitor
GSK 9311 hydrochloride		Control	Bromodomains	Negative control for GSK 6853
FPS ZM1		Antagonist	RAGE	High affinity antagonist of RAGE
H 151			STING-Dependent Signaling	STING antagonist
FIN 56		Activator	Ferroptosis	Ferroptosis activator
4-Octyl itaconate			Nrf2	Nrf2 activator; cell permeable
UCLA GP130 2		Agonist	Cytokines	gp130 agonist; brain penetrant and neuroprotectant
CMA			STING-Dependent Signaling	Murine-selective STING agonist
Mefloquine hydrochloride		Blocker	Gap Channels	Cx36 and Cx50 gap channel blocker; also antimalarial and antischistosomal
AA 147		Other	Other ER stress/UPR	ER proteostasis regulator

Compound Name	Target Class	Action	Primary Target	Brief Description
SAK 3	Ion Channels	Activator	Cav3.x Channels	Potent CaV3.1 and 3.3 activator; orally bioavailable
GSK 1702934A			TRPC	Potent and selective TRPC3/6 activator
Jedi2			Piezo Channels	Piezo1 channel activator
GI 530159			Two-P Potassium Channels	K2P2.1 (TREK-1) and K2P10.1 (TREK-2) channel activator
ML 67-33			Two-P Potassium Channels	K2P2.1 (TREK-1), K2P10.1 (TREK-2) and K2P4.1 (TRAAK) channel activator
ML 402			Two-P Potassium Channels	Selective TREK channel activator
JNJ 55511118		Modulator	AMPA Receptors	High affinity and selective negative modulator of AMPA receptors containing TARP-γ8
UoS 12258			AMPA Receptors	Positive allosteric modulator of AMPA receptors
GNE 9278			NMDA Receptors	Positive allosteric modulator of NMDA receptors; acts in transmembrane domain
Dooku 1			Piezo Channels	Reversibly blocks Yoda1 activity; does not affect constitutive Piezo1 activity
B 973B			Nicotinic (a7) Receptors	Positive allosteric modulator of α7 nAChRs; analgesic
ABT 594 hydrochloride		Agonist	Nicotinic (a4b2) Receptors	Selective α4β2 nAChR agonist
AMG 333		Antagonist	TRPM	Potent and selective TRPM8 antagonist; active in vivo
Z 944		Blocker	Cav3.x Channels	CaV3.x blocker
Ivabradine hydrochloride			HCN Channels	HCN channel blocker; inhibits If pacemaker current
CBA			TRPM	Selective TRPM4 blocker
AC 1903			TRPC	Selective TRPC5 blocker

Compound Name	Target Class	Action	Primary Target	Brief Description
ABT 639	Ion Channels	Blocker	Cav3.x Channels	CaV3.2 and CaV3.1 channel blocker; orally bioavailable
VU 0134992			Inward rectifier Potassium Channels	Kir4.1 blocker
ML 418			Inward rectifier Potassium Channels	Kir 7.1 inhibitor; also inhibits Kir 6.2
A 1899			Two-P Potassium Channels	Potent K2P3.1 (TASK-1) and K2P9.1 (TASK-3) blocker
OB-1		Other	Piezo Channels	Stomatin-like protein-3 (STOML3) oligomerization inhibitor
XY 018	Nuclear Receptors	Antagonist	Retinoic Acid-related Orphan Receptors	RORγ antagonist; inhibits AR expression
SR 16832			PPARgamma Receptors	Dual site PPARγ inhibitor
Megestrol Acetate		Agonist	Progesterone Receptor	Synthetic progesterone analog
Tamoxifen		Modulator	Estrogen and Related Receptors	Estrogen receptor partial agonist/antagonist
GT 949	Transporter	Modulator	Glutamate Transporters	Potent and selective positive allosteric modulator of EAAT2
DMSO - Control	N/A			Polar, aprotic organic solvent

Appendix 4. Summary of Results from High-Throughput Drug Screening Assay

Table 2. Results of the drug screening assay and statistical significance of response variation across the culture systems, colors correspond to the legends presented in scatter plot in Figure 14 (Data reported as normalized Mean, n=3, multiple unpaired t-test (*) $p < 0.05$, (**) $p < 0.01$).

Compound Name	Average in PS	Average in 2D	Average in 3D	Significance in 2D vs PS (Figure 14A)	Significance in 3D vs PS (Figure 14B)	Significance in 2D vs 3D (Figure 14C)
Aprepitant	51.56	88.47	126.27	**	*	NS
Ciclopirox	2.17	100.57	7.08	*	NS	*
XY 018	4.35	50.44	12.70	*	NS	*
EHop 016	-1.21	79.64	54.29	*	NS	NS
Obatoclax mesylate	14.67	53.02	44.69	*	NS	NS
BAY 826	45.88	72.52	77.36	*	NS	NS
Fendiline Hydrochloride	59.63	83.74	67.79	*	NS	NS
LY 450139	172.04	84.41	97.32	***	**	NS
A 77-01	234.25	68.66	97.87	***	**	NS
Jedi2	195.26	76.30	127.47	***	*	NS
LJI308	174.86	67.84	24.52	**	***	NS
ML 67-33	127.94	42.76	32.63	**	**	NS
AC 1903	224.12	67.24	83.50	**	**	NS
MB 05032	200.35	85.49	111.90	**	*	NS
PA 8	222.98	70.15	108.71	**	*	NS
4-Octyl itaconate	223.34	78.64	113.76	**	*	NS
PF 04449913 maleate	163.80	72.46	138.94	**	NS	*
BRD 73954	142.42	63.56	66.16	**	NS	NS
MS 21570	178.23	86.12	95.20	**	NS	NS
1A-116	138.85	72.48	95.08	**	NS	NS
Roflumilast	225.42	68.84	108.86	**	NS	NS
NGI 1	156.45	52.61	68.91	**	NS	NS
ABT 594 hydrochloride	105.87	67.11	86.96	**	NS	NS
MRK 740	121.47	69.65	20.94	*	**	*
TM 5441	157.08	96.70	101.79	*	**	NS
Rosuvastatin calcium	191.40	97.09	40.07	*	**	NS
16673-34-0 NLRP3i	107.50	77.75	55.21	*	**	NS
B 973B	161.73	80.46	47.10	*	**	NS
WM 1119	189.02	75.47	94.37	*	*	NS
AP C5	214.23	79.40	108.09	*	*	NS

Compound Name	Average in PS	Average in 2D	Average in 3D	Significance in 2D vs PS (Figure 14A)	Significance in 3D vs PS (Figure 14B)	Significance in 2D vs 3D (Figure 14C)
Acetazolamide	211.81	75.69	89.28	*	*	NS
TC SL C5	139.56	63.89	42.71	*	*	NS
CBA	210.31	53.96	107.75	*	*	NS
ABT 639	135.12	74.29	76.95	*	*	NS
TH 257	93.97	69.59	94.99	*	NS	*
AZD 2098	160.34	50.14	126.97	*	NS	*
CID 1375606	154.06	74.17	141.31	*	NS	*
Avagacestat	128.51	82.81	107.08	*	NS	NS
CU CPT 9a	104.15	75.79	73.63	*	NS	NS
Phentolamine Mesylate	110.64	82.13	44.34	*	NS	NS
GSK 9311 hydrochloride	125.69	89.42	98.59	*	NS	NS
Tamoxifen	135.33	96.07	77.37	*	NS	NS
TH 5427 hydrochloride	157.57	68.87	130.75	*	NS	NS
Pyridone 6	76.93	33.14	54.02	*	NS	NS
OD 36 hydrochloride	114.61	59.07	81.19	*	NS	NS
Silodosin	202.43	47.59	112.64	*	NS	NS
ML 184	141.62	75.86	120.52	*	NS	NS
GSK 2018682	204.08	83.03	102.13	*	NS	NS
UCLA GP130 2	119.53	67.96	100.00	*	NS	NS
CMA	202.35	89.22	118.29	*	NS	NS
FM19G11	149.52	65.03	99.39	*	NS	NS
BAY 87-2243	81.29	40.50	62.65	*	NS	NS
GI 530159	152.80	88.32	111.31	*	NS	NS
Ivabradine hydrochloride	204.91	55.59	128.24	*	NS	NS
OB-1	93.65	51.86	57.44	*	NS	NS
(R)-ZINC 3573	158.95	99.41	28.20	NS	**	*
JTP 103237	152.63	89.11	53.86	NS	*	*
Quizartinib	138.80	73.04	11.87	NS	*	*
Dasatinib	63.71	68.39	21.09	NS	*	*
OUL 35	151.26	122.55	36.47	NS	*	*
JNJ 0966	66.21	79.93	13.83	NS	*	*
TAK 375	90.83	88.44	50.66	NS	*	*
AA 147	173.99	83.25	11.12	NS	*	*

Compound Name	Average in PS	Average in 2D	Average in 3D	Significance in 2D vs PS (Figure 14A)	Significance in 3D vs PS (Figure 14B)	Significance in 2D vs 3D (Figure 14C)
AMG 333	150.91	73.78	28.51	NS	*	*
VU 0134992	117.05	52.29	14.40	NS	*	*
Idasanutlin	79.09	74.79	37.68	NS	*	NS
AZD 5363	62.03	45.17	17.45	NS	*	NS
TR 14035	119.45	98.98	55.64	NS	**	NS
H 151	34.10	41.24	8.66	NS	**	NS
Darapladib	1.38	34.69	5.21	NS	*	NS
SLM 6031434 hydrochloride	79.94	53.04	18.18	NS	*	NS
J 2156	145.76	85.89	53.43	NS	*	NS
PF 04628935	137.96	94.01	31.82	NS	*	NS
L Moses dihydrochloride	153.68	82.86	59.28	NS	*	NS
A 410099.1	99.50	64.19	22.58	NS	*	NS
FITM	138.04	80.29	31.63	NS	*	NS
RGFP 966	42.15	27.56	14.68	NS	*	NS
Autophinib	133.73	107.60	20.17	NS	NS	*
CP 43	61.30	28.41	116.64	NS	NS	**
SPRi 3	117.28	47.38	80.10	NS	NS	*
LY 2033298	81.25	60.96	86.50	NS	NS	*
CHS 828	3.42	0.05	1.73	**	NS	NS
ML 418	1.17	-0.98	3.72	**	**	**
MS 275	0.31	-1.72	2.46	**	NS	*
A 485	13.70	21.95	4.96	*	NS	*
YM 155	0.70	-1.25	2.52	*	NS	*
Cytarabine	1.44	1.11	4.95	NS	**	**
SR 16832	-1.76	0.13	1.78	NS	*	*
Afatinib dimaleate	-0.84	-0.80	3.23	NS	*	**
XMU MP 1	0.40	-1.59	2.52	NS	*	**
LY 2603618	1.33	15.19	4.49	NS	**	NS
CC 401 dihydrochloride	18.17	11.18	1.14	NS	*	NS
ZAP 180013	4.15	-0.88	3.57	NS	NS	**
SGC GAK 1	2.35	-1.66	2.53	NS	NS	**
Dacomitinib	-1.14	21.04	1.14	NS	NS	NS
ML 210	1.00	4.76	2.81	NS	NS	NS

Compound Name	Average in PS	Average in 2D	Average in 3D	Significance in 2D vs PS (Figure 14A)	Significance in 3D vs PS (Figure 14B)	Significance in 2D vs 3D (Figure 14C)
Brequinar sodium	18.56	23.54	44.26	NS	NS	NS
ABT 199	4.98	1.30	4.39	NS	NS	NS
Givinostat hydrochloride	-0.09	-1.28	1.33	NS	NS	NS
Pelitinib	1.16	1.02	1.30	NS	NS	NS
BAY 293	0.11	39.95	7.92	NS	NS	NS
CRT 0105950	58.23	22.09	3.02	NS	NS	NS
Saxagliptin hydrochloride	31.85	17.73	5.07	NS	NS	NS
Rucaparib camsylate	110.07	82.80	60.14	NS	NS	NS
O8 OGG1 Inhibitor	105.55	89.34	44.03	NS	NS	NS
SM 16	98.93	89.25	58.53	NS	NS	NS
JH-II-127	41.77	30.67	17.76	NS	NS	NS
Lenalidomide	191.02	135.11	50.91	NS	NS	NS
Tadalafil	164.41	115.50	50.34	NS	NS	NS
CBM 301940	192.68	97.13	50.43	NS	NS	NS
ESI 05	108.24	99.47	43.37	NS	NS	NS
AZ 5704	118.94	84.53	40.84	NS	NS	NS
Epiblastin A	68.69	40.94	60.02	NS	NS	NS
PF 5006739	81.86	100.74	33.61	NS	NS	NS
Squarunkin A hydrochloride	122.85	93.57	79.41	NS	NS	NS
PF 04457845	27.28	72.74	21.75	NS	NS	NS
PF 05180999	91.20	93.84	47.57	NS	NS	NS
ML 323	73.11	84.04	34.16	NS	NS	NS
BRD 6989	63.45	72.54	34.71	NS	NS	NS
ML 351	104.93	68.79	44.78	NS	NS	NS
GSK'872	53.21	76.03	78.18	NS	NS	NS
Avasimibe	83.15	81.48	56.76	NS	NS	NS
PF 06551600 malonate	77.35	82.78	78.06	NS	NS	NS
SSR 149415	139.98	79.29	89.17	NS	NS	NS
Bosentan	103.59	101.08	42.93	NS	NS	NS
JNJ 39758979 dihydrochloride	188.29	102.05	50.05	NS	NS	NS
Trazodone hydrochloride	196.41	88.05	79.22	NS	NS	NS

Compound Name	Average in PS	Average in 2D	Average in 3D	Significance in 2D vs PS (Figure 14A)	Significance in 3D vs PS (Figure 14B)	Significance in 2D vs 3D (Figure 14C)
Vilazodone hydrochloride	80.64	63.32	24.33	NS	NS	NS
Arformoterol tartrate	152.71	105.53	115.71	NS	NS	NS
MS 15203	187.19	118.98	75.30	NS	NS	NS
tBPC	113.56	79.25	96.70	NS	NS	NS
GSK 6853	82.34	82.72	53.84	NS	NS	NS
ML 385	78.20	87.75	39.25	NS	NS	NS
Nelarabine	148.34	97.70	88.43	NS	NS	NS
FPS ZM1	100.59	83.00	44.79	NS	NS	NS
FIN 56	29.67	44.67	16.24	NS	NS	NS
Megestrol Acetate	112.04	70.59	67.22	NS	NS	NS
SAK 3	102.73	83.81	56.03	NS	NS	NS
GSK 1702934A	117.18	88.11	88.98	NS	NS	NS
JNJ 55511118	118.81	71.55	41.81	NS	NS	NS
UoS 12258	111.28	96.25	52.81	NS	NS	NS
GNE 9278	102.75	117.16	45.37	NS	NS	NS
Z 944	101.15	106.37	56.53	NS	NS	NS
SGC AAK1 1	48.39	47.34	89.20	NS	NS	NS
UNC 2881	100.79	47.12	78.53	NS	NS	NS
Darunavir	203.67	81.24	95.43	NS	NS	NS
Raphin 1	181.36	94.46	69.49	NS	NS	NS
Sitagliptin phosphate	139.00	71.40	66.11	NS	NS	NS
Conivaptan hydrochloride	91.86	79.80	22.83	NS	NS	NS
FTBMT	101.74	94.54	46.21	NS	NS	NS
KI-7	78.17	88.23	55.21	NS	NS	NS
VU 6005649	94.01	69.35	99.34	NS	NS	NS
Mefloquine hydrochloride	124.54	51.80	60.87	NS	NS	NS
ML 402	104.88	47.63	55.50	NS	NS	NS
A 1899	93.12	48.46	55.82	NS	NS	NS
Dooku 1	115.48	75.49	81.17	NS	NS	NS
GT 949	115.03	77.99	84.38	NS	NS	NS
VAS 2870	124.80	17.47	74.22	NS	NS	NS

Compound Name	Average in PS	Average in 2D	Average in 3D	Significance in 2D vs PS (Figure 14A)	Significance in 3D vs PS (Figure 14B)	Significance in 2D vs 3D (Figure 14C)
Thiorizadine	8.09	5.88	3.53	NS	NS	NS